NATIONAL TECHNICAL UNIVERSITY OF ATHENS

SCHOOL OF APPLIED MATHEMATICS

AND PHYSICAL SCIENCES

APPROXIMATE DYNAMICAL SYMMETRIES IN COLLECTIVE MODELS OF NUCLEAR STRUTURE

DOCTORAL THESIS
SOFIA G. KARAMPAGIA
Graduate of the School of Applied Mathematical and Physical Sciences, NTUA

Supervisor: Dennis Bonatsos,
Director of Research, National Center of Scientific Research "Demokritos"

October 2014

NATIONAL TECHNICAL UNIVERSITY OF ATHENS

SCHOOL OF APPLIED MATHEMATICS
AND PHYSICAL SCIENCES

APPROXIMATE DYNAMICAL SYMMETRIES
IN COLLECTIVE MODELS
OF NUCLEAR STRUTURE

DOCTORAL THESIS
SOFIA G. KARAMPAGIA
Graduate of the School of Applied Mathematical and Physical Sciences, NTUA

THREE MEMBER ADVISORY COMMITTEE:
D. Bonatsos, Direc. of Res. NCSR "D"
G. Kutsubas, Ass. Prof. NTUA
K. Papadopoulos, Ass. Prof. NTUA

SEVEN MEMBER ADVISORY COMMITTEE:
D. Bonatsos, Direc. of Res. NCSR "D"
G. Kutsubas, Ass. Prof. NTUA
K. Papadopoulos, Ass. Prof. NTUA
E. Mavrommati, Ass. Prof. NTUA
G. Lalazisis, Prof. NTUA
M. Axenidis, Princ. Inv. NCSR "D"
S. Charisopoulos, Direc. of Res. NCSR "D"

Athens, October 2014

Contents

Acknowledgements

Abstract

Symmetries play a central role in physics. A Hamiltonian is said to have a given symmetry, or is said to be invariant under transformations of a symmetry group, when the generators of the symmetry group commute with the Hamiltonian. A consequence of the existence of a symmetry is the occurence of degeneracies in the spectrum of the Hamiltonian. A dynamical symmetry arises when the Hamiltonian can be written in terms of Casimir (or invariant) operators of a chain of groups. (Casimir operators of a group are combinations of generators of the group.) Now, the eigenstates of the Hamiltonian are characterized by the characteristic quantum numbers of all the symmetries of the groups involved, but the degeneracy of the spectrum is relaxed.

Dynamical symmetries have long been used in the study of nuclear structure. One of the first uses of dynamical symmetries was in the context of the SU(3) Elliott model, that focused on light nonspherical nuclei in the s-d shell. In the context of the shell model, an analogous try for the description of deformed nuclei was achieved with the Nilsson model, which calculated binding energies of nucleons in a deformed potential. Another characteristic and extensively used example of dynamical symmetries is in the context of the Interacting Boson Model (IBM) or Interacting Boson Approximation (IBA), with its three dynamical symmetries U(5), SU(3) and O(6), which describe spherical vibrators, prolate axially symmetric nuclei and nuclei soft with respect to axial asymmetry (γ-soft), respectively.

The breaking of a symmetry could lead to the appearence of approximate symmetries, which could be identified, among other methods, with chaotic measures. The breaking of the SU(3) Elliott symmetry for heavy nuclei, has lead to the development of a model based on an approximate SU(3) symmetry, the pseudo-SU(3) scheme, appropriate for the description of heavy nuclei. The breaking of symmetries in the context of the IBA, has lead to new approximate symmetries, the extended concepts of Partial Dynamical Symmetries and Quasi Dynamical Symmetries, which in general have to do with the persistence of a symmetry or part of a symmetry, in spite of strong symmetry breaking interactions.

In the first part of this study, statistical measures of chaos are used, in order to study the emergence of regularity among chaos, in the context of the IBM. Symmetry breaking leads the IBM Hamiltonian away from its dynamical symmetries, so one would also expect, away from regularity. However, the existence of approximate symmetries in the parameter space of IBM, leads to the emergence of semiregular

regions, based on these approximate symmetries, among totally chaotic regions. A well known such region, based on an unknown approximate symmetry, is the the arc of regularity. It was found that no matter how many bosons are used, a small number, or a large one, the position of the arc of regularity is unaltered. Also, from a study of chaos as a function of energy it was found that even for chaotic points, as the energy increases, chaos gives its place to regularity.

Next, the nature of the approximate symmetry underlying the arc of regularity was studied. A line of approximate SU(3) symmetry was analytically derived in the parameter space of the IBM. The derivation of the line is based on the idea that in order to have an SU(3) symmetry the IBM Hamiltonian has to commute with the generators of SU(3). The line was extracted by the study of Hamiltonians that in the large boson limit of the IBM, approximately commute with the SU(3) generators. This line closely follows the arc of regularity and gives an explanation to its existence.

Last, the onset of deformation in nuclei is studied, in the context of the Nilsson model, through the calculation of the overlaps of the wavefunctions of the last filled proton and neutron in the Nilsson diagrams. Maximum values of overlaps are related to wavefunctions that differ by 0[110] in their Nilsson quantum numbers and also to nuclei for which deformation has just set in. 0[110] proton-neutron partners have led to the suggestion of a new coupling scheme, similar in spirit to the idea of pseudo-SU(3), but different in content, based also on an approximate SU(3) symmetry.

Chapter 1

Introduction

1.1 Collectivity in nuclei

In order to understand the low energy structure of nuclei, the spherical shell model has been extensively used. In the spherical shell model, nucleons move around a central potential, which produces shell structure and major shell closings, which provide the well known magic numbers. The spherical shell model can describe well nuclei which are near closed shells. These nuclei have spherical shape. Collectivity is interpreted as coherent motion of the nucleons. As valence nucleons are added, the pairing interaction, which favors the spherical coupling of identical nucleons, starts competing with the quadrupole-quadrupole interaction, between unlike nucleons, which favors deformation. While pairing is proportional to the number of valence nucleons, the quadrupole interaction goes as its square. So, gradually deformation wins. Nuclei with expressed collectivity, can no longer be described by the spherical shell model. As deformation sets in, the use of a deformed potential, instead of the spherical potential in the shell model, has been proved probably one of the more successful models for the description of deformed nuclei, called Nilsson model [1]. Deformed nuclei have also been described with algebraic models. It has been shown that the spectrum of deformed light nuclei (belonging maximum to the sd shell) resembles that of the 3D harmonic oscillator, which is known to have an SU(3) symmetry. So, the SU(3)-Elliott [2] model, appropriate for the description of these nuclei has been developed. For heavier nuclei, the spin-orbit coupling breaks the SU(3) symmetry. To account for the breaking of SU(3) symmetry, the pseudo-SU(3) [3, 4] scheme has been developed.

The collective structure of nuclear shapes at low excitation energy is dominated by surface deformations, in which a surface layer of nucleons is vibrating around a spherical shape or gives the nucleus a deformed shape. Deformed nuclei can also rotate. These collective states have been described geometrically in the Bohr model [5]. This model has two structure parameters; β, which defines the shape of the nucleus (if $\beta = 0$, the nucleus is spherical, $\beta > 0$, corresponds to a prolate nucleus, $\beta < 0$ to an oblate) and γ which defines whether a nucleus is axially symmetric or

not (γ-soft). The Bohr model has three analytical solutions. One that describes a spherical harmonic vibrator, one that describes a triaxial, γ-soft nucleus and last, one that describes a solid rotator.

1.1.1   Collective observables

Various features show the onset of collectivity and the resulting change of structure in nuclei. A useful measure of collectivity is the ratio

$$R_{4/2} = \frac{E(4_1^+)}{E(2_1^+)}, \tag{1.1}$$

where $E(J^+)$ is the energy of the level of the ground state band with spin J. In nuclei with a small number of valence nucleons, where collectivity hasn't appeared yet, the ratio $R_{4/2}$ is < 2. A characteristic of the spectrum of these nuclei is that there is a large gap between the 0^+ level and the first excited 2^+ level. As valence nucleons are added, collectivity sets in, in the form of collective vibrations around a spherical shape and the ratio $R_{4/2}$ becomes ≈ 2. Then, the first excited 2^+ level lowers in energy. As more nucleons are added, the nucleus becomes deformed and its levels follow the $L(L+1)$ rule. Then, $R_{4/2} \approx 3.33$. Now, the 2^+ level is even more lowered in energy. In Fig. (1.1), an example is given of how the ratio $R_{4/2}$ and the characteristic features of the specta of nuclei vary between the various limits. For nuclei transitional between these limits, intermediate values of $R_{4/2}$ are encountered. In Fig. (1.1) the $B(E2; 2_1^+ \to 0_1^+)$ transition is also drawn. In fact, the thickness of the arrow is proportional to its strength. So, the $B(E2; 2_1^+ \to 0_1^+)$ transition can be thought of as another measure of collectivity, since the more collective the nucleus is, the more strong the transition.

1.2   Interacting Boson Model

The Interacting Boson Model [6, 7], introduced by Arima and Iachello [8, 9, 10, 11], provides an algebraic framework to describe collective motion in even-even nuclei. Only valence nucleons are taken into account, which are treated as bosons, coupled to angular momentum 0 or 2. In this version of the model, which is the simplest one, no distinction is made between proton and neutron bosons. The number of bosons is half the number of valence protons and neutrons. Valence protons and neutrons are counted from the nearest closed shell and depending on whether less than the half of the shell or more than the half of the shell is filled, they can be either particles or holes.

    States and operators in the IBM are constructed from boson creation and annihilation operators. As already mentioned, nucleons are coupled either to angular momentum $L = 0$, so they create an s boson, which has no magnetical substate, or to angular momentum $L = 2$, creating a d boson, with five magnetic substates. The boson creation and annihilation operators are
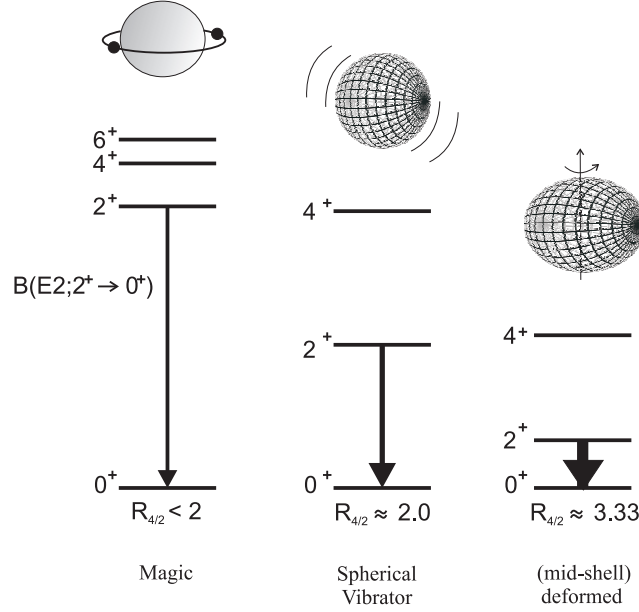
Figure 1.1: From left to right, the variation of the $R_{4/2}$ ratio, for nuclei close to closed shells, where collectivity hasn't appeared yet, for nuclei performing collective vibrations and for deformed nuclei. The arrow refers to the $B(E2; 2_1^+ \rightarrow 0_1^+)$ transition, whose strength is analogous to the thickness of the arrow and of course to the increase of collectivity.

$$\begin{cases} s^\dagger, d_\mu^\dagger & (\mu = 0, \pm 1, \pm 2), \\ s, d_\mu & (\mu = 0, \pm 1, \pm 2), \end{cases}$$

who satisfy Bose commutation relations

$$[s, s^\dagger] = 1, \qquad [s, s] = [s^\dagger, s^\dagger] = 0 \tag{1.2}$$
$$[d_\mu, d_\mu^\dagger] = \delta_{\mu,\mu'}; \qquad [d_\mu, d_{\mu'}] = [d_\mu^\dagger, d_{\mu'}^\dagger] = 0$$
$$[s, d_\mu^\dagger] = [s, d_\mu] = [s^\dagger, d_\mu^\dagger] = [s^\dagger, d_\mu] = 0.$$

For applications, boson operators need to transform like spherical tensors. While the creation operators do have this property, the annihilation operators do not, so new annihilation operators need to be introduced

$$\tilde{s} = s, \quad \tilde{d}_\mu = (-1)^\mu d_{-\mu}. \tag{1.3}$$

With spherical tensors one can form tensor products, whose use will be revealed in the next section. The tensor product of two spherical tensors $T_{\kappa_1}^{k_1}$, $T_{\kappa_2}^{k_2}$ is

$$T_\kappa^k = [T_{\kappa_1}^{k_1} \times T_{\kappa_2}^{k_2}]_\kappa^k = \sum_{\kappa_1 \kappa_2} (k_1 \kappa_1 k_2 \kappa_2 | K\kappa) T_{\kappa_1}^{k_1} T_{\kappa_2}^{k_2}. \tag{1.4}$$

When at the tensor product the spherical tensors are coupled to angular momentum zero, one has a scalar product, defined as

$$(U^{(k)} \cdot V^{(k)}) = (-1)^k (2k+1)^{1/2} [U^{(k)} \times V^{(k)}]_0^{(0)} = \sum_\kappa (-1)^\kappa U_\kappa^{(k)} V_\kappa^{(k)}. \qquad (1.5)$$

1.3   U(6) algebra and Subalgebra Chains

We now introduce the operators - tensor products

$$G_\kappa^{(k)} = [b_l^\dagger \times \tilde{b}_{l'}]_\kappa^{(k)}, \qquad (1.6)$$

where $l, l' = 0, 2 \equiv s, d$. The symbolization means that the objects in the square brackets having angular momentum l and l' respectively, are coupled to create a spherical tensor of angular momentum k.

By writing down all the tensor products of the spherical tensors $\tilde{s}$, $s^\dagger$, $\tilde{d}_\mu$, $d_\mu^\dagger$, of the form (1.6) and by using their commutation relations

$$[G_\kappa^{(k)}(l,l'), G_{\kappa'}^{(k')}(l'',l''')] = \sum_{k'',\kappa''} \sqrt{(2k+1)(2k'+1)} (k\kappa k'\kappa'|k''\kappa'')(-1)^{k-k'}$$

$$\left[(-1)^{k+k'+k''} \begin{Bmatrix} k & k' & k'' \\ l''' & l & l' \end{Bmatrix} \delta_{l'l''} G_{\kappa''}^{(k'')}(l,l''') - \begin{Bmatrix} k & k' & k'' \\ l'' & l' & l \end{Bmatrix} \delta_{ll'''} G_{\kappa''}^{(k'')}(l'',l') \right], \quad (1.7)$$

one can see that the commutation relations of these operators are the same with the commutation relations of the Lie algebra of the group U(6). Thus, they form the generators of U(6). For convenience, at the tensor products, we omit the $\times$ symbol and replace the square brackets [], by parentheses, ().

$$
\begin{aligned}
G_0^{(0)}(s,s) &= (s^\dagger \tilde{s})_0^{(0)} \qquad\qquad\qquad (1.8) \\
G_0^{(0)}(d,d) &= (d^\dagger \tilde{d})_0^{(0)} \\
G_\mu^{(1)}(d,d) &= (d^\dagger \tilde{d})_\mu^{(1)} \\
G_\mu^{(2)}(d,d) &= (d^\dagger \tilde{d})_\mu^{(2)} \\
G_\mu^{(3)}(d,d) &= (d^\dagger \tilde{d})_\mu^{(3)} \\
G_\mu^{(4)}(d,d) &= (d^\dagger \tilde{d})_\mu^{(4)} \\
G_\mu^{(2)}(d,s) &= (d^\dagger \tilde{s})_\mu^{(2)} \\
G_\mu^{(2)}(s,d) &= (s^\dagger \tilde{d})_\mu^{(2)}
\end{aligned}
$$

These 36 operators are the generators of U(6). By selecting specific tensor products, subalgebras of the algebra U(6) are revealed and chains of subalgebras are constructed. For applications in nuclear physics, states should be characterized by good angular momentum, so each chain should contain the O(3) algebra. After this restriction is taken into account, three possible chains of subalgebras are constructed

$$U(6) \supset U(5) \supset O(5) \supset O(3) \quad \text{(I)} \tag{1.9}$$
$$U(6) \supset SU(3) \supset O(3) \quad \text{(II)}$$
$$U(6) \supset O(6) \supset O(5) \supset O(3) \quad \text{(III)}$$

and the dynamical symmetries [12] U(5), SU(3) and O(6) are revealed, which are the dynamical symmetries of the model.

We can see explicitly how these subalgebras are revealed, after selecting the appropriate tensor products, whose commutation relations close under the specific algebras. For the first chain, (I), one omits from the 36 generators of U(6) those that contain s bosons and the remaining 25 operators, $(d^\dagger \tilde{d})_0^{(0)}$, $(d^\dagger \tilde{d})_\mu^{(1)}$, $(d^\dagger \tilde{d})_\mu^{(2)}$, $(d^\dagger \tilde{d})_\mu^{(3)}$, $(d^\dagger \tilde{d})_\mu^{(4)}$, which are obtained, have commutation relations that close under the algebra U(5), so they are the generators of U(5). By keeping now the ten operators $(d^\dagger \tilde{d})_\mu^{(1)}$, $(d^\dagger \tilde{d})_\mu^{(3)}$, the orthogonal algebra in five dimensions, O(5), is obtained. Last, the three operators $(d^\dagger \tilde{d})_\mu^{(1)}$, are the generators of the O(3) algebra.

For the second chain, (II), one considers the operators $(s^\dagger \tilde{s})_0^{(0)} + \sqrt{5}(d^\dagger \tilde{d})_0^{(0)}$, $(d^\dagger \tilde{d})_\mu^{(1)}$, $(d^\dagger \tilde{s} + s^\dagger \tilde{d})_\mu^{(2)} \pm \frac{1}{2}\sqrt{7}(d^\dagger \tilde{d})_\mu^{(2)}$. These operators close under commutation and form the algebra U(3). The $(d^\dagger \tilde{s} + s^\dagger \tilde{d})_\mu^{(2)} \pm \frac{1}{2}\sqrt{7}(d^\dagger \tilde{d})_\mu^{(2)}$ operator has a $\pm$ sign. The +, corresponds to prolate nuclear shape, while the -, to oblate nuclear shape. The operator $(s^\dagger \tilde{s})_0^{(0)} + \sqrt{5}(d^\dagger \tilde{d})_0^{(0)}$ is the total number operator, $\hat{N}$. In the IBM, the total N is conserved and the eigenvalues of $\hat{N}$ are constant, so they can be omitted and the remaining operators form the SU(3) algebra. Last, the rotational, O(3), algebra is reached by keeping just the $(d^\dagger \tilde{d})_\mu^{(1)}$ operator.

The last chain, (III), is obtained if first, one keeps the fifteen operators $(d^\dagger \tilde{d})_\mu^{(1)}$, $(d^\dagger \tilde{d})_\mu^{(3)}$, $(d^\dagger \tilde{s} + s^\dagger \tilde{d})_\mu^{(2)}$, which form the algerba O(6), then by keeping the ten operators $(d^\dagger \tilde{d})_\mu^{(1)}$, $(d^\dagger \tilde{d})_\mu^{(3)}$ the O(5) algebra is generated, which, by keeping just the $(d^\dagger \tilde{d})_\mu^{(1)}$ the last algebra of the chain, O(3) comes into play.

1.3.1 Construction of Bases

The construction of algebra chains allows the construction of bases in which the Hamiltonian can be diagonalised. The bases states of each chain will be written in terms of the quantum numbers which characterize the irreducible representations (irreps) of the algebras which appear in the chains. One needs to know which are the allowed quantum numbers of the irreps of an algebra G′, given the values of the quantum numbers of the irreps of the algebra which contains it, G (G ⊃ G′). The representations are interpreted as quantum mechanical states and the bracket notation is used.

Chain I

In general, the corresponding Young tableaux [13] of the representations of U(n) are denoted as $[f_1, ..., f_n]$. The representations of U(n) which describe bosons are totally symmetric and the corresponding Young tableaux are denoted as, $[N, 0, 0, \ldots, 0] \equiv [N]$, where there are n-1 zeros. So, the irreps of U(6) will be denoted by

$$U(6): \qquad [N, 0, 0, 0, 0, 0] \equiv [N], \tag{1.10}$$

where N is the total number of bosons. Similarly, the irreps of U(5) will be

$$U(5): \qquad [n_d, 0, 0, 0, 0, 0] \equiv [n_d], \tag{1.11}$$

where n_d is the number of d bosons. The allowed values of n_d are $n_d = N, N - 1, \ldots, 0$. For the general case of O(n), the number of quantum numbers needed to describe the totally symmetric irreps is either n/2, for n=even, or (n-1)/2 for n odd. So, the irreps of O(5) will be

$$O(5): \qquad [v, 0] \equiv [v], \tag{1.12}$$

where v is called seniority and is the number of boson pairs not coupled to zero angular momentum. The allowed values of v are $v = n_d, n_d - 2, \ldots, 1$ or 0, for n_d=odd or even. The irreps of the last algebra of this chain, O(3), are denoted by just one quantum number, the angular momentum, L. When trying to find the allowed values of L, a problem arises, that more than one states with a given value of L are contained in a given representation v of O(5). An additional quantum number is needed to characterize the states uniquely, the n_Δ, which is the number of boson triplets coupled to zero angular momentum. In order to find the values of L contained in each representation v, first one partitions n_d as $n_d = 2n_\beta + 3n_\Delta + \lambda$, where $n_\Delta = 0, 1, \ldots$, and $n_\beta = (n_d - v)/2 = 0, 1, \ldots, \frac{n_d}{2}$ or $\frac{n_d - 1}{2}$. Then, $L = \lambda, \lambda + 1, \ldots, 2\lambda - 2, 2\lambda$. The basis will be $|Nn_d v n_\Delta L>$.

Chain II

As above, the irreps of U(6) are labelled by $[N]$. The irreps of SU(3) are labelled by the Elliott quantum numbers (λ, μ) [2].

$$SU(3): \qquad (\lambda, \mu). \tag{1.13}$$

The values of (λ, μ) contained in $[N]$ are

$$
\begin{aligned}
(2N, 0) \oplus (2N - 4, 2) \oplus \ldots &\quad \oplus \left\{ \begin{array}{ll} (0, N) & N = even \\ (2, N - 1) & N = 0dd \end{array} \right\} \oplus \\
(2N - 6, 0) \oplus (2N - 10, 2) \oplus \ldots &\quad \oplus \left\{ \begin{array}{ll} (0, N - 3) & N - 3 = even \\ (2, N - 4) & N - 3 = 0dd \end{array} \right\} \oplus \\
(2N - 12, 0) \oplus (2N - 16, 2) \oplus \ldots &\quad \oplus \left\{ \begin{array}{ll} (0, N - 6) & N - 6 = even \\ (2, N - 7) & N - 6 = 0dd \end{array} \right\} \oplus \ldots
\end{aligned}
\tag{1.14}
$$

For the last algebra in the chain, O(3), whose irreps are denoted by L, an additional quantum number is needed to find the values of L contained in each (λ, μ), the K quantum number. Then, $L = K, K + 1, K + 2, \ldots, (K + max\{\lambda, \mu\})$, where $K = $ integer $= min\{\lambda, \mu\}, min\{\lambda, \mu\} - 2, \ldots, 1$or 0 and for $K = 0$, $L = max\{\lambda, \mu\}, max\{\lambda, \mu\} - 2, \ldots, 1$ or 0. The basis will be $|N(\lambda, \mu)KL>$.

Chain III

For the last chain, again, the irreps of U(6) are labelled by $[N]$. The irreps of O(6) are

$$O(6): \qquad [\sigma, 0, 0, 0] \equiv \sigma, \tag{1.15}$$

where the allowed quantum numbers of σ are $\sigma = N, N - 2, \ldots, 1$ or 0. The irreps of O(5) are

$$O(5): \qquad [\tau, 0] \equiv \tau, \tag{1.16}$$

where the allowed quantum numbers of τ are $\tau = \sigma, \sigma - 1, \ldots, 1, 0$. For the irreps of O(3), denoted by L, again, an additional quantum number is needed to find the allowed values of L, called ν_Δ. In order to find the values of L contained in each representation τ, one partitions τ as $\tau = 3\nu_\Delta + \lambda$, where $\nu_\Delta = 0, 1, \ldots$. Then, $L = \lambda, \lambda + 1, \ldots, 2\lambda - 2, 2\lambda$. The basis will be $|N\sigma \ \tau\nu_\Delta L>$.

1.3.2 Dynamical Symmetries

A dynamical symmetry arises when the Hamiltonian H can be written as a sum of certain operators, called Casimir operators of a chain of algebras

$$G \supset G' \supset \cdots, \tag{1.17}$$

i.e. $H = aC(G) + a'C(G') + \cdots$, where $C(G)$ is a Casimir operator of the algebra G. Casimir operators are linear or higher order combinations of the generators of the algebra G. They also commute with all the generators of the algebra G. Casimir operators are also diagonal in the representation of the corresponding algebra G and have eigenvalues that are functions only of the characteristic quantum numbers of that particular algebra. This has direct application to the algebra chains described before. So, when the Hamiltonian is written in terms only of Casimir operators of a complete chain of subalgebras of U(6), the Hamiltonian will be diagonal in the basis of the corresponding chain and the eigenvalue problem of the IBM Hamiltonian can be solved analytically. In IBM there are three algebra chains, so there are 3 dynamical symmetries.

An important property of the dynamical symmetry is that the representations of an algebra are split in energy, but not admixed with other representations of the algebras involved in the chain. The way the representations of an algebra are split in energy is by moving to the next subalgebra. For example, the states of a representation of an algebra are all characterized by the same quantum number, so

they are degenerate. The degeneracy is broken when going to the next algebra of the chain, where the levels are subclassified according to another quantum number. In that way, the representations are split in energy, but not mixed. This is seen in a characteristic way in Fig. (1.2).
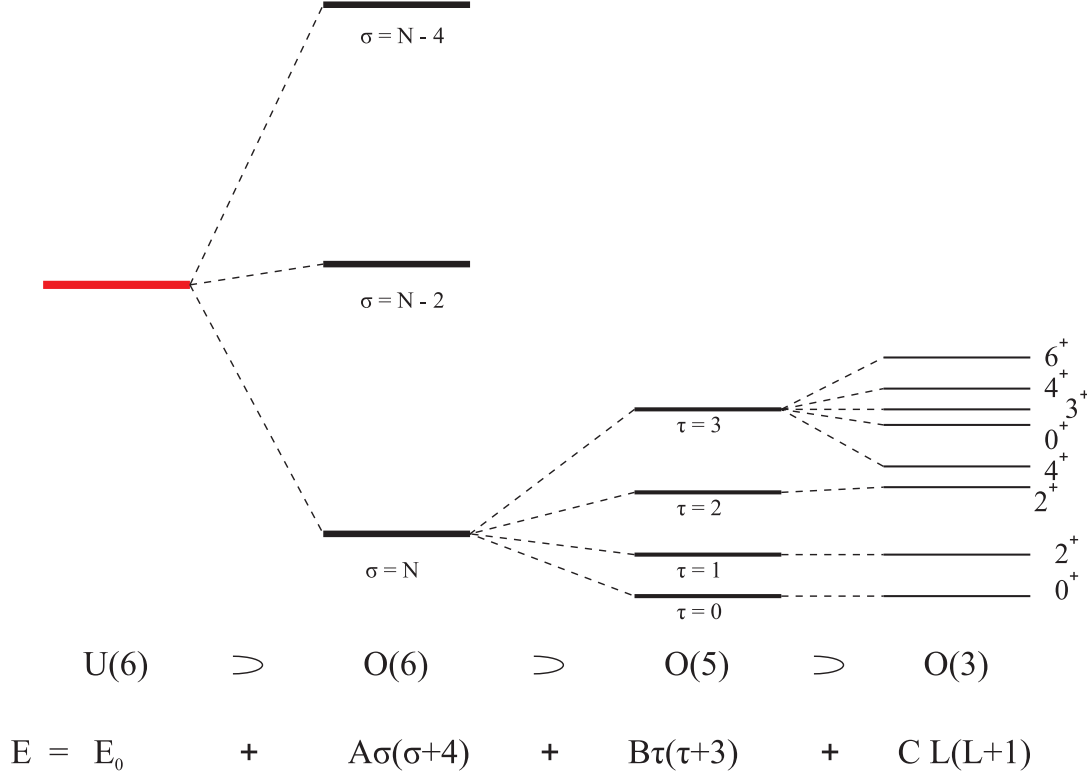
Figure 1.2: Degeneracy breaking when moving to the next algebra of the chain (the example is for the O(6) chain). The representations are split in energy, but not admixed, by the quantum number of the next group of the chain. Figure taken by [14].

Casimir operators

The list of Casimir operators [15] of the subalgebras of U(6) are listed below

$$
\begin{aligned}
C_1(U(6)) &= (s^\dagger \tilde{s})_0^{(0)} + \sqrt{5}(d^\dagger \tilde{d})_0^{(0)} = \hat{n}_s + \hat{n}_d = \hat{N} \\
C_1(U(5)) &= \sqrt{5}(d^\dagger \tilde{d})_0^{(0)} = \hat{n}_d \\
C_2(U(5)) &= \sum_{k=0}^{4}(d^\dagger \tilde{d})^{(k)} \cdot (d^\dagger \tilde{d})^{(k)} = \hat{n}_d(\hat{n}_d + 4) \\
C_2(SU(3)) &= \frac{4}{3}\left((d^\dagger \tilde{s} + s^\dagger \tilde{d})^{(2)} - \frac{\sqrt{7}}{2}(d^\dagger \tilde{d})^{(2)}\right) \cdot \left((d^\dagger \tilde{s} + s^\dagger \tilde{d})^{(2)} - \frac{\sqrt{7}}{2}(d^\dagger \tilde{d})^{(2)}\right) \\
&\quad + 5(d^\dagger \tilde{d})^{(1)} \cdot (d^\dagger \tilde{d})^{(1)} = \frac{4}{3}\hat{Q} \cdot \hat{Q} + \frac{1}{2}\hat{L} \cdot \hat{L}
\end{aligned}
$$

$$(1.18)$$

$$
\begin{aligned}
C_2(O(6)) &= 2(d^\dagger \tilde{s} + s^\dagger \tilde{d})^{(2)} \cdot (d^\dagger \tilde{s} + s^\dagger \tilde{d})^{(2)} + 4 \sum_{k=1,3} (d^\dagger \tilde{d})^{(k)} \cdot (d^\dagger \tilde{d})^{(k)} \\
&= 2\hat{N}(\hat{N}+4) - 8\,\hat{P}^\dagger \cdot \hat{P} \\
C_2(O(5)) &= 4 \sum_{k=1,3} (d^\dagger \tilde{d})^{(k)} \cdot (d^\dagger \tilde{d})^{(k)} = \frac{2}{5}\hat{L} \cdot \hat{L} + 4\,\hat{T}_3 \cdot \hat{T}_3 \\
C_2(O(3)) &= 20(d^\dagger \tilde{d})^{(1)} \cdot (d^\dagger \tilde{d})^{(1)} = 2\,\hat{L} \cdot \hat{L},
\end{aligned}
$$

where $\hat{P} = \frac{1}{2}(\tilde{d} \cdot \tilde{d}) - \frac{1}{2}(\tilde{s} \cdot \tilde{s})$ is the pairing operator, $\hat{L} = \sqrt{10}(d^\dagger \tilde{d})^{(1)}$ is the angular momentum operator, $\hat{Q} = (d^\dagger \tilde{s} + s^\dagger \tilde{d})^{(2)} - \frac{\sqrt{7}}{2}(d^\dagger \tilde{d})^{(2)}$ is the quadrupole operator and $\hat{T}_3 = (d^\dagger \tilde{d})^{(3)}$ is the M3 transition operator.

The eigenvalues of Casimir operators in the representation in which they are diagonal are

$$
\begin{aligned}
\langle [N] | C_1(U(6)) | [N] \rangle &= N & (1.19) \\
\langle [n_d] | C_1(U(5)) | [n_d] \rangle &= n_d \\
\langle [n_d] | C_2(U(5)) | [n_d] \rangle &= n_d(n_d + 4) \\
\langle (\lambda, \mu) | C_2(SU(3)) | (\lambda, \mu) \rangle &= \lambda^2 + \mu^2 + \lambda\mu + 3\lambda + 3\mu \\
\langle (\sigma, 0, 0) | C_2(O(6)) | (\sigma, 0, 0) \rangle &= \sigma(\sigma + 4) \\
\langle (\tau, 0) | C_2(O(5)) | (\tau, 0) \rangle &= \tau(\tau + 3) \\
\langle (L) | C_2(O(3)) | (L) \rangle &= L(L+1).
\end{aligned}
$$

Dynamical Symmetry I

So, the dynamical symmetry of the first chain of algebras $U(6) \supset U(5) \supset O(5) \supset O(3)$ occurs when the Hamiltonian can be written in terms of the Casimir operators of the algebras of the chain, that is

$$
H^{(I)} = E_0 + \epsilon C_1(U(5)) + a C_2(U(5)) + \beta C_2(O(5)) + \gamma C_2(O(3)). \qquad (1.20)
$$

The eigenvalues in the basis $|Nn_d u n_\Delta L >$ according to the section 1.3.2 are

$$
E^{(I)} = E_0 + \epsilon n_d + a n_d(n_d + 4) + \beta \upsilon(\upsilon + 3) + \gamma L(L+1). \qquad (1.21)
$$

A typical spectrum is seen in Fig. 1.3(a). The main characteristics of the spectrum, the equispaced levels, the triplet of states with $L = 0, 2, 4$ at $n_d = 2$, at about twice the energy of the state with $L = 2$ with $n_d = 1$, indicate that it is a vibrational spectrum. This is a $U(5)$ dynamical symmetry.

Dynamical Symmetry II

The Hamiltonian of the second chain of algebras $U(6) \supset SU(3) \supset O(3)$ in terms of the Casimir operators of the algebras of the chain, is written as

$$
H^{(I)} = E_0 + \kappa C_2(SU(3)) + \kappa' C_2(O(3)). \qquad (1.22)
$$

The eigenvalues in the basis $|N(\lambda, \mu)KL>$ are

$$E^{(II)} = E_0 + \kappa(\lambda^2 + \mu^2 + \lambda\mu + 3\lambda + 3\mu) + \kappa' L(L+1). \qquad (1.23)$$

A typical spectrum is seen in Fig. 1.3(b). It is equivalent to the spectrum of axially symmetric rotational nuclei in the sense that the energies in each band increase following the $L(L+1)$ rule. The bands which belong to the $(2,2)$ irrep (in fact to the $(2N-4,2)$ irrep) with $K = 0$ and $K = 2$ are refered as β_1 and γ_1 bands respectively. Bands belonging to the $(2N-8,4)$ irrep are refered to as β_2 and γ_2, etc. A characteristic of the SU(3) dynamical symmetry spectrum is that bands having the same angular momentum, belonging to the same irrep, are degenerate. The $(2N,0)$ irrep, where the ground state band belongs, is called the most leading irrep, because it maximizes the value of the $C_2(SU(3))$, which means that the quadrupole-quadrupole $(\hat{Q} \cdot \hat{Q})$ interaction is maximized for this irrep.

Dynamical Symmetry III

The Hamiltonian of the third chain of algebras U(6) $\supset$ O(6) $\supset$ O(5) $\supset$ O(3) in terms of the Casimir operators of the algebras of the chain, is written as

$$H^{(I)} = E_0 + AC_2(O(6)) + BC_2(SO(5)) + C \, C_2(O(3)). \qquad (1.24)$$

The eigenvalues in the basis $|N\sigma \, \tau\nu_\Delta L>$ are

$$E^{(III)} = E_0 + A\sigma(\sigma + 4) + B\tau(\tau + 3) + C \, L(L+1). \qquad (1.25)$$

A typical spectrum is seen in Fig. 1.3(c). A characteristic property of the O(6) dynamical symmetry spectrum is the repeated occurence of the states $0^+, 2^+$ and the doublet $2^+, 4^+$, where the energy difference between the doublet and the 0^+ is about 2.5 times as large as the energy difference between the 2^+ and 0^+ levels. The spectrum corresponds to the spectrum of a γ-unstable nucleus.
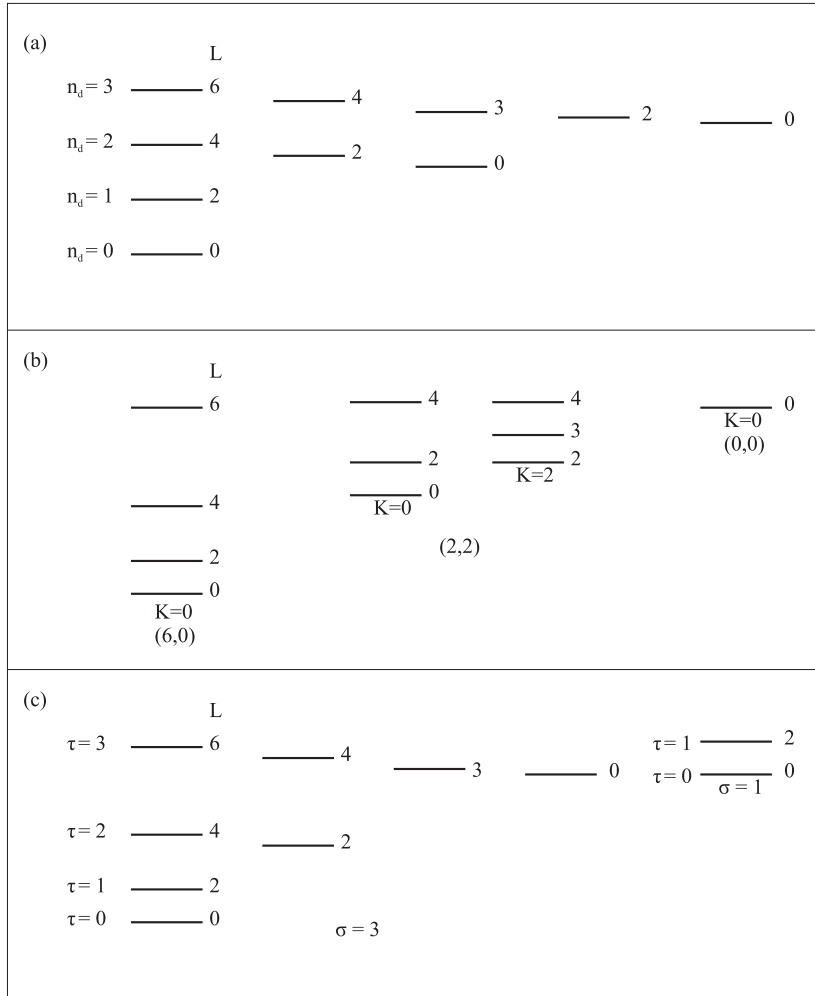
Figure 1.3: The spectra of the three dynamical symmetries of the U(6) algebra of the IBM, for N=3. (a) is the spectrum of the U(5) dynamical symmetry U(6) ⊃ U(5) ⊃ O(5) ⊃ O(3), (b) is the spectrum of the SU(3) dynamical symmetry U(6) ⊃ SU(3) ⊃ O(3) and (c) is the spectrum of the O(6) dynamical symmetry U(6) ⊃ O(6) ⊃ O(5) ⊃ O(3). Figure taken by [15].

1.3.3   IBM Hamiltonian

Till now we have avoided writing a general Hamiltonian for the model. Many Hamiltonian expressions have been proposed, but the one that is usually used for applications to nuclear strucrure has the form [16, 17]

$$\hat{H}(\zeta, \chi) = c \left[(1 - \zeta)\hat{n}_d - \frac{\zeta}{4N}\hat{Q}^\chi \cdot \hat{Q}^\chi \right], \qquad (1.26)$$

where the $\hat{n}_d = d^\dagger \cdot \tilde{d}$ is the number of d-bosons (the first order Casimir operator of U(5)) and $\hat{Q}^\chi = (d^\dagger \tilde{s} + s^\dagger \tilde{d})^{(2)} + \chi(d^\dagger \tilde{d})^{(2)}$ is the quadrupole operator, while N is the number of valence bosons and c a scaling factor. This Hamiltonian satisfies the invariance requirements of boson number conservation (the Hamiltonian commutes with the boson number operator), by having as many creation, as annihilation operatos and the angular momentum conservation (the Hamiltonian commutes with the angular momentum operator), by coupling all the terms to zero angular momentum. In this parametrization, which is called consistent-Q formalism, the quadrupole operator used in the Hamiltonian and in the E2 transition operator, $T^{(E2)} = e_B \hat{Q}^\chi$, are the same, where e_B represents the boson effective charge. The Hamiltonian has two parameters, ζ and χ, which serve for symmetry breaking. ζ ranges from 0 to 1 and χ ranges from 0 to $-\frac{\sqrt{7}}{2}$. By varying ζ and χ, the three dynamical symmetries of the model can be reached and nuclei with properties among the three dynamical symmetries can be described. U(5), which describes vibrational nuclei, corresponds to $\zeta = 0$, SU(3), which describes axially symmetric rotational nuclei, corresponds to $(\zeta, \chi) = (1, -\frac{\sqrt{7}}{2})$ and O(6), which describes deformed γ-soft nuclei, corresponds to $(\zeta, \chi) = (1, 0)$. These dynamical symmetries are placed at the vertices of the symmetry triangle (Casten's triangle) [14, 18], (Fig. 1.4) which is the parameter space of the model. ζ augments when heading from the U(5) vertex to the O(6)-SU(3) line of the triangle and has a constant value on the lines which are parallel to the O(6)-SU(3) line. χ changes values when going from the SU(3) to the O(6) vetrices of the triangle and has constant value on the lines which join the U(5) vertex to the O(6)-SU(3) line.

An interesting subject in nuclear structure is the study of shape/phase transitions in nuclei, which refer to the change of the structure of the ground state band of the nucleus, from spherical to deformed. A shape/phase transition occurs when an observable changes abruptly as a function of a control parameter. Empirically, various observables have been examined, e.g. level energies, separation energies [19], which show sharp discontinuities in behavior at a specific point, called critical point.

According to Ehrenfest classification, a shape/phase transition is of first order if the first derivative of the observable is discontinuous at the critical point or of second order if the discontinuity is presented at the second derivative. The shape/phase transitions have been studied in the context of the IBM [20], by using the classical limit of the model [21, 22]. According to Ehrenfest classification, it was found that a first order shape/phase transition occurs between U(5) and SU(3) limits

and a second order shape/phase transition between U(5) and O(6) limits. These shape/phase transitions are placed on the symmetry triangle (Fig. 1.4). In general, the triangle is divided into two regions, spherical and deformed, by a narrow shape coexistence region [23] (the slanted lines shown in Fig. 1.4), extending around the line connecting the two points where shape/phase transitions occur. Shape/phase transitions have also been studied in a geometrical framework. The critical point symmetries E(5) [24] and X(5) [25] have been developed to describe shape/phase transitions, with E(5) found to correspond to the second order critical point between U(5) and O(6) and X(5) to the first order critical point between U(5) and SU(3), using special solutions of the Bohr Hamiltonian [5]. Although not relevant to IBM, E(5) and X(5) are also placed on the symmetry triangle for the sake of completeness.

Arc of regularity

As already mentioned, the parameters of the Hamiltonian (1.26) serve for symmetry breaking. The breaking of a symmetry could lead to the appearence of approximate symmetries, which could be identified, among other methods, with chaotic measures. Twenty years ago, Alhassid and Whelan, studied the interplay between regular and chaotic behavior in the context of the Interacting Boson Model (IBM), using both classical and quantum measures of chaos [26, 27, 28, 29, 30]. In their study, they had found integrability at the three dynamical symmetry limits of the symmetry triangle of the IBM, as well as at the O(6)-U(5) side of the triangle, while away from these integrable regions chaos prevailed. The study of the interior of the symmetry triangle of the IBM, brought to the surface a surprising result, a region of nearly regular behavior [27], connecting the U(5) and SU(3) vertices, called the "Alhassid–Whelan arc of regularity", or simply "arc of regularity". This semiregular region is seen in Fig. 1.4. It is the arc moving inside the symmetry triangle, connecting the U(5) and SU(3) vetrices.

Alhassid and Whelan used a different parametrization of the IBM Hamiltonian, where ζ parameter is replaced by η, while χ remains the same (Fig. 1.4 (b)). In this parametrization the IBM Hamiltonian changes form and is written as

$$\hat{H}(\eta, \chi) = c \left[\eta \, \hat{n}_d - \frac{\eta - 1}{N} \hat{Q}^\chi \cdot \hat{Q}^\chi \right], \tag{1.27}$$

where η and ζ are connected through the relationship

$$\eta = \frac{4(\zeta - 1)}{3\zeta - 4}. \tag{1.28}$$

The points on the arc are given by the relationship, $\chi(\eta) = \frac{\sqrt{7}-1}{2}\eta - \frac{\sqrt{7}}{2}$ [29]. Throughout the rest of the text, we will be using this parametrization of the Hamiltonian.

1.3.4 Quasi-Dynamical and Partial Dynamical Symmetry

In the previous section, the dynamical symmetries of the U(6) symmetry were presented. The merits of having a dynamical symmetry is more than evident. The
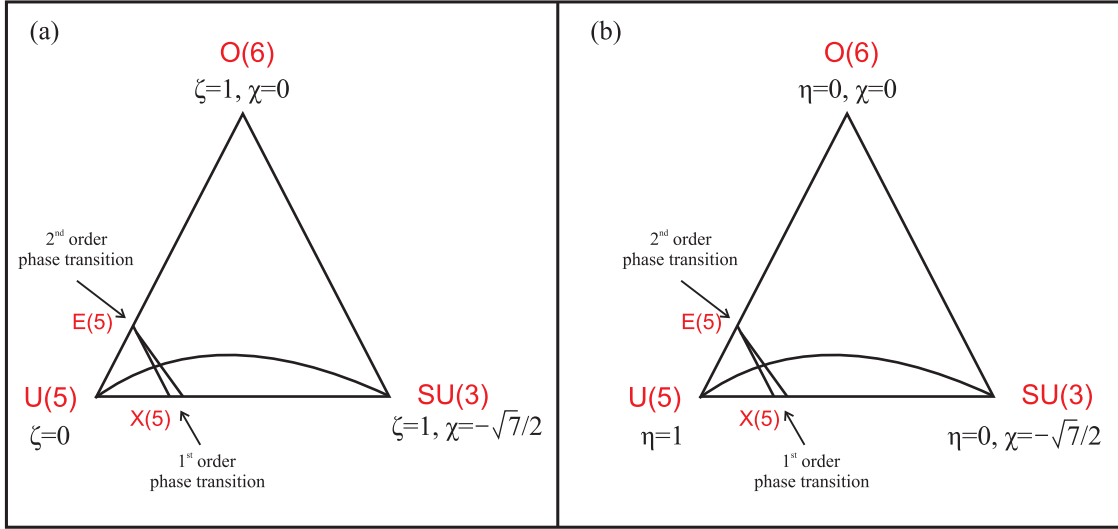
Figure 1.4: The symmetry triangle of the IBM in two different paramertizations. The slanted lines close the coexistence region. The two lines become one, near the second order shape/phase transition (X(5)). The arc moving inside the triangle, connecting the U(5) and SU(3) vertices is the arc of regularity.

eigenstates of the dynamical symmetry are easy to obtain and analytic expressions of energies on the dynamical symmetry limit and other observables are easy to find. However, dynamical symmetries rarely do apply in real nuclei. For example, the degeneracies predicted by dynamical symmetries are rarely shown in real nuclei. While dynamical symmetries appear solely on the vertices of the symmetry triangle of the IBM, the search of more generalized symmetries in the parameter space of the IBM can become possible by applying symmetry breaking. In that way, the concepts of partial dynamical symmetries (PDS) and quasi-dynamical symmetries (QDS) are revealed.

A PDS is achieved when the symmetry breaking keeps some, but not all, of the characteristics of a dynamical symmetry. There are three types of PDS [31, 32, 33, 34, 35]. In Type I, part of the states preserves all the dynamical symmetry. In type II, all the states preserve part of the dynamical symmetry. In Type III, part of the states preserve part of the dynamical symmetry. QDS [36, 37, 38, 39, 40] are defined as the situation where, several observables associated with a particular subset of eigenstates may be consistent with a certain symmetry, despite strong symmetry breaking. The apparent persistence of symmetry is due to the coherent nature of the mixing in the wave functions of these states. Recently, a link has been found between a PDS and a QDS [41]. In [41], they found a region of almost exact ground-state-band O(6) symmetry, away from the O(6) dynamical symmetry, by decomposing the yrast states into O(6) basis states. At this region, the σ quantum number is conserved. At the same time, they found that for the same states, the decomposition of the states into SU(3) basis states, showed that the SU(3) was broken, due to mixing of SU(3) representations, but at the same time this mixing

was coherent (L independent), a hallmark of SU(3) quasidynamical symmetry. So, coherent mixing of one symmetry (SU(3) here) may result in the purity of a quantum number associated with partial conservation of a different, incompatible symmetry (O(6) here).

Chapter 2

Random Matrix Theory and Quantum Chaos

Before giving a definition of quantum chaos, it would be interesting to describe how chaos reveales itself in classical mechanics. The solutions of equations of motion for systems in classical mechanics can be visualised as trajectories which start from specific points in phase space, at certain time t_0 and then evolve with time in the available phase space. In general, trajectories that have arbitrarily small deviations in initial conditions should lie close in phase space.

An interesting feature of some systems with nonlinear equations of motion [42], is that arbitrarily small deviations in initial conditions may lead to exponential divergence in time, of their trajectories. This behavior is called chaos. The phase space of a fully chaotic system is filled with such chaotic trajectories and is void of islands with regular dynamics.

Quantum mechanical systems are not represented by points in phase space but, rather, by vectors in Hilbert spaces. The time evolution of these vectors is governed by the linear Schrödinger equation. So, the term quantum chaos could be confusing, since the Schrödinger equation is linear and hence its solutions cannot be chaotic. However, quantum chaos must be understood as refering to quantum systems that are chaotic in the classical limit [43, 44].

The tools used to study quantum chaos include random matrix theory [45, 46, 47], level dynamics [44] and periodic orbit expansions [43]. Here, we will be studying the former method which applies well to nuclei. In particular, we will be interested in the fluctuation properties of eigenvalues and eigenvectors of the IBM Hamiltonian.

2.1 Random Matrix Theory

Random Matrices were introduced to nuclear physics in the 1960s by Wigner, Dyson and others to explain neutron resonances observed in the scattering of slow neutrons by medium–weight and heavy nuclei (e.g. [48, 49]). In the absence of a dynamical nuclear theory (the nuclear shell model had only just been discovered and had not

yet found universal acceptance), emphasis was focused on the statistical aspects of nuclear spectra as revealed in neutron scattering data.

In order to develop a statistical theory of spectra [50, 51, 52, 53, 54, 55], Random Matrix Theory (RMT) was used. Instead of considering the actual nuclear Hamiltonian, an ensemble of Hamiltonians was used, each given in matrix form and each having a certain probability. The use of ensembles is a common procedure in statistical mechanics, but differs a lot from the way the ensemble is used in RMT. In statistical mechanics, one considers an ensemble of identical physical systems, all governed by the same Hamiltonian, but differing in initial conditions and calculates thermodynamic functions by averaging over this ensemble. So, while in statistical mechanics the members of the ensemble are different states of the same Hamiltonian, in RMT, the members are different Hamiltonians. The Hamiltonians of the ensemble have common symmetry properties (time invariance, rotation invariance, half-integer total angular momentum), depending on the symmetries of the system. RMT takes no account of the specific properties of the nuclear Hamiltonian, e.g. its two body nature, its large pairing, the quadrupole moments, but only the invariances dictated by the symmetry of the matrices. So, attention is focused on the generic properties which are common to (almost) all members of the ensemble and which are determined by the underlying fundamental symmetries. The application of the results obtained within this approach to individual physical systems is justified provided there exists a suitable ergodic theorem (see next section). RMT does not aim at producing spectra for comparison with the data, but rather at calculating spectral fluctuation measures (see next sections) as averages over the ensemble.

The ensembles of Hamiltonian matrices considered by Wigner and Dyson [56, 57, 58, 59, 60, 61, 62, 63, 64] are defined in terms of invariance requirements. With every Hamiltonian matrix belonging to the ensemble, all matrices generated by suitable unitary transformations of Hilbert space are likewise members of the ensemble. With these assumptions, they introduced three ensembles of random matrices. These are the Gaussian orthogonal ensemble (GOE), the Gaussian unitary ensemble (GUE) and the Gaussian symplectic ensemble (GSE).

- The first, GOE, is used for time–reversal invariant systems with rotational symmetry. For such systems, the Hamiltonian matrix can be chosen real and symmetric. Time–reversal invariant systems with integer spin and broken rotational symmetry also belong to this ensemble. This ensemble is used for the study of nuclei.

- The GUE is the Gaussian ensemble of Hermitian (but not necessarily) real matrices. This ensemble plays a role for systems in which time–reversal invariance is violated.

- Last, comes the GSE, which applies to systems with half integer spin that are invariant under time reversal, but with broken rotational symmetry. The GSE does not apply to nuclei directly.

All three ensembles are invariant respectively under orthogonal, unitary, and symplectic transformations. They are often distinguished by the label β, which indicates the degree of level repulsion [65], as two eigenvalues approach each other. Orthogonal, unitary, and symplectic canonical transformations correspond to level repulsion of, respectively, linear, quadratic, and quartic degree ($\beta = 1$, $\beta = 2$, $\beta = 4$). Of the three degrees of level repulsion, only the linear and quadratic have been observed experimentally. First experimental evidence for linear repulsion came from nuclear physics [45, 50, 66, 67], later, confirmation came from microwaves [68, 69, 70, 71], molecular [72, 73] and atomic [74] spectroscopy and sound waves [75, 76]. Quadratic level repulsion hasn't been observed to nuclei, since the breaking of time-reversal invariance is too feeble to become visible in level spacing distributions. The first experimental observation of quadratic level repulsion was in microwave experiments [77, 78], while the first experimentally realizable example in a quantum system came later [79, 80].

Since nuclei are invariant under time reversal and the nuclear Hamiltonian can be chosen real and symmetric, the random matrix ensemble considered from now on will be the GOE.

2.2 The Gaussian Orthogonal Ensemble

For the GOE one considers the family of real symmetric random matrices, of dimension N. With $i, j = 1, \ldots, N$, the matrix elements obey $H_{ij} = H_{ji} = H_{ij}^*$. Any matrix in this family depends on $N(N+1)/2$ random variables, namely, the elements H_{ij} with $i \leq j$. It is assumed that these random variables are independent and identically distributed. The remaining elements are determined by symmetry.

What one is seeking is a probability density $P(H)$ for the independent matrix elements H_{ij} normalized as

$$\int_{-\infty}^{\infty} \prod_{i \leq j} dH_{ij} P(H) = 1 \tag{2.1}$$

and subject to two conditions. First, $P(H)$ must be invariant under any orthogonal transformation, so that for any real orthogonal matrix O,

$$P(H) = P(OH\tilde{O}), \tag{2.2}$$

where $\tilde{O} = O^{-1}$.

Second, the random matrix elements H_{ij} must be statistically independent, thus the function $P(H)$ must be a product of the probability densities of each H_{ij}.

$$P(H) = \prod_{i \leq j} P_{ij}(H_{ij}). \tag{2.3}$$

It is found that subject to these two conditions, the matrix elements H_{ij} must be Gaussian distributed. The probability density can be rewritten in the form

$$
\begin{aligned}
P(H) &= N_0\, exp\left(-\frac{1}{4\sigma^2}\left(\sum_j H_{jj}^2 + 2\sum_{i<j} H_{ij}^2\right)\right) \\
&= N_0\, exp\left(-\frac{1}{4\sigma^2}\sum_{i,j} H_{ij}^2\right)
\end{aligned}
\tag{2.4}
$$

In this expression all the matrix elements have mean 0, the diagonal elements have variance $2\sigma^2$ and the off-diagonal have variance σ^2.

By observing that $\sum_{i,j}(H_{ij})^2 = \sum_{i,j} H_{ij}H_{ji} = (H)_{ii}^2$, equation (2.4) can be rewritten in the form

$$
\begin{aligned}
P(H) &= N_0\, exp\left(-\frac{1}{4\sigma^2}\sum_i (H^2)_{ii}\right) \\
&= N_0\, exp\left(-\frac{1}{4\sigma^2}Tr(H^2)\right).
\end{aligned}
\tag{2.5}
$$

Using (2.4) one can derive the probability distribution of the eigenvalues. Briefly, one rewrites the Hamiltonian as $H = O\,diag(E_1, E_2, \ldots, E_N)\,\tilde{O}$, where O is an orthogonal matrix which can be determined by at most $N(N-1)/2$ parameters and $diag(E_1, E_2, \ldots, E_N)$ is a diagonal matrix containing the eigenvalues. This Hamiltonian expresses the H_{ij}s as a function of $E_1, \ldots, E_N$. Last, by using the Jacobian of the transformation, the distribution of the eigenvalues takes the form

$$
P(E_1, \ldots, E_N) = N_0 \prod_{i<j} |E_i - E_j| \cdot exp\left(-\frac{1}{4\sigma^2}\sum_i E_i^2\right)
\tag{2.6}
$$

The factor $\prod_{i<j} |E_i - E_j|$ gives a manifestation of level repulsion. When two eigenvalues approach each other, the distribution of eigenvalues goes to zero.

A striking feature of RMT (and of GOE of course), which also makes it successful, is the universality of the local eigenvalue statistics. (Here, local statistics means that one rescales the eigenvalues such that the average spacing is of order one. This procedure is called unfolding of spectra and will be explained later.) There is evidence that when the size of a matrix is very large, $N \to \infty$, then the eigenvalue distribution tends towards a limiting distribution, independently of the initial probability law imposed on the matrix entries (e.g. the initial probability law imposed on the matrix entries of GOE is the Gaussian distribution). In the limit $N \to \infty$, the spectral fluctuations are universal. By the term universal, one means that systems that are completely different from each other (see Fig. 2.1), but are dominated by the same symmetries and invariances, have spectral fluctuations that show the same behavior. So, the distributions of empirically observed eigenvalues (e.g. spectra of nuclei), obey the same statistics as random matrix models.
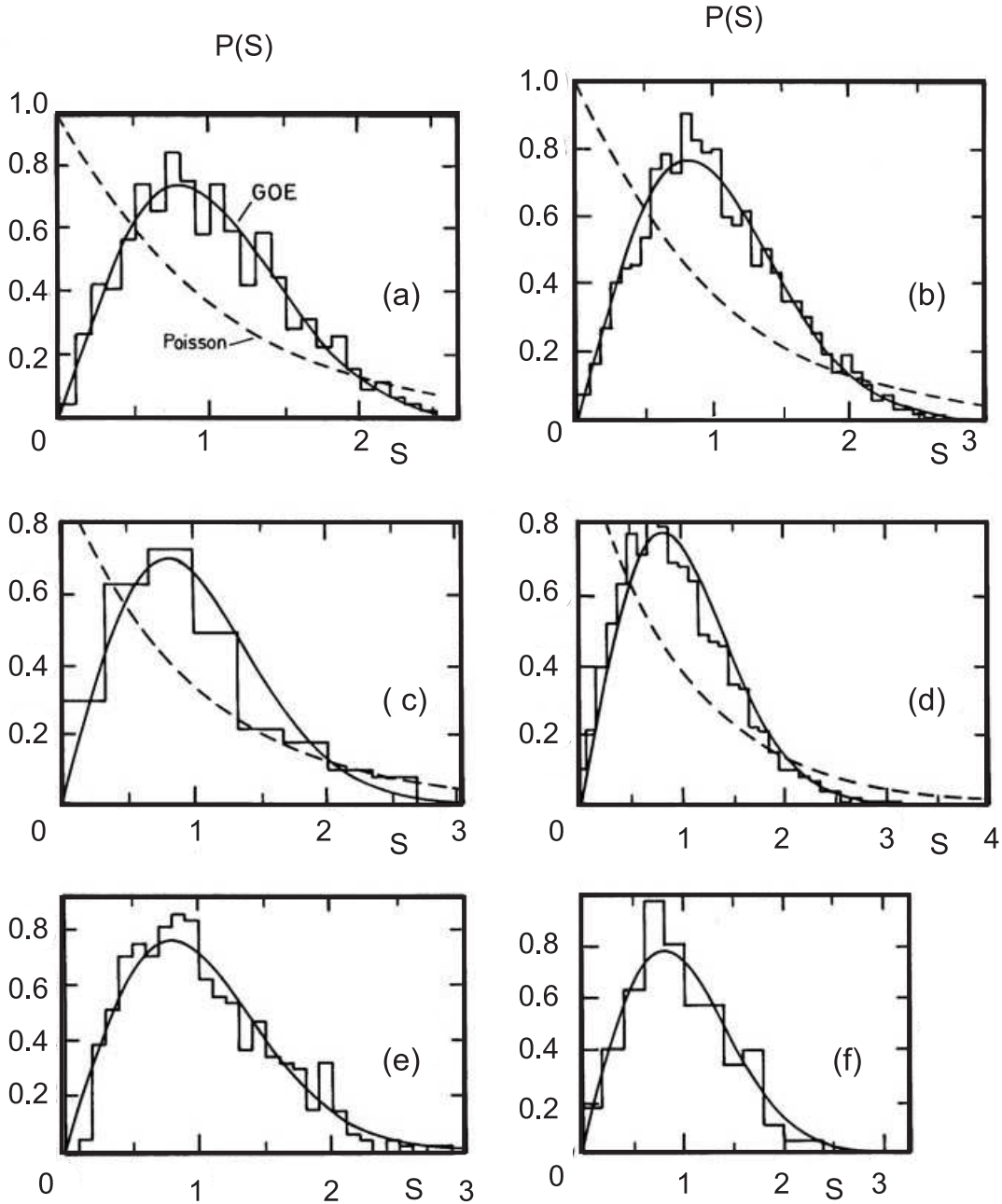
Figure 2.1: Level spacing distributions for (a) the Sinai billiard [67], (b) a hydrogen atom in a strong magnetic field [81], (c) an NO$_2$ molecule [72], (d) a vibrating quartz block shaped like a three dimensional Sinai billiard [82], (e) the microwave spectrum of a three-dimensional chaotic cavity [83], (f) a vibrating elastic disk shaped like a quarter stadium [84]. Figure taken by Haake [44].

In RMT, the various quantities are calculated as averages over the ensemble of Hamiltonians. However, in physical systems there is a single Hamiltonian. The obvious question is how can GOE be applicable to individual physical systems which have a single Hamiltonian, such as nuclei. The answer is by the property of ergodicity of GOE. Ergodicity [85], states that the ensemble average of an observable is equal to the running average of this observable, where the running average is the average calculated for a single member of the ensemble.

One last question that needs to be answered is how RMT is connected with the study of chaos in nuclei. The answer is given by the "Bohigas conjecture" which established a link between RMT and the spectral fluctuation properties of classically chaotic quantum systems with few degrees of freedom. It was already known that experimental data aquiered by scattering of low energy neutrons and protons by nuclei, that were combined to make the "Nuclear Data Ensemble", a total of 1726 level spacings, were in agreement with the GOE [86]. In 1984, Bohigas, Giannoni and Schmit [67] investigated the quantum spectra of the Sinai billiard [87], a classicaly chaotic system and produced a set of data consisting of more than 700 eigenenergies, which then compared with the GOE predictions. The good agreement between the spectra fluctuations calculated from the data and the corresponding GOE results caused the authors to formulate the following conjecture: "Spectra of time-reversal invariant systems whose classical analogues are systems which exhibit strong chaos, show the same fluctuation properties as predicted by the GOE. "

2.3   GOE fluctuation measures, Unfolding Spectra

2.3.1   Nearest neighbour spacing distribution

As already mentioned, RMT does not aim at producing spectra for comparison with the data, but rather at calculating spectral fluctuation measures or statistics for comparison with the data. The first statistic introduced here is the nearest neighbour spacing distribution, commonly used to study the short range fluctuations of the spectrum. It is denoted by $P(S)$ and it is equal to the probability density for two neighboring levels having a spacing S, where S is the actual level spacing over the mean level spacing. When the Hamiltonian is integrable, but with irrational frequencies, then the distribution gets a Poisson form [88]

$$P_P(S) = exp(-S). \tag{2.7}$$

For the GOE, $P(S)$ cannot be determined analytically, but an excellent approximation is given by Wigner, known as Wigner surmise, which is the exact spacing distribution for a 2×2 matrix model, given by the joint distribution (2.6), if $\int SP(S)dS = 1 = \langle S \rangle$, with the normalization $\int_0^\infty P(S)dS = 1$,

$$P_{GOE}(S) = \frac{\pi}{2} S exp(-\pi S^2/4). \tag{2.8}$$

Universality is evident in this relation, since the gaussian form of $P(S)$ is not related to the gaussian factor of the GOE joint probability, but has to do with the fact that large and zero spacings are unlikely to occur. The exact expression for $P(S)$ was first derived by [53]. $P(S)$ for the integral (Poisson form) and the chaotic case (GOE) are displayed in Fig. 2.2.
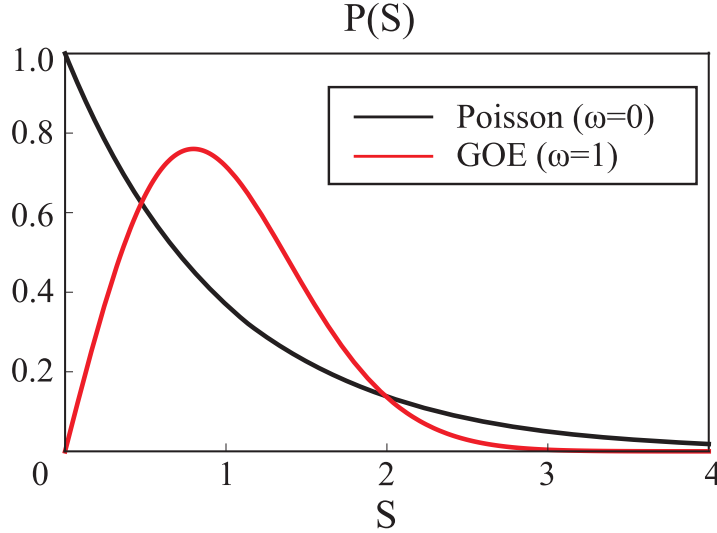
Figure 2.2: The form of the nearest spacing distribution for the Poisson and the GOE case. The ω corresponds to the parameter of the Brody distribution which is going to be introduced in section 2.4.

2.3.2 The Δ_3 statistics

The spectral rigidity, $\Delta_3(L)$, is a measure for the deviation from equal spacing and it is used to measure long range correlations. It was introduced by Dyson and Mehta [63], who defined the function

$$\Delta_3(L) = \frac{1}{L} min_{A,B} \left\langle \int_a^{a+L} [N(E) - (AE + B)]^2 dE \right\rangle_a, \qquad (2.9)$$

where the constants A and B will give the best local fit to $N(E)$ in the interval $a \leq E < a + L$. The angular brackets denote an average over a, while L is the energy length of the interval. For a random Poisson spectrum (integral case) Δ_3 takes the form

$$\Delta_3^P(L) = \frac{L}{15}. \qquad (2.10)$$

For the GOE case there is an approximate expression, for large L,

$$\Delta_3^{GOE}(L) = \frac{1}{\pi^2}(logL - 0.0687). \qquad (2.11)$$

The exact expression, good for all L, is also known [86],

$$\Delta_3^{GOE}(L) = \frac{2}{L^4} \int_0^L (L^3 - 2L^2 r + r^3) \Sigma^2(r) dr. \tag{2.12}$$

It is related to the fluctuation measure of number variance, $\Sigma^2(L) = \overline{n^2(a,L)} - \overline{(n(a,L))^2}$, where $n(a,L)$ is the number of energy levels in the interval $[a, a+L]$. There is an analytic expression for $\Sigma^2(L)$ as well [86],

$$\Sigma^2(L) = \frac{2}{\pi^2} \left(ln(2\pi L) + \gamma + 1 + \frac{1}{2}(Si(\pi L))^2 - \frac{1}{2}\pi Si(\pi L) - \cos(2\pi L) \right.$$

$$\left. -Ci(2\pi L) + \pi^2 L[1 - \frac{2}{\pi}Si(2\pi L)] \right). \tag{2.13}$$

Figure 2.3 shows the form of $\Delta_3(L)$ for the GOE and the Poisson case.
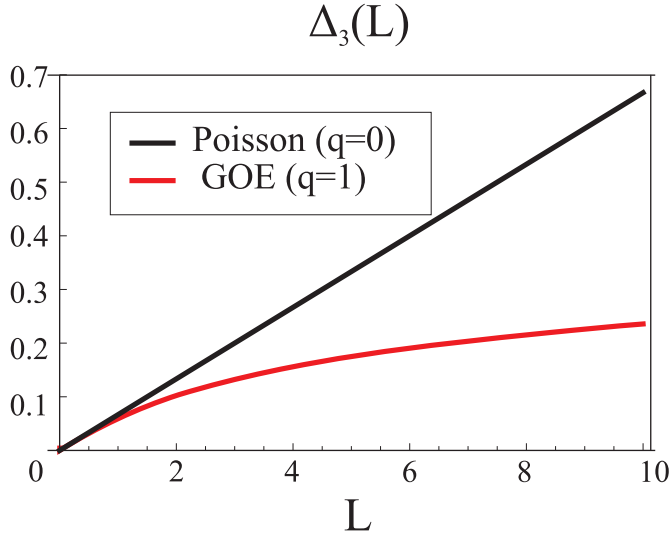
Figure 2.3: The form of the distribution of the Δ_3 statistics for the Poisson and the GOE case. q is a parameter introduced in section 2.4 which characterises the system as regular or chaotic.

2.3.3   Porter-Thomas distribution

Besides the energy level fluctuations, one can consider the fluctuations of the transition strenghts from one level of the excited nucleus to another. Porter and Thomas assumed that the transition matrix elements connecting states of the nuclear spectra, may be treated as random, identical independent variables having a Gaussian distribution centered at zero. The resulting distribution for the GOE case is the Porter-Thomas distribution [54]

$$P_{GOE}(y) = \frac{1}{\sqrt{2\pi <y>}} \frac{1}{\sqrt{y}} exp(-y/2 <y>), \tag{2.14}$$

where y is the relevant transition intensity considered, e.g $B(E0)$ or $B(E2)$. There is no universal distribution for the regular case, but one expects to see fewer transition strenghts compared to the chaotic case. It is very important, for the calculations to be correct, when one compares the Porter-Thomas distribution with data, to take into consideration the whole set of data and also to consider transitions between states of the same angular momentum. Figure 2.4 shows the form of the Porter-Thomas distribution.
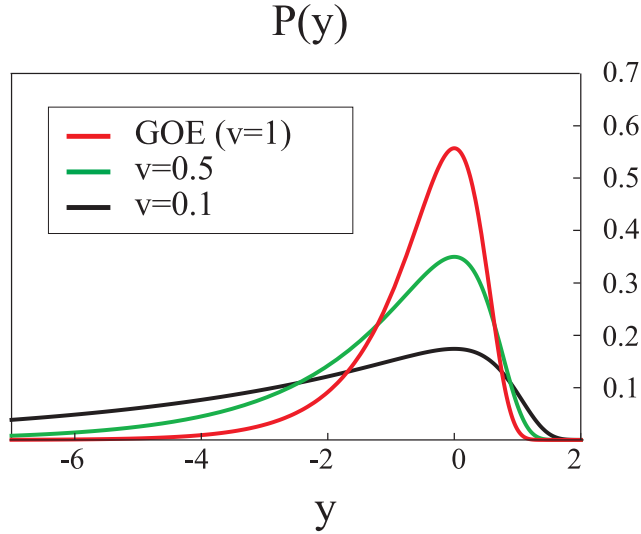
Figure 2.4: The form of the Porter-Thomas distribution for the GOE case ($\nu = 1$) and two cases with less chaos. ν is a parameter introduced in section 2.4 which characterises the system as regular or chaotic.

2.3.4 Unfolding spectra

As already mentioned in Section 2.2, the universality of the statistics is seen when the spectra is unfolded. After a measurement or a calculation, an ordered sequence of levels is produced $(E_1, E_2, \ldots, E_N)$, which form the spectrum. The spectrum has the following characteristic, the low energy levels have consistently larger spacings than the high energy ones. This is reflected in the spectral fluctuation measures, so one needs to unfold the spectra, that is to say, modify the spectrum so that the average level spacing is constant and equal to one, $\langle S \rangle = 1$.

The way unfolding is done is the following: One constructs a staircase function of the data. A staircase function is the number of levels found below some specific energy. It is called staircase, because it resembles a stair. Then, one fits a low order polynomial $N(E)$ to that function [89]. The unfolded energies, which will be called from now on, normalized energies, are found as

$$\epsilon_i = N(E_i). \tag{2.15}$$

The average level spacing of the spectrum of the normalized energies, is equal to one. At the calculation of the spectral fluctuation measures discussed before, the energies used are the normalized energies.

2.4   Quantum Statistical Parameters

The three statistics described in the previous section, have forms to describe either chaotic or regular limits. However, often, the results obtained by some calculation, have character between full chaos and integrability, so, the quantum statistical distributions produced have an intermediate form. It is obvious that it is necessary to find forms of the three relevant statistics that, with the help of some parameter, could fit, chaotic, integrable, as well as results of intermediate character.

For the nearest spacing distribution, the form of the function that could interpolate between regular and chaotic limits is the Brody distribution [45],

$$P_\omega(S) = A\,\alpha(1 + \omega)S^\omega exp(-\alpha S^{1+\omega}), \tag{2.16}$$

where A is a scaling factor and $\alpha = \Gamma[(2 + \omega)/(1 + \omega)]^{1+\omega}$. The value of ω is found by fitting (2.16) to the data by least squares. The Brody distribution takes the form of Poisson statistics when $\omega = 0$ (eq. (2.7)), which characterise a regular system and the Wigner distribution when $\omega = 1$ (eq. (2.8)), which corresponds to a chaotic system (Fig. 2.2). For intermediate cases, larger ω implies more chaos.

For the spectral rigidity, the form of the function should be [45]

$$\Delta_3^q(L) = \Delta_3^{GOE}(qL) + \Delta_3^P((1 - q)L). \tag{2.17}$$

The value of q is again found by fitting the data. For $q = 0$, one gets the regular case, $\Delta_3^P(L)$, given in eq. (2.10), while for $q = 1$, the chaotic limit emerges, given in eqs. (2.11), (2.12). For intermediate values of q the result is between 0 and 1, the behavior being closer to chaos for q closer to 1.

For the last statistic, the interpolating function is [90, 91]

$$P_\nu(y) = A\left(\frac{\nu}{2 < y >}\right)^{\nu/2} \frac{y^{\frac{\nu}{2}-1}exp(-\nu y/2 < y >)}{\Gamma\left(\frac{\nu}{2},\right)}, \tag{2.18}$$

where A is again a scaling factor. ν is found by fitting the data to the interpolating function (2.18). The expression reduces to the GOE result for $\nu = 1$. For small values of ν one expects regularity. There is no formal expression for the regular case.

Chapter 3

Measure of chaos in the IBM Hamiltonian

In this chapter, we will apply the statistical measures introduced before, in order to study the emergence of regularity among chaos, inside the symmetry triangle of the IBM. The interplay between regular and chaotic behavior in the context of the IBM, has already been studied, using both classical and quantum measures of chaos in the original work of Alhassid and Whelan [26, 27, 28, 29, 30]. However, due to calculation limitations of the code used, the authors studied quantum chaos for a smaller number of bosons ($N_B = 25$) than we will do here and for angular momentum greater than $L = 2$, in order to have good statistical significance of the results. In their study, they had found integrability at the three dynamical symmetry limits of the triangle, as well as at the $O(6) - U(5)$ side of the triangle, due to the $O(5)$ subalgebra which is common in the two symmetry limits. Away from these integrable regions, one expected to have chaotic behavior. However, the study of the interior of the symmetry triangle of the IBM led to some puzzling results. The study of Alhassid and Whelan brought to the surface a region inside the triangle where regularity is emerging among chaos [27]. Recently, this region, which is called "Alhassid–Whelan arc of regularity", was experimentally confirmed [92]. The study of the arc of regularity [93] and the symmetry underneath its existence is a subject of research [94, 95, 96]. We will deal with this in the next chapter. In this chapter we will mainly consider 0^+ states and how their eigenvalues and transition strengths behave at four different points of the Casten triangle, specifically on the $SU(3)$ vertex, a point on the arc of regularity and two points above and below the arc. A study of the 0^+ states was also done by Macek et al. [97], where they showed that the bunching pattern of 0^+ states in the Alhassid Whelan arc of regularity is similar to the pattern along the $O(6) - U(5)$ side of the triangle, implying the existence of regularity.

3.1   Numerical results

Calculations were performed at four different points, as is demonstrated in Fig. 3.1, namely on the $SU(3)$ vertex, a point on the arc having parameters $(\eta, \chi) = (0.632, -0.803)$ and at two random points at $(\eta, \chi) = (0.632, -0.7)$ and $(\eta, \chi) = (0.632, -1.1)$. The points on the arc are given by the expression $\chi(\eta) = \frac{\sqrt{7}-1}{2}\eta - \frac{\sqrt{7}}{2}$ and it was found by calculating the values of χ versus η, where σ (a measure of classical chaos) is minimized [29].
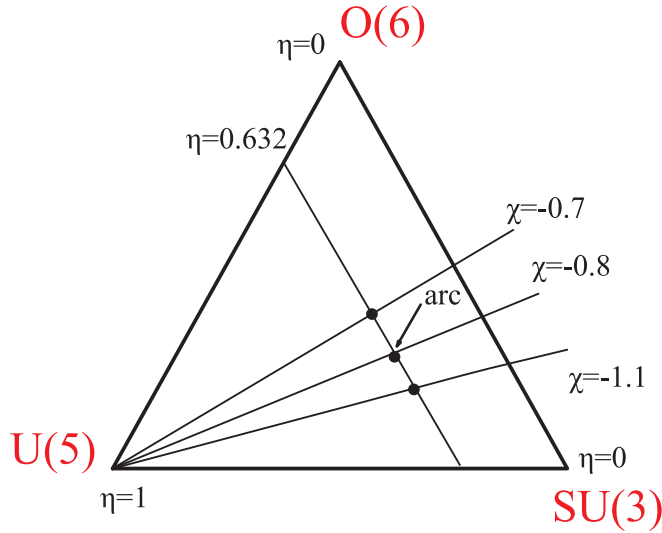
Figure 3.1: The symmetry triangle of the IBM and the four different points where calculations were performed.

In order to have good statistics, we have used $N_B = 175$ number of bosons, for the measures $P(S)$ and $\Delta_3(L)$, which produced 2640 0^+ states. For the statistical measure $P(y)$, we used $N_B = 50$ number of bosons, which produced 54756 possible transition strengths, $B(E0)$s, between the 234 0^+ states. The reason for selecting $N_B = 50$ number of bosons instead of $N_B = 175$, was that in the latter case there are more than 6000000 possible $B(E0)$s between the 2640 0^+ states, something that makes the calculation impossible to run in terms of time, while for $N_B = 50$ number of bosons, the run time is logical and the number of produced $B(E0)$s is already more than enough. The allowed $B(E0)$s differ from point to point in the symmetry trangle of the IBM and their number gets larger, as the point gets more chaotic. Figure 3.2 shows the results for the four points illustrated in Figure 3.1, for the three statistical measures $P(S)$, $\Delta_3(L)$ and $P(y)$. All three different measures of fluctuations show the same consistent results. The $SU(3)$ vertex is the more regular point, followed by the point on the arc of regularity, which appears to also have regular behavior. Then come, the points labelled $\chi = -0.7$, $\chi = -1.1$ which are indeed chaotic, with the $\chi = -0.7$ being less chaotic than the $\chi = -1.1$ point. The fitting of the interpolating function of the last statistic, $P(y)$, on the $SU(3)$ vertex

is rather poor, which reflects the fact that the expression (2.18) does not reduce to the regular case for any value of ν.
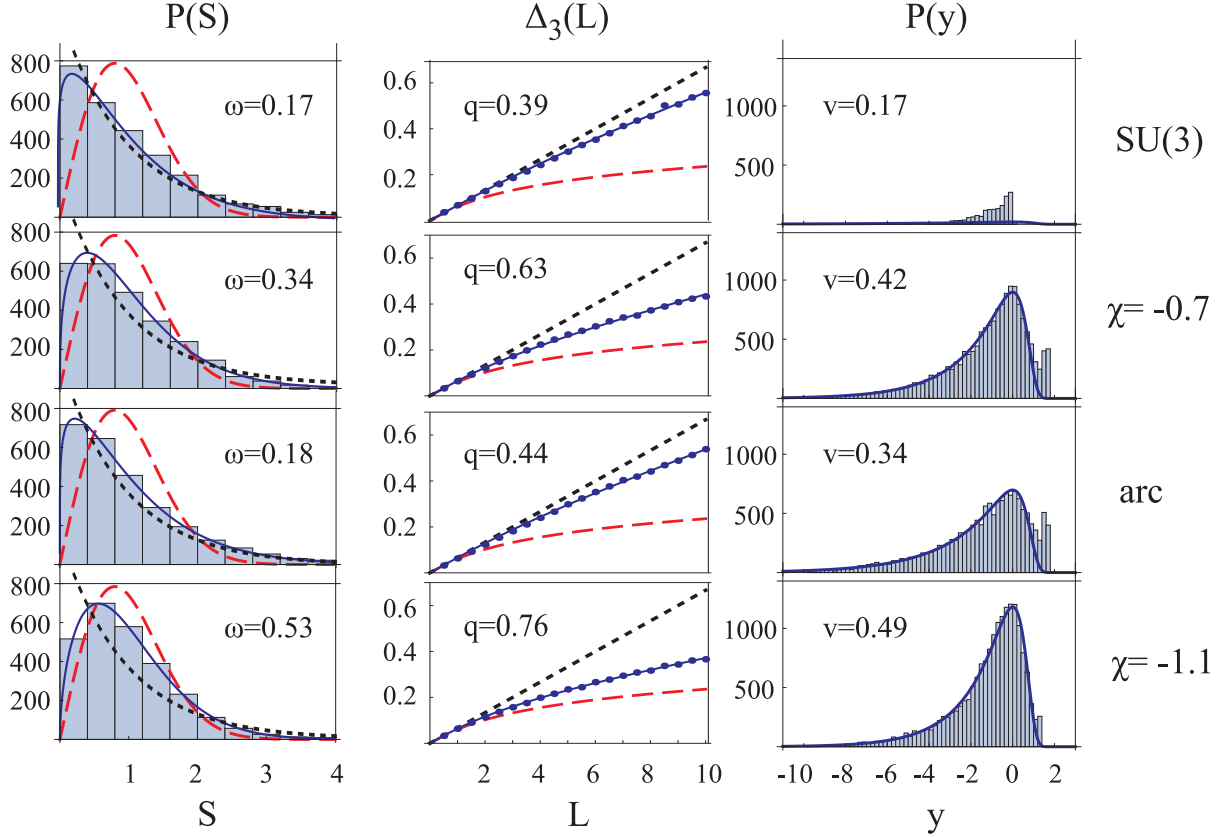
Figure 3.2: Results for the four points shown in Fig. 3.1, for $N_B = 175$ number of bosons and $L = 0$ states, using the fluctuation measures $P(S)$, $\Delta_3(L)$ and for $N_B = 50$ number of bosons and $L = 0$ states, for the fluctuation measure $P(y)$. The black line shows the regular limit, the red line describes the chaotic limit, while the blue line is the fit to the distribution. It is evident from the values of ω, q and ν, that the $SU(3)$ vertex and the point on the arc are regular compared to the other two random points above and below the arc.

3.2   Study of chaos in 0^+ states

3.2.1   Chaos in 0^+ states as a function of energy

The study of chaos as a function of energy has already been performed classically [30], but not quantum mechanically, since the small number of bosons used, produced a small number of states, which didn't allow for good statistics. For $N_B = 175$ number of bosons and $L = 0$, the number of states is 2640, so one can divide the spectrum and study each part quantum mechanically, without worrying about the statistics. In Figures 3.3 and 3.4 the spectrum is divided in 8 parts of 330 states each. The division of the spectrum in parts of equal number of states, is the same as the division of the spectrum in parts having equal energy difference, due to the normalization of the spectrum which has led to neighboring energies differing by 1. The results for ω and q are displayed in Tables 3.1 and 3.2.

The results show a surprising similarity with the expectations of the classical case and there is also consistency, once again, between the fluctuation measures. Indeed, at the low part of the spectrum (at the first interval), the results are almost the same as these expected for the whole spectrum. As the energy increases, there is a big jump, where the motion becomes chaotic, while at even larger energies the amount of chaos decreases significantly, even for the chaotic points, a behavior which is also evident for the classical results. The $SU(3)$ point, which is of course regular, seems not to follow the behavior of the other points. Indeed, if one observes the results of the $SU(3)$, these display chaos, for large energies.

The points above and bellow the arc, even if they obey at the same behavior, as the one described above, increase of chaoticity as the energy increases, decrease of chaoticity for even larger values of energy, they still have chaotic behavior spread all over the spectrum. However, chaotic behavior is confined to less intervals at the arc or the $SU(3)$ vertex.

Table 3.1: Numerical values of ω, for the 8 parts of each spectrum. The states 1-330 are labelled as interval 1, the states 2311-2640 are labelled as interval 8.

interval	SU(3)	arc	$\chi = -0.7$	$\chi = -1.1$
P(S)	ω	ω	ω	ω
1	0.30	0.26	0.51	0.54
2	0.17	0.50	0.67	0.82
3	0.14	0.31	0.67	1.02
4	0.00	0.16	0.39	0.85
5	0.06	0.10	0.18	0.54
6	0.10	0.22	0.22	0.35
7	0.14	0.04	0.23	0.18
8	0.32	0.03	0.10	0.16

Table 3.2: Numerical values of q, for the 8 parts of each spectrum. The states 1-330 are labelled as interval 1, the states 2311-2640 are labelled as interval 8.

interval	SU(3)	arc	$\chi = -0.7$	$\chi = -1.1$
$\Delta_3(L)$	q	q	q	q
1	0.01	0.43	0.67	0.86
2	0.48	0.84	0.91	0.92
3	0.52	0.57	0.79	1.94
4	0.26	0.32	0.64	0.97
5	0.40	0.27	0.37	0.77
6	0.51	0.41	0.53	0.60
7	0.54	0.002	0.53	0.45
8	0.66	0.26	0.46	0.44
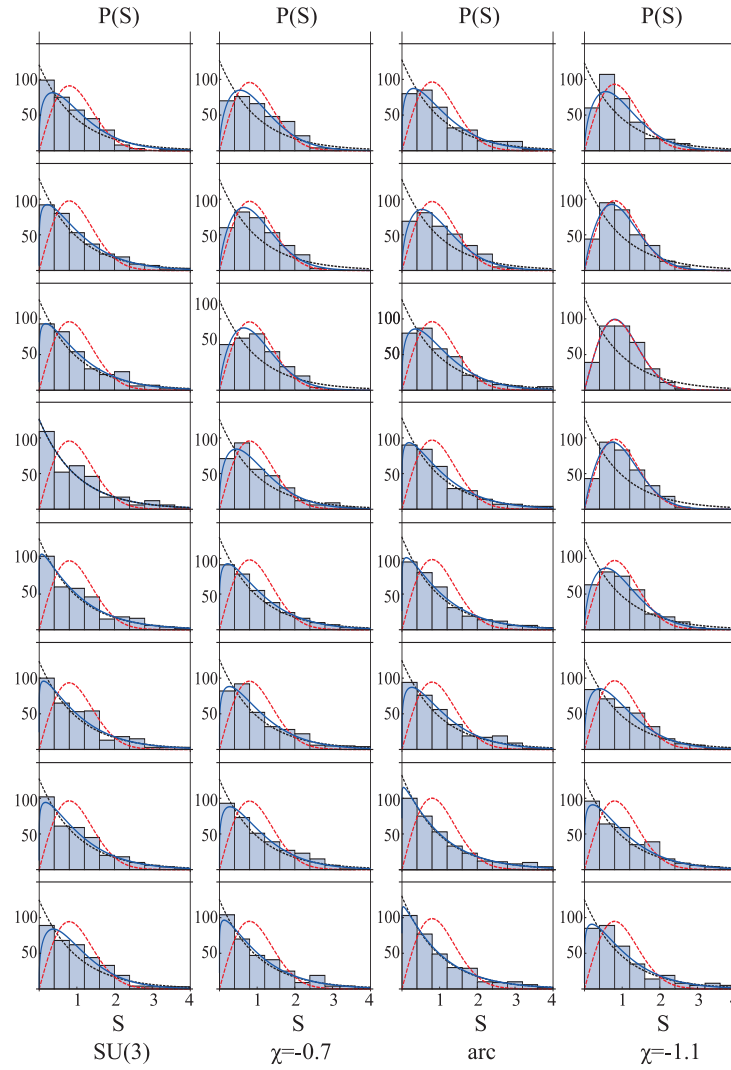
Figure 3.3: Results obtained for the nearest spacing distribution, P(S), for each of the cases shown in Fig. 3.1, for N=175 number of bosons and, when the set of $L = 0$ states is divided into 8 sets of 330 states each. The states 1-330, (labelled as interval 1 in Table 3.1) appear on the top, the states 2311-2640 (labelled as interval 8 in Table 3.1) appear at the bottom.
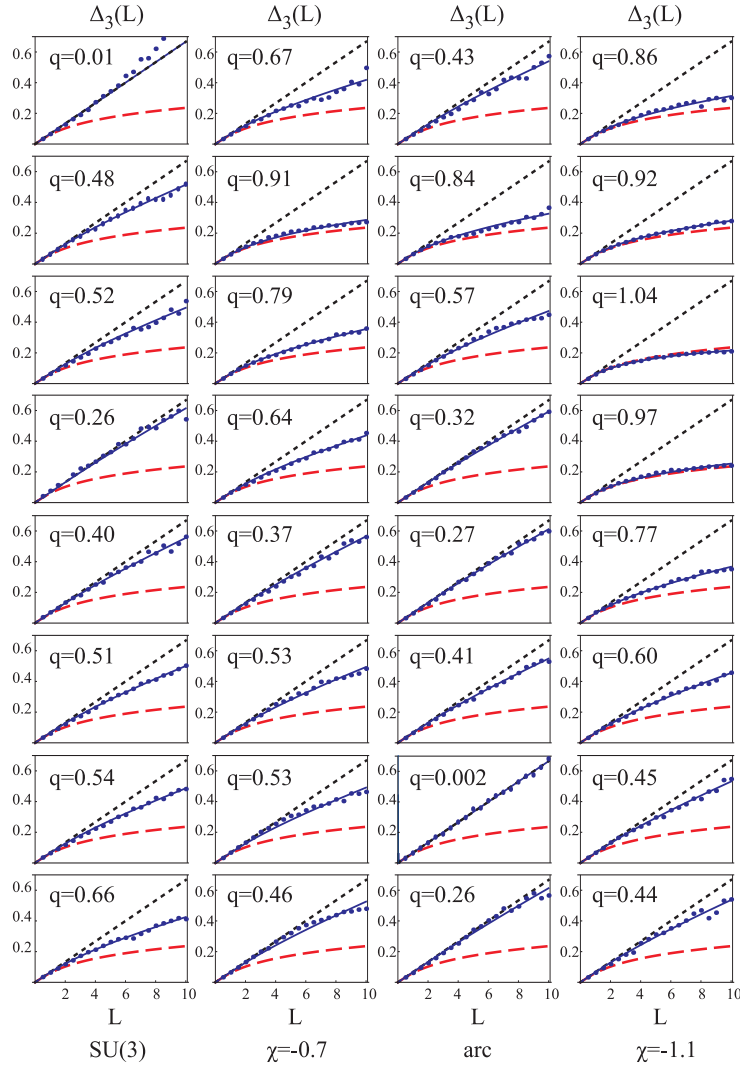
Figure 3.4: Results obtained for the spectral rigidity measure, $\Delta_3(L)$, for each of the cases shown in Fig. 3.1, for N=175 number of bosons and, when the set of $L = 0$ states is divided into 8 sets of 330 states each. The states 1-330, (labelled as interval 1 in Table 3.2) appear on the top, the states 2311-2640 (labelled as interval 8 in Table 3.2) appear at the bottom.

3.2.2   Chaos in 0^+ states as a function of the parameter χ

The results of the quantum statistical parameters, ω and q, as a function of the parameter χ, along the $\eta = 0.632$ line of the triangle are seen in Fig. 3.5. First, being on the $SU(3)$–$U(5)$ line of the triangle $((\eta, \chi) = (0.632, -1.32))$ chaotic behavior is displayed, which keeps diminishing as one reaches the arc of regularity $((\eta, \chi) = (0.632, -0.803))$, where there is a minimum. Then, as one moves to greater values of χ, chaoticity emerges again, but again gives its place to regular behavior as one reaches the $O(6)$–$U(5)$ line of the triangle $((\eta, \chi) = (0.632, 0))$, where the $O(5)$ symmetry causes integrability. These results, for the 0^+ states, are in complete agreement with the work of Alhassid and Whelan, who found the existence of the arc of regularity at the same point using $N = 25$ number of bosons and $L = 10$ angular momentum.
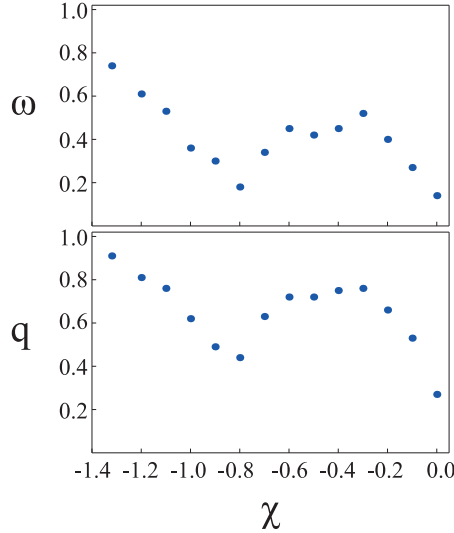
Figure 3.5: Results obtained for the quantum statistical parameters ω and q, for various values of χ along the $\eta = 0.632$ line of the triangle. The calculations were performed for $N = 175$ number of bosons and $L = 0$.

3.2.3   Chaos in 0^+ states as a function of the number of bosons N

The results of the quantum statistical parameters, ω and q, as a function of the number of bosons N are seen in Fig. 3.6. The first observation one can make, is that there is a quick drop of the values of the measured quantum statistical parameters as the number of bosons N increases, while for much larger values of N (larger than $N = 175$ bosons), the drop is very small and the quantum statistical parameters seem to have reached steady values. The reason for this drop, at small values of bosons, is that the number of states is small compared to larger values of bosons, something that affects the statistical results. For example, at $N = 25$ there

are only 65 number of states, while for $N = 175$ there are 2640 number of states, so statistical analysis of eigenvalues has more value at the second case. The second observation, is that despite the, large or much smaller, drop of quantum statistical parameters, as the number of bosons N increases, the point on the arc always has the least values compared with the other two points $\chi = -0.7$ and $\chi = -1.1$ and the point $\chi = -0.7$ is always less chaotic than $\chi = -1.1$. So, as the number of bosons increases, the arc of regularity survives and is stable when changing N.
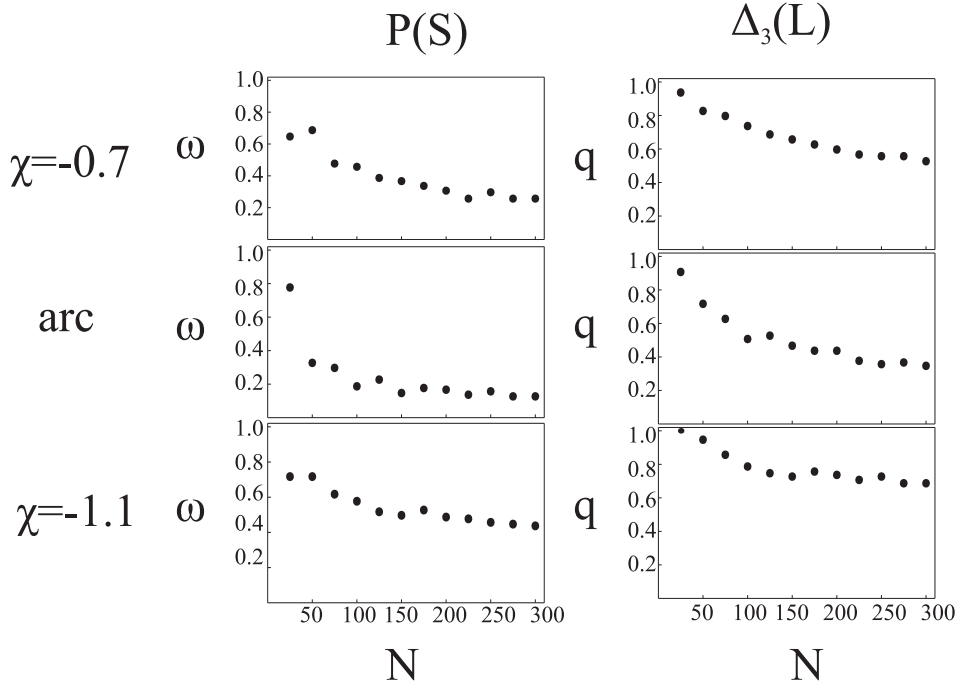
Figure 3.6: Results obtained for the quantum statistical parameters ω and q, for various values of N at the three points mentioned before inside Casten's triangle.

3.3 Study of chaos in the $BE0$ intensities

In addition to the spectral fluctuations, the transition from chaos to regularity and vice versa, can be studied using transition intensities, whose statistical fuctuations provide an equally sensitive measure of chaos. In this section the $B(E0)$ intensities are analysed using the statistical measure $P(y)$.

3.3.1 Chaos in the $BE0$ intensities as a function of the parameter χ

The results of the quantum statistical parameter ν, as a function of the parameter χ, along the $\eta = 0.632$ line of the triangle are seen in Fig. 3.7. For these calculations

we used $N_B = 50$ number of bosons, which gave 54756 $BE0$s between the 234 0^+ states.

The results show the same general behavior, as these of the statistics of the eigenvalues of the 0^+ states. Once again the regularity of the point on the arc is made evident from the minimum of the curve at $\chi = -0.8$. Chaotic behavior is encountered at the regions before and after the arc of regularity, while at the $O(6)$–$U(5)$ line of the triangle $((\eta, \chi) = (0.632, 0))$, regularity emerges again. The study of chaoticity of the $BE0$ intensities distribution gives results which are in complete agreement with the study of chaoticity of the $BE2$ intensities distribution of the work of Alhassid and Whelan.
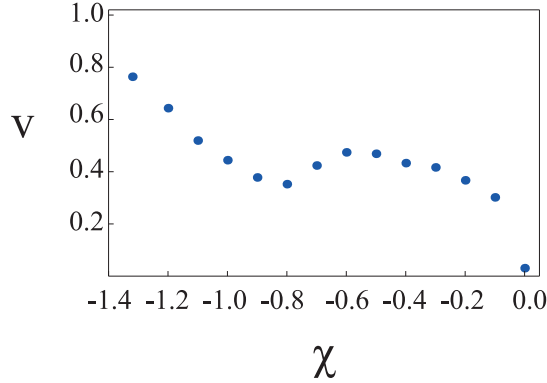

Figure 3.7: Results obtained for the quantum statistical parameter ν, for various values of χ along the $\eta = 0.632$ line of the triangle. The calculations were performed for $N = 50$ number of bosons and $L = 0$.

3.3.2   Chaos in the $B(E0)$ intensities as a function of energy

The study of chaos in the $B(E0)$ intensities as a function of energy was done in the following way. The 234 0^+ states were divided into 7 parts of 30 states each and one part of 24 states. For the first 30 0^+ states, the statistical measure $P(y)$ was applied to the $B(E0)$ intensities, produced by these 30 0^+ states, the same for the next 30 0^+ states and so on. The results are displayed in Table 3.3. The $SU(3)$ point is missing from the Table. As already mentioned, points possessing some dynamical symmetry, as the SU(3) point which is characterized by regularity, have a smaller number of $B(E0)$ intensities compared to other points characterized by chaotic dynamics. In addition to the great dispersion of these few $B(E0)$ intensities, the study of chaos as a function of energy at the $SU(3)$ limit, using $N_B = 50$ number of bosons, was impossible statistically.

At the low part of the spectrum (at the first interval), the statistics of the $B(E0)$ intensities show intermediate chaoticity, which is increased as the energy increases. At even larger energies, the amount of chaos decreases significantly, even for the chaotic points. The points above and bellow the arc, show more chaotic behavior,

compared to the point on the arc, in all the energy intervals. The point $\chi = -1.1$ is definitely more chaotic than the other two points.

The most fascinating observation though, is that both the statistics of the $B(E0)$ intensities and those of eigenvalues, show consistency in the degree of chaos as a function of energy. In all cases, there is a jump in the degree of chaoticity as one passes the low part of the spectum, which is replaced by regularity as one gets at the upper part of the spectrum. These results are in accordance with those found in [94], where the authors, using spectral lattices, observed that regularity is not restricted to low energies, but is found also in high energies.

Table 3.3: Numerical values of ν, for the 8 parts of each spectrum. The states 1-30 are labelled as interval 1, the states 211-234 are labelled as interval 8.

interval	arc	$\chi = -0.7$	$\chi = -1.1$
P(y)	ν	ν	ν
1	0.40	0.62	0.44
2	0.48	0.81	0.84
3	0.39	0.60	0.87
4	0.32	0.49	0.77
5	0.29	0.35	0.54
6	0.23	0.26	0.37
7	0.21	0.21	0.30
8	0.21	0.27	0.22
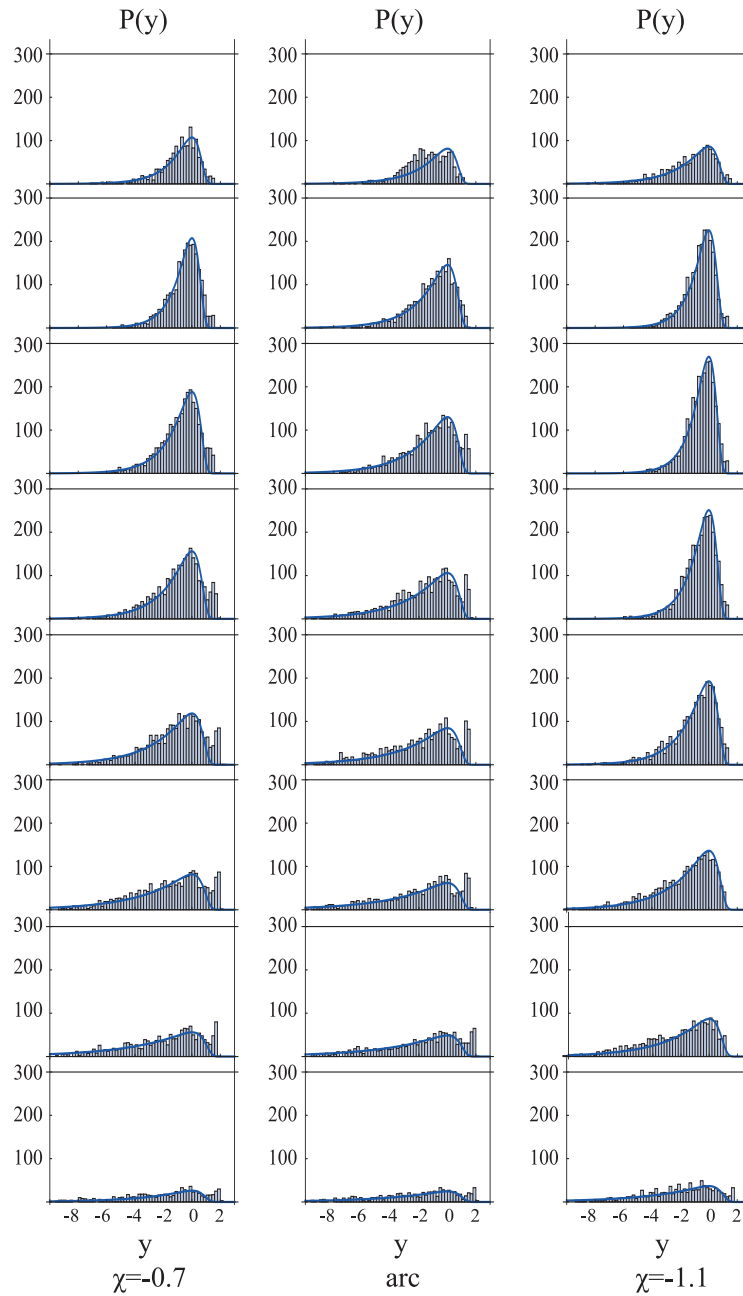
Figure 3.8: Results obtained for the statistical measure, $P(y)$, for each of the cases shown in Fig. 3.1, for N=50 number of bosons and, when the set of 234 $L = 0$ states is divided into 7 sets of 30 states and one set of 24 states. The states 1-30, (labelled as interval 1 in Table 3.3) appear on the top, the states 211-234 (labelled as interval 8 in Table 3.3) appear at the bottom.

Chapter 4

Analytic derivation of an approximate SU(3) symmetry inside the symmetry triangle of the IBM

In the previous chapter we studied the emergence of regularity among chaos inside the symmetry triangle of the IBM, by applying statistical measures of chaos at points around the arc of regularity. As already mentioned, the arc of regularity is a semiregular region inside the symmetry triangle, found by Alhassid and Whelan [98, 99], using both classical and quantum measures of chaos, whose underlying symmetry was unknown.

The authors of [100] have used the notion of wave-function entropy, to quantify the departure of transitional IBM-1 Hamiltonians from the particular dynamical symmetries of the model. (In the context of IBM-1, the wave-function entropy is a measure that quantifies the eigenstate localisation of a particular transitional IBM-1 Hamiltonian in a given dynamical symmetry basis. Chaos is established as the degree of eigenstate localisation in the given dynamical symmetry basis decreases.) They have found that on the arc of regularity, there is indeed an increased localisation in the symmetry bases. However, they couldn't give an explanation of this behavior. From the empirical point of view, it has been found [92] that the line corresponding to the degeneracy of the β_1 and γ_1 bandheads ($2^+_{\gamma_1} = 0^+_{\beta_1}$) closely follows the arc of regularity and 12 nuclei closely exhibiting this behavior have been located. Recently, it has been realized [101] that the locus of the $2^+_{\gamma_1} = 0^+_{\beta_1}$ degeneracy closely follows the line of change of stability of γ vibrations at low energies.

The presence of (near) regularity presupposes the existence of some underlying (approximate) symmetry. From the extensive analysis of the low part of the spectrum in [95], it was suggested that the underlying symmetry of the arc is an SU(3)-QDS. A hallmark of SU(3) is the degeneracies between the levels of the β band and those, with the same even L, of the γ band. The authors, by keeping η constant and varying χ, they tried to find the point where $E(2^+_\beta) = E(2^+_\gamma)$. With

39

this procedure they found a locus of points where not only the $E(2_\beta^+) = E(2_\gamma^+)$ condition was met, but at this locus simultaneously one also had $E(L_\beta^+) = E(L_\gamma^+)$, that is the same degeneracies that characterise SU(3). Also, not only the β and γ bands, but all low lying bands had the same degeneracies as in SU(3), to an excellent approximation. This locus of points lies very close to the arc and for N=250 it ranges from $(\eta, \chi) \sim$ (0.8, -0.5) to (0, -1.32) at SU(3), with weak dependence on N, except near the coexistence region [102] (separating spherical from prolate deformed shapes). This result extends the notion of quasidynamical symmetry (QDS), originally introduced [103, 104, 105, 106, 107] for describing the persistence of limiting symmetries along the U(5)-O(6) and U(5)-SU(3) legs of the IBA, to the interior of the triangle. The domain of validity of the SU(3) QDS inside the IBA symmetry triangle has also been considered by mean field techniques [108]. The analysis of Ref. [95] was limited to the low-lying part of the spectrum, while regularity in the midst of chaoticity was discovered by Alhassid and Whelan and was studied in the previous section, through the study of the whole spectrum [98, 99]. The properties of high-lying rotational bands built on axially deformed ground states have been studied recently [109] in the IBA, showing signatures of an SU(3) QDS extending to the highest part of the IBA spectrum. The authors have studied the occurence of rotational bands at low, intermediate and high energy domains and how this is related with the appearence of regularity. They have found that the regular part of the spectrum is inhabited by SU(3)-like rotational bands. At the arc of regularity they found increased regularity, even for the highest accessible energies $E \approx E_{max}$, accompanied by the highest occurence of rotational bands.

In the present chapter, we will analytically derive a line of approximate SU(3) symmetry inside the symmetry triangle of the IBM. The derivation of the line is based on this idea: In order to have an SU(3) symmetry, the IBM Hamiltonian has to commute with the generators of SU(3). The line will be extracted by the study of Hamiltonians that, in the large-boson-limit of the IBA, approximately commute with the SU(3) generators. The analytical identification of an approximate symmetry takes advantage of the well known contraction [110] of the SU(3) algebra to the $[R^5]$SO(3) algebra [111, 112]. Furthermore, using the contraction of O(6) to the $[R^5]$SO(5) algebra [113, 114] of the γ-unstable rotator, we prove that no line related to the O(6) symmetry exists in the triangle. For a detailed analysis of the İnőnű - Wigner contraction method and the analytic derivation of the contractions of the SU(3) algebra to the $[R^5]$SO(3) algebra and the O(6) to the $[R^5]$SO(5) algebra, the reader is referred to the appendices E, F, G.

4.1   The SU(3) symmetry

In this section we will try to find the locus of points where the IBA Hamiltonian commutes with the generators of SU(3). For convenience the IBA Hamiltonian is given again

$$\hat{H}(\eta, \chi) = \hat{H}_1 + \hat{H}_2 = c\left[\eta\hat{n}_d - \frac{\eta-1}{N}\hat{Q}_\chi^{(2)} \cdot \hat{Q}_\chi^{(2)}\right], \tag{4.1}$$

where the operators $\hat{n}_d$ and $\hat{Q}_\chi^{(2)}$ are given by

$$\hat{n}_d = d^\dagger \cdot \tilde{d} = \sqrt{5}(d^\dagger\tilde{d})^{(0)}, \tag{4.2}$$

$$\hat{Q}_{\chi,\xi}^{(2)} = (s^\dagger\tilde{d} + d^\dagger s)_\xi^{(2)} + \chi(d^\dagger\tilde{d})_\xi^{(2)}. \tag{4.3}$$

The SU(3) algebra [6] is generated by the angular momentum operators

$$\hat{L}_\xi = \sqrt{10}(d^\dagger\tilde{d})_\xi^{(1)}, \tag{4.4}$$

and the quadrupole operators

$$\hat{Q}_{SU(3),\xi}^{(2)} = (s^\dagger\tilde{d} + d^\dagger s)_\xi^{(2)} - \frac{\sqrt{7}}{2}(d^\dagger\tilde{d})_\xi^{(2)}. \tag{4.5}$$

4.1.1 Commutation relations

The first step is to see whether the Hamiltonian commutes with the angular momentum operators, $\hat{L}_\xi$. The Hamiltonian does commute with $\hat{L}_\xi$, by construction. The next step is to examine the special conditions under which the Hamiltonian also commutes (approximately) with the quadrupole operators. In order to calculate the commutation relations, a special expression is used, found in [6], Eq. (2.6) or in [15], Eq. (7.51). The products of boson creation ($b_l^\dagger$) and annihilation ($\tilde{b}_{l'}$) operators are written in coupled form, as

$$G_\kappa^{(k)}(l, l') = [b_l^\dagger \times \tilde{b}_{l'}]_\kappa^{(k)}, \qquad (l, l' = 0, 2). \tag{4.6}$$

For reasons of convenience, usually the symbol $\times$ is omitted and the brackets are replaced by parentheses, so one has, $G_\kappa^{(k)}(l, l') = (b_l^\dagger\tilde{b}_{l'})_\kappa^{(k)}$. Then, the commutation relations of the operators of Eq. (4.6) are

$$[G_\kappa^{(k)}(l, l'), G_{\kappa'}^{(k')}(l'', l''')] = \sum_{k'', \kappa''} \sqrt{(2k+1)(2k'+1)}(k\kappa k'\kappa'|k''\kappa'')(-1)^{k-k'}$$

$$\left[(-1)^{k+k'+k''}\begin{Bmatrix} k & k' & k'' \\ l''' & l & l' \end{Bmatrix}\delta_{l'l''}G_{\kappa''}^{(k'')}(l, l''') - \begin{Bmatrix} k & k' & k'' \\ l'' & l' & l \end{Bmatrix}\delta_{ll'''}G_{\kappa''}^{(k'')}(l'', l')\right]. \tag{4.7}$$

The commutation relations needed for this task, as well as some examples of calculating commutation relations are listed in the appendix B. The commutator of the first term of the Hamiltonian with the quadrupole operators gives

$$[\hat{H}_1, \hat{Q}_{SU(3),\nu}^{(2)}] = c\eta[\hat{n}_d, \hat{Q}_{SU(3),\nu}^{(2)}] = c\eta(d^\dagger s - s^\dagger\tilde{d})_\nu^{(2)}. \tag{4.8}$$

For the commutator of the second term of the Hamiltonian with the quadrupole operators,

$$[\hat{H}_2, \hat{Q}^{(2)}_{SU(3),\nu}] = c\frac{\eta - 1}{N}[\hat{Q}^{(2)}_\chi \cdot \hat{Q}^{(2)}_\chi, \hat{Q}^{(2)}_{SU(3),\nu}], \tag{4.9}$$

one rewrites the scalar product $\hat{Q}^{(2)}_\chi \cdot \hat{Q}^{(2)}_\chi$ as ([6], Eq. (1.14))

$$\hat{Q}^{(2)}_{\chi,\xi} \cdot \hat{Q}^{(2)}_{\chi,\xi} = \sum_\xi (-1)^\xi \, \hat{Q}^{(2)}_{\chi,\xi} \, \hat{Q}^{(2)}_{\chi,-\xi} \tag{4.10}$$

and also uses the

$$\hat{Q}^{(2)}_{\chi,\xi} = \hat{Q}^{(2)}_{SU(3),\xi} + \left(\chi + \frac{\sqrt{7}}{2}\right)(d^\dagger \tilde{d})^{(2)}_\xi \tag{4.11}$$

and of course,

$$\hat{Q}^{(2)}_{\chi,-\xi} = \hat{Q}^{(2)}_{SU(3),-\xi} + \left(\chi + \frac{\sqrt{7}}{2}\right)(d^\dagger \tilde{d})^{(2)}_{-\xi} \tag{4.12}$$

in order to get the intermediate result

$$[\hat{Q}^{(2)}_\chi \cdot \hat{Q}^{(2)}_\chi, \hat{Q}^{(2)}_{SU(3),\nu}] = \sum_\xi (-1)^\xi \left\{ [\hat{Q}^{(2)}_{SU(3),\xi}, \hat{Q}^{(2)}_{SU(3),\nu}]\hat{Q}^{(2)}_{\chi,-\xi} + \hat{Q}^{(2)}_{\chi,\xi}[\hat{Q}^{(2)}_{SU(3),-\xi}, \hat{Q}^{(2)}_{SU(3),\nu}] \right.$$

$$\left. + \left(\chi + \frac{\sqrt{7}}{2}\right) \left\{ [(d^\dagger \tilde{d})^{(2)}_\xi, \hat{Q}^{(2)}_{SU(3),\nu}]\hat{Q}^{(2)}_{\chi,-\xi} + \hat{Q}^{(2)}_{\chi,\xi}[(d^\dagger \tilde{d})^{(2)}_{-\xi}, \hat{Q}^{(2)}_{SU(3),\nu}] \right\} \right\}. \tag{4.13}$$

By calculating explicitly the commutators of (4.13) and by using the tensor product

$$[T^{(k_1)} \times T^{(k_2)}]^{(k)}_q = \sum_{q_1=-k_1}^{k_1} \sum_{q_2=-k_2}^{k_2} <k_1 q_1 k_2 q_2 | kq> T^{(k_1)}_{q_1} T^{(k_2)}_{q_2}, \tag{4.14}$$

(for details on the calculation see appendix D), equation (4.13) can be rewritten in the form

$$[\hat{Q}^{(2)}_\chi \cdot \hat{Q}^{(2)}_\chi, \hat{Q}^{(2)}_{SU(3),\nu}] = \frac{3\sqrt{15}}{4}[((d^\dagger \tilde{d})^{(1)}\hat{Q}^{(2)}_x)^{(2)}_\nu - (\hat{Q}^{(2)}_x(d^\dagger \tilde{d})^{(1)})^{(2)}_\nu]$$

$$+ \left(\chi + \frac{\sqrt{7}}{2}\right)[((d^\dagger s - s^\dagger \tilde{d})^{(2)}\hat{Q}^{(2)}_\chi)^{(2)}_\nu + (\hat{Q}^{(2)}_\chi(d^\dagger s - s^\dagger \tilde{d})^{(2)})^{(2)}_\nu]$$

$$+ \left(\chi + \frac{\sqrt{7}}{2}\right) \sum_{k=1,3} \sqrt{35(2k+1)} \begin{Bmatrix} 2 & 2 & k \\ 2 & 2 & 2 \end{Bmatrix} [((d^\dagger \tilde{d})^{(k)}\hat{Q}^{(2)}_\chi)^{(2)}_\nu - (\hat{Q}^{(2)}_\chi(d^\dagger \tilde{d})^{(k)})^{(2)}_\nu].$$

$$\tag{4.15}$$

In order to obtain the conditions under which the Hamiltonian of Eq. (4.1) commutes with the generators of SU(3), we exploit a simplification of Eq. (4.13) that occurs in the large-N limit. In this limit, the eigenvalue expression for the second-order Casimir of SU(3) [see Eq. (77)] reduces to just the λ^2 term for SU(3)-irreducible representations (irreps) (λ, μ) with $\lambda >> \mu$. Then, the ground state

band, which belongs to the (2N,0) irrep, becomes energetically isolated from all the other excitations. This situation is formally known as the contraction of SU(3) to $R^5[SO(3)]$ [111, 112] and it occurs when the $Q^{(2)}_{SU(3)}$ operators are replaced by quantities that are mutually commuting. (For a detailed explanation, see in appendix F the discussion leading to Eq. (80).) If the $Q^{(2)}_{SU(3)}$ operators can be approximated by mutually commuting quantities, Eq. (4.13) and Eq. (4.15) greatly simplify.

In the large-N limit, where contraction occurs, the commutators in the first two terms in Eq. (4.13) vanish. Also, the first term of Eq. (4.15) vanishes as well, as it comes from these commutators. This can be better justified, since, in the large-N limit, the vanishing of the commutator

$$[\hat{Q}^{(2)}_{SU(3),\xi}, \hat{Q}^{(2)}_{SU(3),\nu}] = \frac{15}{4}(2\xi 2\nu|1\xi + \nu)(d^\dagger \tilde{d})^{(1)}_{\xi+\nu} \tag{4.16}$$

implies that the terms containing $(d^\dagger \tilde{d})^{(1)}$ can be ignored. This fact can be understood qualitatively as a consequence of the relevant dominance of s bosons over d bosons within the ground-state band, especially for relatively low-lying states in the large boson number limit.

Another simplification that occurs in the large-N limit is that the terms containing $(d^\dagger \tilde{d})^{(k)}$ can be omitted. Furthermore, $\hat{Q}^{(2)}_\chi$ can be replaced by $\hat{Q}^{(2)}_{SU(3)}$, since, as seen from Eq. (4.11), they differ by the terms $(d^\dagger \tilde{d})^{(2)}$, which are small. In addition, in this limit, $\hat{Q}^{(2)}_{SU(3)}$ can be replaced by the intrinsic quadrupole moment, which is a scalar, which is $N\sqrt{2}$ in the present case (see appendix F). This result is perhaps familiar in the context of the well-known property of SU(3), that $B(E2 : 2^+_1 \to 0^+_1)$ increases with N^2 [6]-that is the collectivity of yrast transition strengths increases quadratically with boson number. Then, in the large-N limit, one is left with

$$[\hat{Q}^{(2)}_\chi \cdot \hat{Q}^{(2)}_\chi, \hat{Q}^{(2)}_{SU(3),\nu}] = 2\sqrt{2}N\left(\chi + \frac{\sqrt{7}}{2}\right)(d^\dagger s - s^\dagger \tilde{d})^{(2)}_\nu. \tag{4.17}$$

So, in the large-N limit, the commutator for the second part of the Hamiltonian reads

$$[\hat{H}_2, \hat{Q}^{(2)}_{SU(3),\nu}] = c(\eta - 1)2\sqrt{2}\left(\chi + \frac{\sqrt{7}}{2}\right)(d^\dagger s - s^\dagger \tilde{d})^{(2)}_\nu. \tag{4.18}$$

In total, the commutator of the first and the second part of the Hamiltonian with the quadrupole operators gives

$$\begin{aligned}[\hat{H}, \hat{Q}^{(2)}_{SU(3),\nu}] &= [\hat{H}_1 + \hat{H}_1, \hat{Q}^{(2)}_{SU(3),\nu}] \\ &= \left(c\eta + c(\eta - 1)2\sqrt{2}\left(\chi + \frac{\sqrt{7}}{2}\right)\right)(d^\dagger s - s^\dagger \tilde{d})^{(2)}_\nu. \end{aligned} \tag{4.19}$$

In order to get a vanishing commutator, the coefficients should cancel, leading in the large-N limit to the condition

$$\chi(\eta) = \frac{1}{2\sqrt{2}} \frac{\eta}{(1 - \eta)} - \frac{\sqrt{7}}{2}. \qquad (4.20)$$

When χ takes values between $-\sqrt{7}/2$ and 0, the parameter η takes values between 1 and 0.789. From the formulas reported in Ref. [92] and [115] it is clear that the critical line in the large-N limit corresponds to $\eta_{crit} = 0.8$ for $\chi = 0$ and to $\eta_{crit} = 9/11 = 0.818$ for $\chi = -\sqrt{7}/2$. Thus, the line described by Eq. (4.20) cannot reach the critical line, confined in the region between the critical line and the SU(3) vertex.

It should be reminded that the arc of regularity found in Refs. [27, 29] has been approximately described in Ref. [93]:

$$\chi(\eta) = \frac{\sqrt{7} - 1}{2} \eta - \frac{\sqrt{7}}{2}. \qquad (4.21)$$

The similarity between the lines described in Eqs. (4.20) and (4.21) can be seen in Fig. 4.1. Indeed, the two equations give very similar predictions for values of η between 0 and 0.6 - that is, from the SU(3) vetrex until quite close to the critical line.
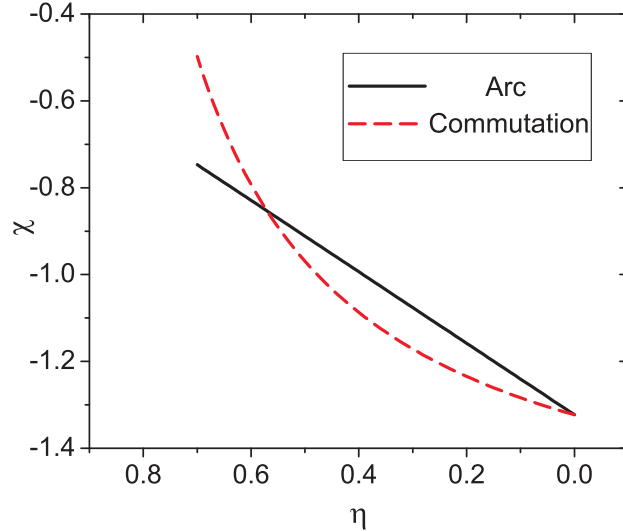
Figure 4.1: Location of the arc of regularity, as described by the original Eq. (4.21) and as predicted by the findings of the present work, Eq. (4.20). The η axis has been reversed, in order to correspond directly to Fig. 4.2.

The symmetry triangle of IBA in the Alhassid-Whelan parametrization is shown in Fig. 4.2(a), together with the arc corresponding to Eq. (4.21) and the line of Eq. (4.20). The degeneracy line corresponding to $E(2_\beta^+) = E(2_\gamma^+)$, found in Ref. [95], is also shown (to the right of the critical line) for comparison.

We see that the present line remains very close to both the $E(2_\beta^+) = E(2_\gamma^+)$ degeneracy line and the original arc line from the SU(3) vertex till quite close to the

critical region, where both the $E(2_\beta^+) = E(2_\gamma^+)$ degeneracy line and the present line turn upward, avoiding meeting the critical line.

In Figs. 4.2(b) and 4.2(c), the ν and $\overline{\lambda}$ (ν is the quantum statistical parameter introduced in Section 2.4 and $\overline{\lambda}$ is the average leading Lyapunov exponent, used to quantify the degree of classical chaos) diagrams are reproduced from Ref. [29], with the lines of Fig. 4.2(a) plotted in them. We see that the present line remains within the valley corresponding to the arc of regularity for most of the way from the SU(3) vertex toward the critical line, turning upward a little before reaching the critical line.

It should be noted that the present study is greatly facilitated by the fact that the position of the arc of regularity appears to be practically independent of the number of bosons, as already seen numerically in the previous chapter, using quantum statistical measures of chaos and as already remarked in Refs. [27, 29] and corroborated in Ref. [95].

In summary, we have achieved by now two goals:

(1) To prove analytically the existence of a line in the parameter space of the IBA, along which the Hamiltonian approximately commutes with the SU(3) generators in the large-N limit.

(2) To prove that this line closely follows the Alhassid-Whelan arc of regularity in the region between the SU(3) vertex and the critical line of the first-order shape/phase transition.
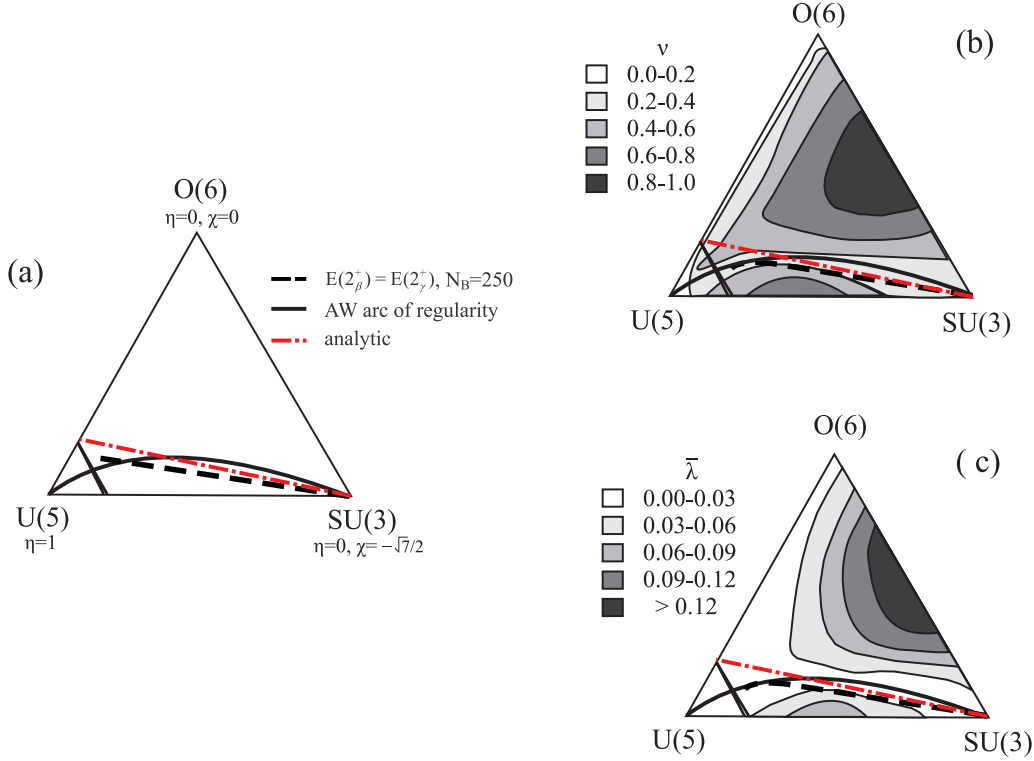
Figure 4.2: The IBA symmetry triangle in the parametrization of Eq. (4.1), with the three dynamical symmetries, the Alhassid-Whelan arc of regularity, Eq. (4.21) and the present line of Eq. (4.20) labeled as analytic. The shape coexistence region between spherical and deformed shapes is shown by slanted lines, near the U(5) vertex. In addition, the loci of the degeneracies $E(2_\beta^+) = E(2_\gamma^+)$ is shown, which is the black dashed line on the right, corresponding to the SU(3) quasidynamical symmetries discussed in Ref. [95]. In panels (b) and (c), the ν and $\bar{\lambda}$ diagrams, respectively, are shown, based on Ref. [99].

4.2   The $\overline{\mathrm{SU(3)}}$ symmetry

The question is now raised about what happens in the triangle formed by U(5), O(6), and $\overline{\mathrm{SU(3)}}$ [6]– the latter of which is the algebra containing the quadrupole operators with $\chi = +\sqrt{7}/2$, which is known to correspond to oblate nuclei, while SU(3) is related to prolate nuclei.

It turns out that the relevant calculation follows the same steps, with two notable differences:

1) $-\sqrt{7}/2$ is replaced by $+\sqrt{7}/2$ everywhere.

2) The intrinsic quadrupole moment changes sign (see Appendix BBB), in agreement to the well known fact that the intrinsic quadrupole moment has positive values for prolate nuclei and negative values for oblate nuclei [14].

As a result of these two changes, Eq. (4.20) takes the form

$$\chi(\eta) = -\frac{1}{2\sqrt{2}}\frac{\eta}{1-\eta} + \frac{\sqrt{7}}{2}. \tag{4.22}$$

It then becomes clear that for a given η, in this case χ acquires the opposite value from the one it gets within the U(5)-O(6)-SU(3) triangle. This is in agreement with the well known fact that properties within the U(5)-O(6)-$\overline{\text{SU(3)}}$ triangle are mirror images of the properties appearing within the U(5)-O(6)-SU(3) triangle [6].

4.3 The O(6) symmetry

The successful determination of a line in the symmetry triangle characterized by approximate SU(3) symmetry raises the question of whether a similar line related to the O(6) symmetry can be determined. The O(6) algebra [6] is generated by the angular momentum operators of Eq. (4.4) and the operators $(d^\dagger \tilde{d})^{(3)}_\xi$, which together form the O(5) subalgebra, plus the quadrupole operators

$$\hat{Q}^{(2)}_{O(6),\xi} = (s^\dagger \tilde{d} + d^\dagger s)^{(2)}_\xi. \tag{4.23}$$

Following the same procedure as in Section 3, we are going to examine the conditions under which the Hamiltonian commutes with the generators of the O(6) algebra. The needed commutation relations are listed in appendix B. We already know that the angular momentum operators of Eq. (4.4) commute with the Hamiltonian, so we will proceed with the calculation of the commutator of the Hamiltonian with the quadrupole operators of Eq. (4.23). We shall leave for the next section the commutator of the Hamiltonian with the $(d^\dagger \tilde{d})^{(3)}_\xi$ operators.

4.3.1 Commutation relations

The first term of the Hamiltonian gives

$$[\hat{H}_1, \hat{Q}^{(2)}_{O(6),\nu}] = c\eta[\hat{n}_d, \hat{Q}^{(2)}_{O(6),\nu}] = c\eta[(d^\dagger s - s^\dagger \tilde{d})]^{(2)}_\nu, \tag{4.24}$$

which is similar to Eq. (4.8).

Using

$$\hat{Q}^{(2)}_{\chi,\xi} = \hat{Q}^{(2)}_{O(6),\xi} + \chi(d^\dagger \tilde{d})^{(2)}_\xi, \tag{4.25}$$

in the second term of the Hamiltonian, one gets the intermediate result

$$[\hat{Q}^{(2)}_\chi \cdot \hat{Q}^{(2)}_\chi, \hat{Q}^{(2)}_{O(6),\nu}] = \sum_\xi (-1)^\xi \left\{ [\hat{Q}^{(2)}_{O(6),\xi}, \hat{Q}^{(2)}_{O(6),\nu}]\hat{Q}^{(2)}_{\chi,-\xi} + \hat{Q}^{(2)}_{\chi,\xi}[\hat{Q}^{(2)}_{O(6),-\xi}, \hat{Q}^{(2)}_{O(6),\nu}] \right.$$

$$\left. + \chi \left\{ [(d^\dagger \tilde{d})^{(2)}_\xi, \hat{Q}^{(2)}_{O(6),\nu}]\hat{Q}^{(2)}_{\chi,-\xi} + \hat{Q}^{(2)}_{\chi,\xi}[(d^\dagger \tilde{d})^{(2)}_{-\xi}, \hat{Q}^{(2)}_{O(6),\nu}]. \right\} \right\} \tag{4.26}$$

Eq. (4.26) can be rewritten, without using any approximations yet, as

$$[\hat{Q}^{(2)}_\chi \cdot \hat{Q}^{(2)}_\chi, \hat{Q}^{(2)}_{O(6),\nu}] = \sum_{k=1,3} 2\sqrt{\frac{2k+1}{5}} [((d^\dagger \tilde{d})^{(k)}\hat{Q}^{(2)}_\chi)^{(2)}_\nu - (\hat{Q}^{(2)}_\chi (d^\dagger \tilde{d})^{(k)})^{(2)}_\nu]$$

$$+\chi[((d^\dagger s - s^\dagger \tilde{d})^{(2)}\hat{Q}_\chi^{(2)})_\nu^{(2)} + (\hat{Q}_\chi^{(2)}(d^\dagger s - s^\dagger \tilde{d})^{(2)})_\nu^{(2)}]. \tag{4.27}$$

Again, the expressions (4.26), (4.27) can be simplified in the large-N limit, since in this limit the contraction of O(6) to $R^5[SO(5)]$ [113, 114] takes place (see appendix G). This means that the commutators in the first two terms of (4.26) will vanish. Since

$$[\hat{Q}_{O(6),\xi}^{(2)}, \hat{Q}_{O(6),\nu}^{(2)}] = 2(2\xi 2\nu|1\xi + \nu)(d^\dagger \tilde{d})_{\xi+\nu}^{(1)} + 2(2\xi 2\nu|3\xi + \nu)(d^\dagger \tilde{d})_{\xi+\nu}^{(3)}, \tag{4.28}$$

the vanishing of this commutator implies that terms of the form $(d^\dagger \tilde{d})^{(k)}$ can be ignored. In addition, at this limit, $\hat{Q}_{O(6)}^{(2)}$ can be replaced by the intrinsic quadrupole moment (a scalar), which is N in the present case (see appendix G). Then, in the large-N limit one is left with

$$[\hat{Q}_\chi^{(2)} \cdot \hat{Q}_\chi^{(2)}, \hat{Q}_{O(6),\nu}^{(2)}] = 2N\chi[(d^\dagger s - s^\dagger \tilde{d})]_\nu^{(2)}. \tag{4.29}$$

The commutator for the second part of the Hamiltonian in the large-N limit then reads

$$[\hat{H}_2, \hat{Q}_{O(6),\nu}^{(2)}] = -2c(1 - \eta)\chi[(d^\dagger s - s^\dagger \tilde{d})]_\nu^{(2)}. \tag{4.30}$$

In order to get a vanishing commutator, the coefficients of $(d^\dagger s - s^\dagger \tilde{d})_\nu^{(2)}$ in Eqs. (4.24) and (4.30) should cancel, leading in the large-N limit to the condition

$$\chi(\eta) = \frac{\eta}{2(\eta - 1)}. \tag{4.31}$$

However, this does not yet suffice yet to guarantee the existence of a line corresponding to the O(6) symmetry. One has also to consider the commutators of the Hamiltonian with the $(d^\dagger \tilde{d})_\xi^{(3)}$ generators of O(5), to be considered in the next section.

4.4   The O(5) symmetry

As has already been mentioned, the O(5) algebra is generated by the angular momentum operators of Eq. (4.4) and the operators $(d^\dagger \tilde{d})_\xi^{(3)}$. We should examine the conditions under which the commutator of the Hamiltonian with $(d^\dagger \tilde{d})_\mu^{(3)}$ vanishes.

In this case, the first term of the Hamiltonian makes no contribution, since $\hat{n}_d$ is known to be an O(5) scalar [116]. Taking advantage of the fact that $\hat{Q}_{O(6)}^{(2)} \cdot \hat{Q}_{O(6)}^{(2)}$ is also an O(6) scalar [116] in order to simplify the calculation, one obtains

$$[\hat{H}, (d^\dagger \tilde{d})_\nu^{(3)}] = \frac{15}{7}\chi[((d^\dagger \tilde{d})^{(2)}(s^\dagger \tilde{d} + d^\dagger s)^{(2)})_\nu^{(3)} - ((s^\dagger \tilde{d} + d^\dagger s)^{(2)}(d^\dagger \tilde{d})^{(2)})_\nu^{(3)}]$$

$$-\frac{3}{7}\sqrt{10}\chi[((d^\dagger \tilde{d})^{(4)}(s^\dagger \tilde{d} + d^\dagger s)^{(2)})_\nu^{(3)} - ((s^\dagger \tilde{d} + d^\dagger s)^{(2)}(d^\dagger \tilde{d})^{(4)})_\nu^{(3)}]$$

$$-\frac{3}{7}\sqrt{10}\chi^2[((d^\dagger\tilde{d})^{(4)}(d^\dagger\tilde{d})^{(2)})^{(3)}_\nu - ((d^\dagger\tilde{d})^{(2)}(d^\dagger\tilde{d})^{(4)})^{(3)}_\nu]. \qquad (4.32)$$

In this case, no simplification due to contractions can be made. In order to get a vanishing commutator, one needs to put $\chi = 0$, thus being confined on the U(5)-O(6) side of the triangle. This finding is in agreement with the known existence of an O(5) subalgebra along the U(5)-O(6) side of the triangle [116].

Going back to the question of the existence of a line related to the O(6) symmetry, we see that in Eq. (4.31) one has to put $\chi = 0$, as required by the O(5) subalgebra. Then one ends up with $\eta = 0$, which represents the O(6) vertex alone. Thus, no line related to the O(6) symmetry exists within the triangle.

This finding, at first seems to be in contrast with the recent work of Kremer et al. [41], where the authors found a line based on O(6) symmetry, extending from the O(6) vertex, till the U(5)-SU(3) line of the triangle. However, a closer look at their work reveals that with the method used here, no O(6) line could be found. Namely, in [41], by using a measure of σ fluctuations (σ is the quantum number that describes the O(6) symmetry), called, $\Delta\sigma_\psi$, they found a valley of almost vanishing $\Delta\sigma_{g.s.}$ fluctuations, that is, a valley where the ground state wavefunctions have a high degree of purity with respect to the σ quantum number. However, at the same valley the O(5) symmetry is broken. So, in their work, Kremer et al. had a way of dividing the O(6) and O(5) symmetry, by using their characteristic quantum numbers and in that way, they could find a line, based only on O(6) symmetry and not on O(5). A similar division of these two symmetries is not possible in the present case, since the O(6) and O(5) algebras have common generators and so, when one studies the commutators of the O(6) algebra with the Hamiltonian, immediately also studies the commutators of the O(5) algebra with the Hamiltonian. So, since the last one is broken, no line can be found, except the one already known on the U(5)-O(6) line of the triangle.

Chapter 5

Proton-neutron interaction and emergent collectivity in nuclei

The unique role of the residual p-n (proton-neutron) interaction and its relation to the deviation from spherical symmetry of nuclei has long been known [117, 118, 119, 120, 121, 122, 123, 124]. Spherical symmetry is driven by the $J = 0$ pairing interaction between pairs of protons and pairs of neutrons with $T = 1$ (see Fig. 5.1), while deformation is driven by the valence $T = 0$ p-n interaction [125]. In general, the $T = 0$ interaction is nearly always attractive and stronger than the $T = 1$ interaction, which is attractive at the $J = 0$ state, but becomes repulsive as the J value increases. The emergence of collective phenomena is connected to a competition between the pairing and the p-n interactions. If one assumes, in a simplified picture, that the pairing interaction scales as the number of valence protons and neutrons, $N_p + N_n$, while the p-n interaction scales as the valence nucleon product, $N_p N_n$, a measure which indicates the competition between pairing and p-n interaction can be constructed, $P = N_p N_n / (N_p + N_n)$ [126]. $P \approx 5$ signifies the change between spherical and axially deformed shapes.
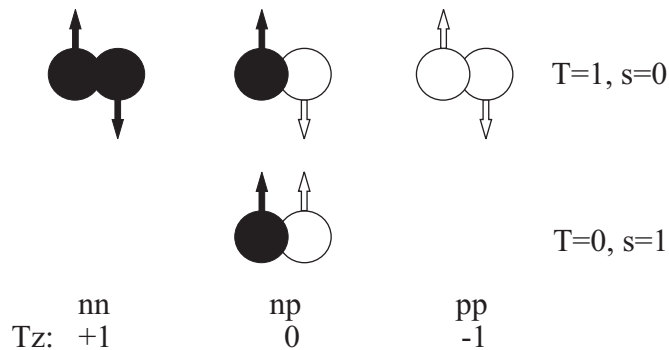
Figure 5.1: The allowed intrinsic angular momentum couplings in the A=2 isobaric triplet. Only a p-n pair is capable of coupling to T = 0, s = 1. Figure taken by [127].

In this chapter we will suggest a simple interpretation of the strong p-n interaction in terms of large spatial overlaps of the wavefunctions of the last proton and

neutron orbitals of a nucleus, in the context of the modified shell model, which describes deformed nuclei, the Nilsson model. We will also show that these pairs of orbitals, that have large spatial overlaps, are nearly synchronously filled in the Nilsson diagram and exactly when they are filled, deformation sets on. This leads to the suggestion of a new coupling scheme, analogous to the pseudo-SU(3) model [3, 4].

5.1 Nilsson Model

In the Spherical Shell Model, a Hamiltonian of the form

$$H = \sum_{i=1}[T_i + U_i] + \frac{1}{2}\sum_{i\neq j} v_{ij} \tag{5.1}$$

is used, where v_{ij} is the two-body residual interaction, which when acting on the unperturbed Hamiltonian $H_0 = \sum_{i=1}[T_i + U_i]$ it breaks its symmetries. When applying the Shrödinger equation to this Hamiltonian, but with no residual interaction, accompanied with a spin-orbit coupling term $l_i \cdot s_i$ [128] and an appropriate potential, the independent single-particle levels and the observed magic numbers are observed.

An analogous try was done by Nilsson, in the context of the shell model, to describe deformed nuclei. The Nilsson Hamiltonian reads

$$H = H_0 + C\mathbf{l}\cdot\mathbf{s} + D\mathbf{l}^2, \tag{5.2}$$

where

$$H_0 = -\frac{\hbar^2}{2m}\nabla^2 + \frac{m}{2}(\omega_x^2(x^2 + y^2) + \omega_z^2 z^2), \tag{5.3}$$

where x, y, z are the coordinates in the system fixed to the nucleus. We have assumed axial symmetry around the z axis ($\omega_x = \omega_y$) and a small deviation from the spherical shape given by a small parameter δ. The oscillator frequencies are defined as $\omega_x^2 = \omega_y^2 = \omega_0^2\left(1 + \frac{2}{3}\delta\right)$ and $\omega_z^2 = \omega_0^2\left(1 - \frac{2}{3}\delta\right)$. The $\mathbf{l}\cdot\mathbf{s}$ and $\mathbf{l}^2$ terms are there to ensure that in the spherical limit, the energies and the order of the levels will be correct. For large deformations, the influence of the $\mathbf{l}\cdot\mathbf{s}$ and $\mathbf{l}^2$ terms is less important, so one can solve the Hamiltonian as a 3D oscillator with cylindrical symmetry, with eigenvalues given by

$$E(n_x, n_y, n_z) = \hbar\omega_x(N - n_z + 1) + \hbar\omega_z(n_z + \frac{1}{2}), \tag{5.4}$$

where $N = n_x + n_y + n_z$. The introduction of the parameter δ enables to write the Hamiltonian in terms of the spherical harmonic Y_{20} as

$$\begin{aligned} H &= \frac{1}{2}\hbar\omega_0(-\nabla^2 + r^2) - \delta\hbar\omega_0\frac{4}{3}\sqrt{\frac{\pi}{5}}r^2 Y_{20} + C\mathbf{l}\cdot\mathbf{s} + D\mathbf{l}^2 \\ &= \bar{H}_0 + H_\delta + C\mathbf{l}\cdot\mathbf{s} + D\mathbf{l}^2 \end{aligned} \tag{5.5}$$

The deformation parameter δ and the analogous parameter of the Bohr Hamiltonian are connected by

$$\delta \simeq \frac{3}{2}\sqrt{\frac{5}{4\pi}}\beta \simeq 0.95\beta. \tag{5.6}$$

It has been customary to label the Nilsson levels with the set of symbols $K^{\pi}[N \; n_z \; \Lambda]$. One can visualize a valence nucleon orbiting around a deformed nucleus, or around a prolate deformed potential (Fig. 5.2). Then, K is the projection of the total angular momentum on the symmetry axis, N is the principal quantum number $N = n_x + n_y + n_z$, n_z is the number of nodes in the wavefunction in the z direction and Λ is the component of the orbital angular momentum on the symmetry axis (the z-axis). By definition, $K = \Lambda + \Sigma = \Lambda \pm \frac{1}{2}$, where Σ is the projection of the intrinsic nucleon spin on the symmetry axis.

The approximate eigenstates of the full Hamiltonian can be expanded as [129]

$$\chi_{N\Omega} = \sum_{l\Lambda} a_{l\Lambda}^{\Omega}|Nl\Lambda\Sigma\rangle. \tag{5.7}$$

The coefficients $a_{l\Lambda}^{\Omega}$ have been calculated for different values of the parameter

$$\eta = \frac{2\hbar\omega_0}{C}\delta \tag{5.8}$$

and are tabulated in Table I of Ref. [1]. These expansions can then be used for calculating overlaps.
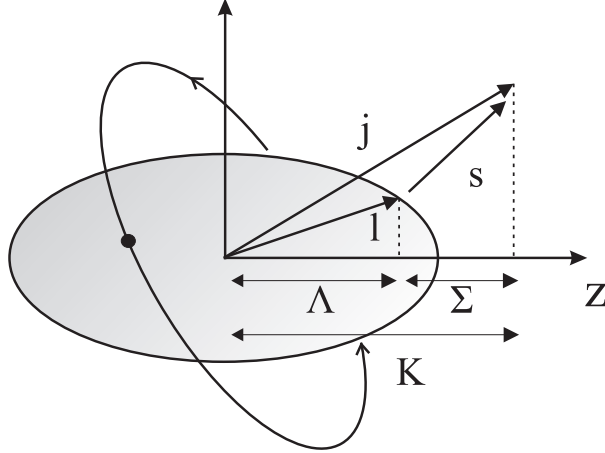
Figure 5.2: A single particle orbiting around a deformed core and the and the resulting Nilsson numbers.

5.1.1 Wave functions in configuration space

The full wave functions corresponding to the vectors $|Nl\Lambda\Sigma\rangle$ are

$$\Psi_{Nl\Lambda\Sigma} = R_{nl}Y_{l\Lambda}f_{s\Sigma}, \tag{5.9}$$

where $Y_{l\Lambda}$ are the usual spherical harmonics, $f_{s\Sigma}$ are the spinors $\begin{pmatrix} 1 \\ 0 \end{pmatrix}$ and $\begin{pmatrix} 0 \\ 1 \end{pmatrix}$ for spin up and spin down respectively, and R_{nl} is the radial wave function of the 3D harmonic oscillator in spherical coordinates, given by [130] (in units in which the mass and the frequency of the oscillator, as well as $\hbar$, are 1)

$$R_{nl} = \sqrt{\frac{2(n!)}{\Gamma\left(n + l + \frac{3}{2}\right)}} e^{-r^2/2} r^l L_n^{l+\frac{1}{2}}(r^2), \tag{5.10}$$

where $\Gamma(x)$ is the Gamma function, $L_n^l(r^2)$ are the Laguerre polynomials, and $N = 2n + l$.

These wave functions can be connected to these appearing in Eq. (8) of Ref. [1] through the relation connecting confluent hypergeometric functions and Laguerre polynomials (p. 149 [131])

$$_1F_1(-n; m + 1; z) = \frac{n!m!}{(n+m)!} L_n^{(m)}(z), \tag{5.11}$$

leading in the present case to

$$_1F_1\left(-n; l + \frac{3}{2}; r^2\right) = \frac{n!\left(l + \frac{1}{2}\right)!}{\left(n + l + \frac{1}{2}\right)!} L_n^{l+\frac{1}{2}}(r^2). \tag{5.12}$$

An alternative basis ($|Nlj\Omega\rangle$) is discussed in the appendix H.

5.2 Empirical p-n interactions

Since the residual p-n interaction is connected with the onset of deformation, one wants to find measures of the strength of the residual p-n interaction that would connect the maximum strength with the change between spherical and deformed shapes. As already mentioned before, a simplified estimation of the p-n strength is the product of the number of valence protons and neutrons, $N_p N_n$ [132], which assumes that the p-n interaction is orbit independent. Orbit dependence gets into play with a refinement of the $N_p N_n$ product, introduced in [133], the integrated quadrupole p-n interaction, $|S_{pn}|$.

Another way of extracting the average p-n interaction of the last nucleons, is by using a specific double difference of binding energies, called δV_{pn} [134]. This is defined for even-even nuclei by

$$|\delta V_{pn}^{ee}(Z, N)| = \frac{1}{4}[(B_{Z,N} - B_{Z,N-2}) - (B_{Z-2,N} - B_{Z-2,N-2})]. \tag{5.13}$$

A schematic illustration of the binding energy differencies of eq. (5.13) is shown in Fig. 5.3, taken by [134]. The first binding energy difference gives the interaction

of the last two neutrons with all the Z protons and with each other, plus the contribution to the average spherical field. The situation is analogous for the second binding energy difference, which is the interaction of the last two neutrons with Z-2 protons and with each other and their contribution to the average spherical field. The double difference of the binding energies results in the subtraction of the p-p, n-n interactions and the contribution to the average spherical field and by dividing with four, one gets the average interaction of each of the last two protons with each of the last two neutrons. Double differences of binding energies for even-odd and odd-odd nuclei have also been defined [135, 136].

$$
\left(\begin{array}{c} \pi \\ \end{array}\right) \otimes \left(\begin{array}{c} \nu \\ \end{array} - \begin{array}{c} \\ \end{array}\right) - \left(\begin{array}{c} \pi \\ \end{array}\right) \otimes \left(\begin{array}{c} \nu \\ \end{array} - \begin{array}{c} \\ \end{array}\right)
$$

(Z) ⊗ [(N)-(N-2)] − (Z-2) ⊗ [(N)-(N-2)]

Figure 5.3: Schematic illustration of the binding energy differencies of eq. (5.13). Figure taken by [134].

It is apparent from the previous schematic and mathematical explanation of δV_{pn}, that this measure works in the following way: when the average p-n interaction is strong, δV_{pn} should have a high value. The behavior of δV_{pn} has been studied much [135, 136, 137, 138, 139, 140, 141, 142, 143, 144, 145]. In Ref. [146] it was found that when the empirical δV_{pn} values were plotted as a function of neutron number for light nuclei, these had characteristic peaks exactly at $N = Z$ for even-even nuclei and at $N = Z - 1$ for even-Z, odd-N nuclei. The peaking of the δV_{pn} values in the vicinity of $N \simeq Z$, which of course signifies strong p-n interaction, was justified by the strong overlaping [117] between neutron and proton orbitals. For $N = Z$ nuclei, protons and neutrons are filling exactly the same orbits, therefore there is strong spatial overlap between the proton and neutron wavefunctions, which leads to large δV_{pn} values. The phenomenon was explained theoritically in terms of Wigner $SU(4)$ supermultiplet theory [135].

One would expect that the characteristic peaking of δV_{pn} values would dissipate for heavier nuclei, since there are no $N = Z$ nuclei beyond $A \sim 100$ and also spin orbit and Coulomb forces grow in importance, so, protons and neutrons start filling different shells, something that would lead to poor overlaping between proton and neutron orbits. However, it was found [146, 147] that heavy nuclei also show similar peaks at the δV_{pn} values, though, while in light nuclei peaks were in an MeV scale, in heavy nuclei the scale moves to keV. In heavy nuclei, δV_{pn} values reach a maximum when the number of valence neutrons equals the number of valence protons, $N_{val} = Z_{val}$, or late in the shells, slightly exceeds the valence proton number. For example, at the left panel of Fig. 5.4, one can see the empirical δV_{pn} values of isotopic chains

of even-Z, even-N nuclei. The elements Sm, Er, Yb and W have maximum δV_{pn} values exactly when $N_{val} = Z_{val}$ $[(N_{val}, Z_{val}) = (12, 12), (18, 18), (20, 20), (24, 24),$ respectively].

Figure 5.4: (a) Empirical δV_{pn} values for even-Z, even-N nuclei. (b) Empirical δV_{pn} values for odd-Z nuclei.

For the elements Gd and Dy, δV_{pn} increases until $N_{val} = Z_{val}$, however, for both elements, this is the last known value of δV_{pn}, so one needs to know the next δV_{pn} value, in order to conclude whether there is a maximum there or not. Last, Hf is the only element which breaks slightly the previous pattern, since δV_{pn} peaks for $(N_{val}, Z_{val}) = (22, 24)$. However, this is not surprising and as we will see later, this has to do with the way protons and neutrons fill the shells. In general, even-even nuclei have a characteristic peak in δV_{pn} for $N_{val} \simeq Z_{val}$.

The same trend is seen in odd-Z, even-N and odd-Z, odd-N nuclei, as seen in the right panel of Fig. 5.4. The phenomenon is more pronounced in odd-odd nuclei, because here the p-n interaction can be better expressed, due to the lack of the pairing force between the two last protons and neutrons of even-even nuclei. The effects of pairing force can even be seen in odd-Z, even-N nuclei, whose δV_{pn} values are always smaller compared to the ones of odd-odd nuclei.

An even more characteristic plot can be seen in Fig. 5.5. This is a color plot of $R_{4/2} \equiv E(4_1^+)/E(2_1^+)$, in the Z=50-82, N=82-126 shells, which varies from < 2 near closed shells to ~ 3.33 for well deformed axial rotors. The black line represents the line where $N_{val} = Z_{val}$, while the white circles are the isotopes of the isotopic chains shown in Fig. 5.4 for which maximum δV_{pn} values are observed. Only the isotopes with confirmed maximum δV_{pn} values are presented. It is observed that both even-even and odd-odd nuclei follow the $N_{val} \simeq Z_{val}$ line, while a possible explanation for the isotopes that slightly deviate from this line, will be given later. What is more impressive is that the line of $N_{val} \simeq Z_{val}$ and the maximum δV_{pn} values are found

exactly there where the onset of deformation occurs for $R_{4/2} > 3.3$, highlighting the link to the evolution and saturation of collectivity.
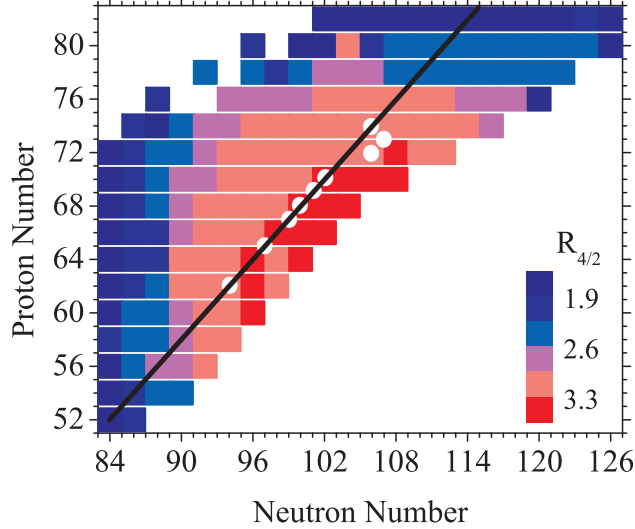
Figure 5.5: Color plot of empirical $R_{4/2}$ values in the Z=50-82, N=82-126 shells. The black line is the locus of points, where $N_{val} = Z_{val}$. The white circles are the nuclei where the largest δV_{pn} is observed.

What was also found [146], is that for the isotopes that had the largest δV_{pn} values, there was a characteristic relationship between the quantum numbers of the orbits occupied by the last protons and neutrons. These nuclei are all well-deformed (except the lighter Sm and Gd isotopes), so a Nilsson description is appropriate. The quantum numbers stated above refer to the Nilsson quantum numbers. For example, the Er isotopes, shown in Fig. 5.4 , have 18 valence protons and 10-20 valence neutrons. If one consults the Nilsson diagram of Fig. 5.6 , it is obvious that the last proton will occupy the 7/2[523] orbital of the $h_{11/2}$ orbit, an intruder orbit in the 50-82 shell, stemming from the upper shell, with an opposite parity compared to the other orbits of the 50-82 shell. Consulting again the Nilsson diagram, one can see that the 10-20 valence neutrons occupy the orbitals, 3/2[651], 3/2[521], 5/2[642], 5/2[523], 7/2[633] and 1/2[521]. The isotope that gives the peaking in δV_{pn} is the one with N=100, whose last neutron, according to the order of the orbitals we just wrote, occupies the 7/2[633] orbital, stemming from the $i_{13/2}$ orbit, which is again an intruder orbit in the 82-126 shell, with an opposite parity compared to the other orbits of this shell. A more careful look at Fig. 5.6, will reveal, that the 7/2[523] and the 7/2[633] orbital, where the last proton and neutron sit on respectively, are like sister orbitals and they also differ by $\Delta K[\Delta N \Delta n_z \Delta \Lambda] = 0[110]$. Physically, this difference means that the wavefunctions of the proton and the neutron have equal numbers of quanta in the x-y plane (the same $n_x + n_y$ values) and protons and neutrons have the same projection of the angular momentum on the symmetry axis. The peaking of δV_{pn} for a specific isotope and the occupancy, by the last proton and neutron of this isotope, of orbitals which differ by $\Delta K[\Delta N \Delta n_z \Delta \Lambda] = 0[110]$

characterize and the other isotopes of the even-even nuclei studied (Yb, Hf, W). So, protons and neutrons, occupying sister orbitals, linked by the 0[110] relationship, imply a high overlap of their wavefunctions which results in strong p-n interaction.
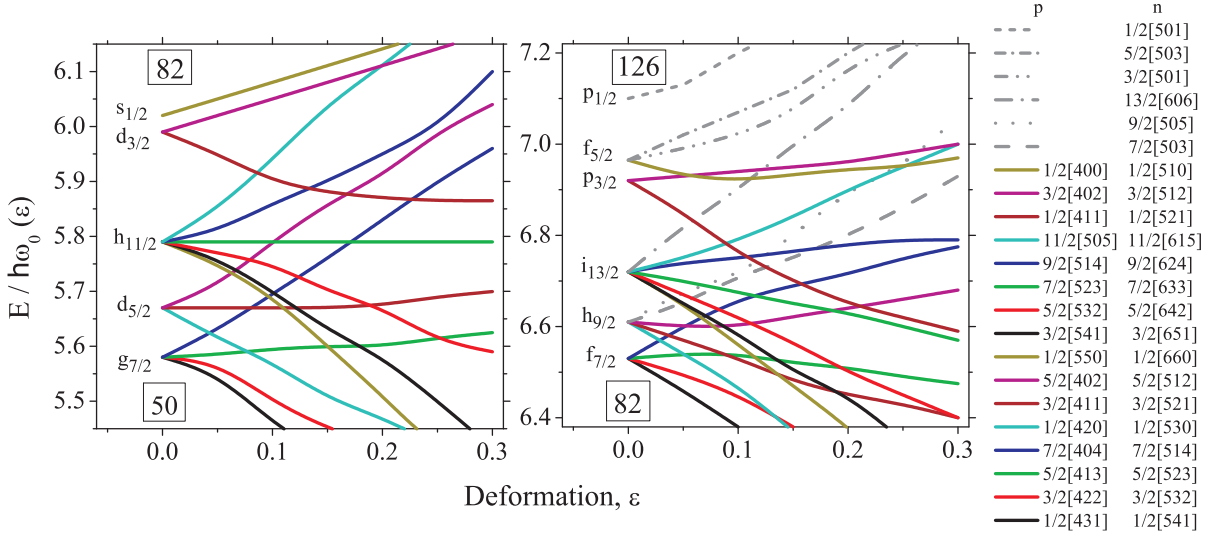
Figure 5.6: Nilsson diagrams of the $Z = 50 - 82$ and $N = 82 - 126$ shells. Different colors are used to indicate sister orbits, pairs of orbits differing by $\Delta K[\Delta N \Delta n_z \Delta \Lambda] = 0[110]$. For most deformations, the sequential filling of 0[110] pairs of orbits is closely followed. Neutron orbitals without 0[110] proton partners (they have $n_z = 0$) are shown as black dashed lines in the neutron 82-126 shell.

5.3   A simple model for the p-n interactions

How can one try to understand the origin and implications of these results? According to Federman and Pittel [119], the criterion for strong p-n correlations to occur, is that protons and neutrons should occupy orbitals with good overlap. And the overlap between two orbitals $(n_N l_N j_N)$, $(n_P l_P j_P)$ is maximum if $n_N = n_P$ and $l_N = l_P \pm 1$. Strong correlations into the rare earth region were expected to occur between $1h_{11/2}$ protons and $1i_{13/2}$ neutrons. This could explain a part of the results. Another way of studying the results is through large scale computationally intensive methods. In Ref. [141], the authors have used density functional theory in order to calculate δV_{pn} values (see Fig. 5.9, right panel). The comparison with the empirical δV_{pn} values of $Z = 50 - 82$, $N = 82 - 126$ shells gives good agreement, however it doesn't reveal the underlying origin of the behavior of δV_{pn}. Here we investigate these interactions from a simpler theoretical perspective, by directly calculating the overlap of proton and neutron Nilsson wavefunctions. Our approach obtains similar results, but now in a way that explicitly exposes, in a physically intuitive way, the underlying origins of the emergent collectivity. It will be apparent that collectivity emerges through the roles of specific orbitals in p-n interactions.

Nilsson wavefunctions in the form [1] $\chi_{N\Omega} = \sum_{l\Lambda} \alpha_{l\Lambda}^{\Omega} |Nl\Lambda\Sigma\rangle$ were used, where Ω, Λ, Σ are the projections of the total particle angular momentum j, the orbital angular momentum l and the spin s on the z axis, while the coefficients $\alpha_{l\Lambda}^{\Omega}$ were calculated by solving the Nilsson Hamiltonian with the standard parameter values, $\kappa = 0.0637$ and $\mu = 0.42$ for neutrons and $\kappa = 0.0637$ and $\mu = 0.6$ for protons. For axially symmetric nuclei, which we will deal here, K, the projection of the total (particle and the rest of the nucleus) angular momentum on the z axis and Ω are the same ($K = \Omega$). In order to calculate spatial overlaps of Nilsson wavefunctions two different expressions were used. The first expression

$$\int \sqrt{\chi_{N_1\Omega_1}^* \chi_{N_1\Omega_1}} \sqrt{\chi_{N_2\Omega_2}^* \chi_{N_2\Omega_2}} \quad r^2 \sin\theta \; dr \; d\theta \; d\phi \tag{5.14}$$

was also tested on hydrogen atom wavefunctions and for orbitals with quantum numbers $(n_1 l_1 m_1)$ and $(n_2 l_2 m_2)$ it was found that all overlaps with $\Delta n = 0$ are larger than the $\Delta n = 1$ overlaps and all overlaps with $\Delta n = 1$ are larger than the $\Delta n = 2$ ones. This is in accordance with [119] and it shows that the n quantum number is the most important one in deciding how large the overlap of two wave functions is. Note that the expression (5.14) is normalised and when $\chi_{N_1\Omega_1} = \chi_{N_2\Omega_2}$, (5.14) is equal to one, while the more the two wavefunctions deviate from each other, the smaller the integral will be.

Eq. (5.14) is not the only possibility for estimating spatial overlaps of the Nilsson orbitals. Overlaps can also be estimated using the integral

$$\frac{\int \chi^*_{N_1\Omega_1}\chi_{N_1\Omega_1}\chi^*_{N_2\Omega_2}\chi_{N_2\Omega_2}dV}{\sqrt{\int \chi^*_{N_1\Omega_1}\chi_{N_1\Omega_1}\chi^*_{N_1\Omega_1}\chi_{N_1\Omega_1}dV}\sqrt{\int \chi^*_{N_2\Omega_2}\chi_{N_2\Omega_2}\chi^*_{N_2\Omega_2}\chi_{N_2\Omega_2}dV}}, \tag{5.15}$$

where $dV = r^2 \sin\theta\, dr\, d\theta\, d\phi$. The normalization factors in the denominator guarantee that the overlap of a wave function with itself is unity. Overlaps were calculated for three different values of the deformation ϵ=0.05, 0.22 and 0.3, allocating nuclei to these categories according to $R_{4/2}$ and extending these choices to unknown nuclei using the P-factor [126]. Expressions (5.14) and (5.15) give identical results, so we will restrict ourselves to the second overlap. Overlaps of the proton orbitals appearing in the 50-82 shell with the neutron orbitals appearing in the 82-126 shell are shown in Tables 5.1, 5.2, 5.3 for the three different values of deformation.

It is instructive to look globally at the overlaps. Fig. 5.7 shows their behavior against correlated differences in K and n_z, as well as against differences in each of the Nilsson quantum numbers. In Fig. 5.7(a) the spatial overlaps are highest when $\Delta K = 1$ and $\Delta n_z = 0$, which includes the 1[000] case. However, large overlaps also occur for $\Delta K = 0$ and $\Delta n_z = 1$ characteristic of the 0[110] transformation and for neighboring values of ΔK and Δn_z. The overlaps generally fall off for larger ΔK and Δn_z values.

One, can note two outlying pink boxes at the upper left of Fig. 5.7(a). These occur for large ΔK differences (3 and even 6), such as for the orbital pair 1/2[431] and 13/2[606] and were at first rather puzzling. To understand these and the other patterns, a further analysis of the overlaps, like the one shown in Fig. 5.7(b) to 5.7(f) is needed. Each point is an average of all the overlaps for that value of the difference in the particular quantum number. In each case, the overlaps fall off steeply as the particular quantum number between the two orbits differs by larger and larger amounts. The overlaps peak either when the difference between the quantum numbers is 0 (ΔK for antiparralel spin, Δn_z, Δn_ρ) or when it is 1 (ΔN, ΔK for parallel spin and $\Delta\Lambda$). Note that the steepest difference is for the Δn_ρ plot at bottom left, where Δn_ρ is the difference in the number of radial nodes with $n_\rho = (N - n_z - \Lambda)/2$. Also, the peak at $\Delta N = 1$ is interesting. Given that the maximum overlaps occur for Δn_z and $\Delta n_\rho = 0$, the peak at $\Delta N = 1$ implies a corresponding peak at $\Delta\Lambda = 1$, which is indeed seen. Now, one can understand the pink boxes with large ΔK in Fig. 5.7(a). They all correspond to cases of $\Delta n_\rho = 0$, for which the large Δn_ρ overlaps compensate for the large ΔK and Δn_z differences. However, such orbit pairs form the ground states only in neutron rich nuclei, not currently accessible.
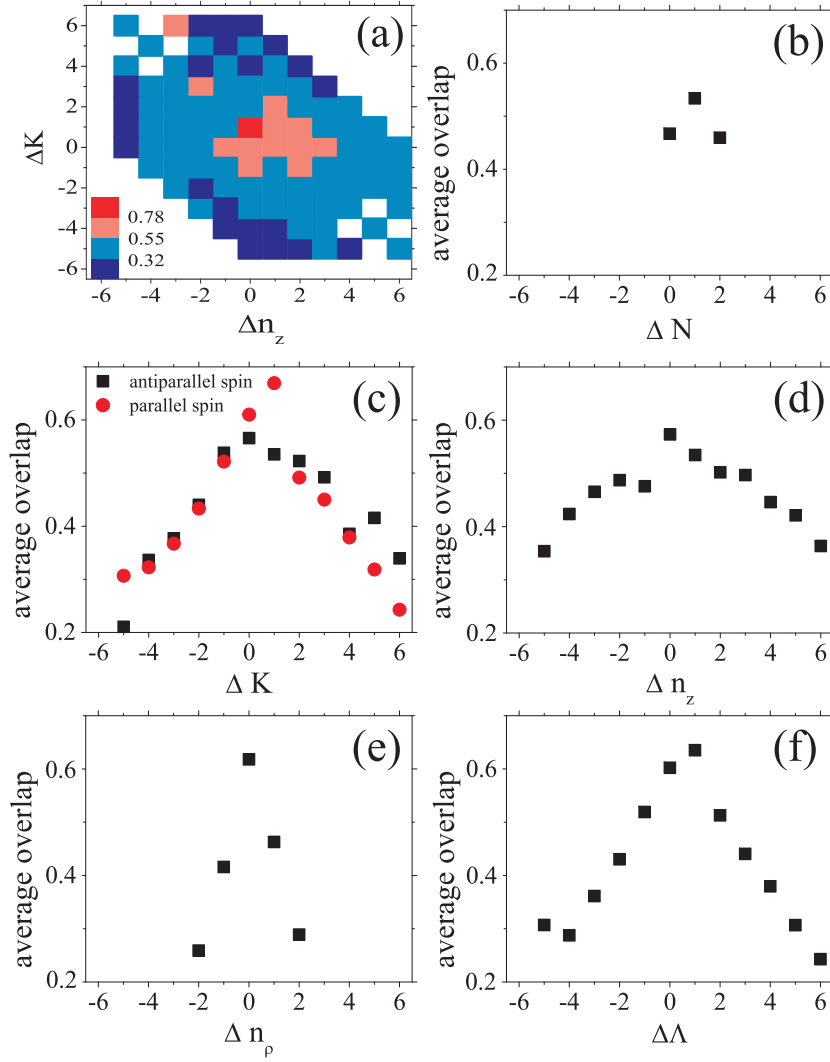
Figure 5.7: Calculated average spatial overlaps (for a deformation $\epsilon = 0.22$) for proton and neutron orbitals in the $Z = 50-82$, $N = 82-126$ shells against the differences (neutron orbit minus proton orbit) in their K and n_z values in a color code. Other panels show average overlaps as a function of differences [(b) ΔN, (c) ΔK, (d) Δn_z, (e) Δn_ρ, (f) $\Delta \Lambda$] in individual Nilsson quantum numbers.

In Fig. 5.8, one can see empirical values of δV_{pn} compared to calculated overlaps for the $Z = 50 - 82$, $N = 82 - 126$ shells. The left black line corresponds to the place where the number of valence protons equals the number of valence neutrons, while the right black line is the line of equal fractional filling of shells. Overall, the agreement is quite good given the simplicity and the parameter free nature of the approach. In both images, large values are found near the two lines and between them, while small values are found away from the diagonal. There is also a region of large values early in the shells. There are occasional pink boxes to the upper left that disagree with the data. They correspond to very neutron deficient isotopes for $Z \sim 72 - 76$. Also, the blue box for Pb at $N = 124$ would be light pink were zero deformation (instead of 0.05) to be used.
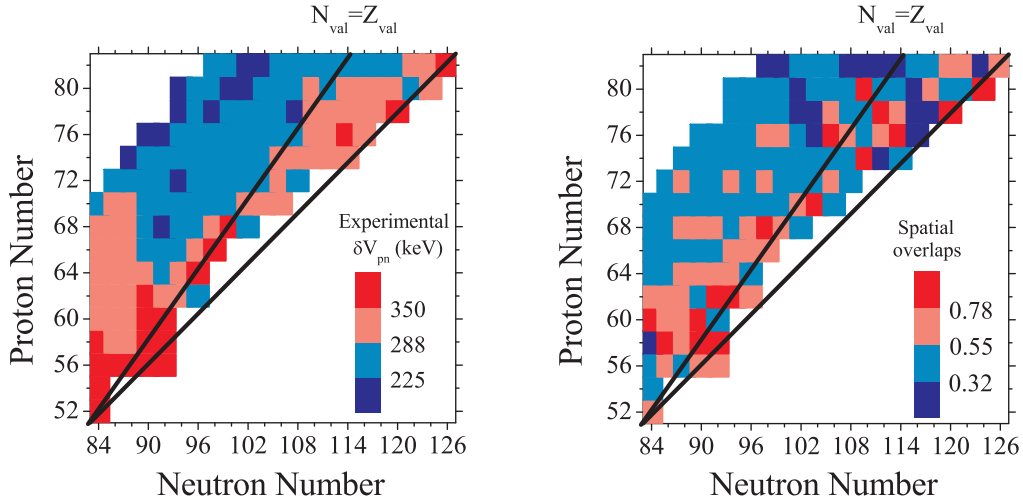
Figure 5.8: Comparison of empirical δV_{pn} values for the $Z = 50 - 82$, $N = 82 - 126$ shells with calculated overlaps. Blue color corresponds to low δV_{pn} values and low spatial overlaps, while red color corresponds to large δV_{pn} values and large spatial overaps.

Calculated overlaps were not limited to known nuclei. Fig. 5.9, left panel, shows overlaps for the whole $Z = 50 - 82$, $N = 82 - 126$ shells compared with δV_{pn} values calculated from density functional theory (DFT) [141]. Highly complicated calculations of δV_{pn} values and very simple calculations of integrals of wavefunctions show an overall agreement. They also reveal a region of large p-n interaction in neutron rich nuclei in the regions $Z \sim 52 - 64$ and $N \sim 92 - 108$. Here, pairs of orbitals, such as 5/2[413] with 5/2[512] and 1/2[420] with 1/2[521], coupled to $S = 0$, are filling (near ^{168}Gd and ^{162}Nd, respectively), that do not satisfy 0[110], which implies $S = 1$.
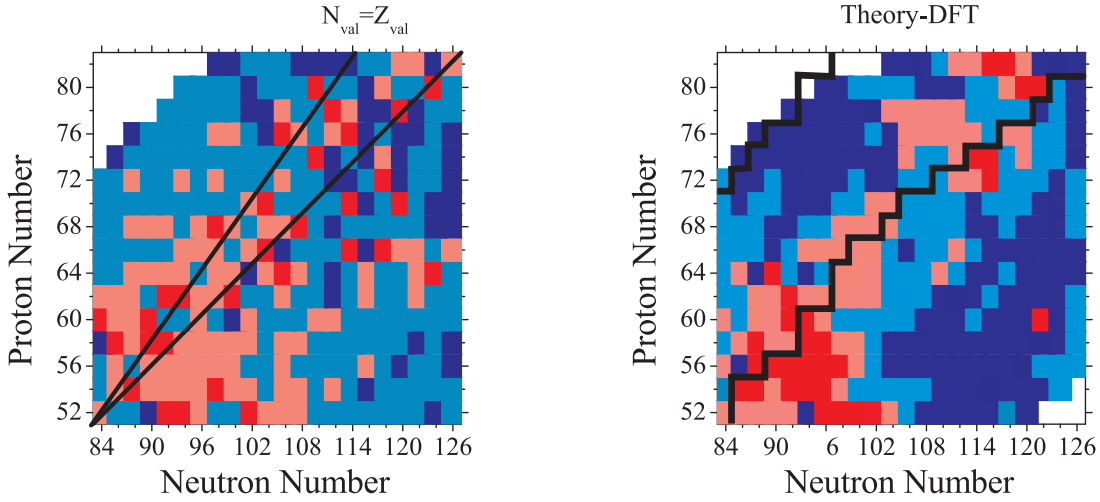
Figure 5.9: Comparison of calculated spatial overlaps, now for the whole $Z = 50-82$, $N = 82-126$ shells (left panel) with δV_{pn} values from density functional theory (DFT) calculations [141].

Table 5.1: Spatial overlaps [Eq. (5.15)] of Nilsson orbitals in the 50–82 proton shell (listed in the first line, in the order appearing in Fig. 5.6) with orbitals in the 82–126 neutron shell (listed in the first column, in the order appearing in Fig. 5.6). a) For deformation $\epsilon_2 = 0.22$.

|	$\frac{1}{2}$[431]	$\frac{3}{2}$[422]	$\frac{5}{2}$[413]	$\frac{7}{2}$[404]	$\frac{1}{2}$[420]	$\frac{3}{2}$[411]	$\frac{5}{2}$[402]	$\frac{1}{2}$[550]	$\frac{3}{2}$[541]	$\frac{5}{2}$[532]	$\frac{7}{2}$[523]	$\frac{9}{2}$[514]	$\frac{11}{2}$[505]	$\frac{1}{2}$[411]	$\frac{3}{2}$[402]	$\frac{1}{2}$[400]
$\frac{1}{2}$[541]	0.691	0.455	0.489	0.310	0.653	0.500	0.347	0.535	0.535	0.409	0.405	0.464	0.266	0.561	0.362	0.461
$\frac{3}{2}$[532]	0.791	0.790	0.606	0.488	0.504	0.636	0.463	0.634	0.714	0.818	0.589	0.440	0.500	0.638	0.482	0.451
$\frac{5}{2}$[523]	0.582	0.901	0.879	0.514	0.408	0.605	0.495	0.621	0.682	0.740	0.941	0.674	0.502	0.606	0.507	0.278
$\frac{7}{2}$[514]	0.595	0.616	0.885	0.671	0.414	0.332	0.519	0.568	0.594	0.642	0.705	0.987	0.627	0.362	0.511	0.132
$\frac{1}{2}$[530]	0.720	0.639	0.532	0.427	0.712	0.509	0.383	0.841	0.694	0.557	0.572	0.409	0.436	0.541	0.398	0.467
$\frac{3}{2}$[521]	0.632	0.665	0.561	0.432	0.664	0.673	0.447	0.619	0.720	0.700	0.446	0.470	0.381	0.682	0.470	0.501
$\frac{5}{2}$[512]	0.461	0.597	0.644	0.368	0.390	0.841	0.550	0.425	0.479	0.555	0.635	0.445	0.287	0.828	0.579	0.357
$\frac{1}{2}$[660]	0.701	0.593	0.524	0.335	0.676	0.437	0.328	0.964	0.784	0.651	0.564	0.482	0.393	0.462	0.338	0.423
$\frac{3}{2}$[651]	0.725	0.653	0.564	0.359	0.583	0.501	0.346	0.837	0.911	0.726	0.601	0.515	0.415	0.511	0.359	0.409
$\frac{5}{2}$[642]	0.690	0.732	0.627	0.385	0.400	0.557	0.366	0.672	0.872	0.853	0.666	0.540	0.437	0.549	0.381	0.345
$\frac{7}{2}$[633]	0.575	0.770	0.714	0.421	0.299	0.534	0.396	0.641	0.608	0.903	0.782	0.596	0.461	0.530	0.534	0.257
$\frac{9}{2}$[624]	0.462	0.697	0.770	0.485	0.339	0.401	0.434	0.548	0.645	0.557	0.931	0.707	0.509	0.424	0.435	0.165
$\frac{11}{2}$[615]	0.523	0.472	0.702	0.602	0.376	0.217	0.452	0.527	0.523	0.594	0.537	0.950	0.612	0.256	0.442	0.091
$\frac{1}{2}$[521]	0.586	0.500	0.351	0.280	0.701	0.667	0.344	0.518	0.545	0.485	0.331	0.226	0.215	0.722	0.372	0.581
$\frac{3}{2}$[512]	0.413	0.516	0.562	0.343	0.464	0.851	0.577	0.369	0.412	0.466	0.504	0.435	0.240	0.861	0.607	0.428
$\frac{1}{2}$[510]	0.463	0.300	0.185	0.120	0.592	0.437	0.261	0.507	0.427	0.266	0.138	0.096	0.091	0.471	0.280	0.595
$\frac{7}{2}$[503]	0.412	0.359	0.438	0.555	0.589	0.416	0.855	0.310	0.325	0.340	0.380	0.472	0.472	0.470	0.848	0.138
$\frac{9}{2}$[505]	0.607	0.554	0.600	0.948	0.273	0.146	0.418	0.472	0.499	0.509	0.546	0.623	0.999	0.140	0.411	0.051
$\frac{13}{2}$[606]	0.578	0.491	0.491	0.820	0.116	0.226	0.398	0.460	0.483	0.474	0.507	0.518	0.957	0.102	0.392	0.0432
$\frac{3}{2}$[501]	0.344	0.397	0.391	0.200	0.355	0.488	0.536	0.287	0.325	0.356	0.348	0.274	0.154	0.517	0.546	0.617
$\frac{5}{2}$[503]	0.403	0.339	0.403	0.530	0.575	0.439	0.854	0.289	0.302	0.314	0.349	0.412	0.456	0.486	0.851	0.148
$\frac{1}{2}$[501]	0.357	0.383	0.364	0.192	0.376	0.463	0.520	0.306	0.331	0.342	0.321	0.253	0.152	0.497	0.529	0.638

Table 5.2: (continued) b) For deformation $\epsilon_2 = 0.05$.

	$\frac{1}{2}$[431]	$\frac{3}{2}$[422]	$\frac{5}{2}$[413]	$\frac{7}{2}$[404]	$\frac{1}{2}$[420]	$\frac{3}{2}$[411]	$\frac{5}{2}$[402]	$\frac{1}{2}$[550]	$\frac{3}{2}$[541]	$\frac{5}{2}$[532]	$\frac{7}{2}$[523]	$\frac{9}{2}$[514]	$\frac{11}{2}$[505]	$\frac{1}{2}$[411]	$\frac{3}{2}$[402]	$\frac{1}{2}$[400]
$\frac{1}{2}$[541]	0.563	0.447	0.379	0.254	0.817	0.597	0.436	0.468	0.456	0.375	0.342	0.318	0.208	0.672	0.485	0.534
$\frac{3}{2}$[532]	0.453	0.568	0.380	0.319	0.719	0.738	0.490	0.408	0.459	0.508	0.433	0.254	0.278	0.741	0.556	0.490
$\frac{5}{2}$[523]	0.346	0.449	0.576	0.335	0.504	0.805	0.597	0.395	0.349	0.410	0.485	0.508	0.249	0.742	0.662	0.353
$\frac{7}{2}$[514]	0.286	0.321	0.397	0.571	0.492	0.439	0.839	0.418	0.275	0.301	0.336	0.399	0.563	0.581	0.821	0.175
$\frac{1}{2}$[530]	0.936	0.718	0.563	0.435	0.533	0.387	0.288	0.730	0.863	0.674	0.611	0.514	0.433	0.430	0.315	0.359
$\frac{3}{2}$[521]	0.828	0.860	0.641	0.476	0.473	0.470	0.319	0.539	0.937	0.914	0.622	0.586	0.460	0.469	0.355	0.347
$\frac{5}{2}$[512]	0.631	0.880	0.764	0.526	0.344	0.522	0.365	0.498	0.711	0.876	0.953	0.579	0.499	0.481	0.403	0.283
$\frac{1}{2}$[660]	0.788	0.583	0.457	0.345	0.533	0.377	0.271	0.756	0.762	0.627	0.533	0.453	0.366	0.420	0.298	0.367
$\frac{3}{2}$[651]	0.778	0.681	0.510	0.380	0.513	0.438	0.298	0.546	0.927	0.727	0.594	0.500	0.401	0.457	0.332	0.373
$\frac{5}{2}$[642]	0.676	0.762	0.569	0.407	0.428	0.489	0.322	0.440	0.884	0.877	0.667	0.538	0.425	0.472	0.360	0.338
$\frac{7}{2}$[633]	0.557	0.770	0.656	0.444	0.341	0.503	0.356	0.553	0.635	0.919	0.812	0.599	0.457	0.471	0.392	0.282
$\frac{9}{2}$[624]	0.476	0.653	0.751	0.510	0.297	0.451	0.401	0.408	0.585	0.629	0.935	0.733	0.509	0.444	0.426	0.213
$\frac{11}{2}$[615]	0.449	0.456	0.750	0.629	0.300	0.328	0.448	0.444	0.493	0.548	0.581	0.950	0.626	0.384	0.451	0.143
$\frac{1}{2}$[521]	0.358	0.378	0.290	0.116	0.618	0.513	0.235	0.432	0.342	0.345	0.299	0.201	0.074	0.673	0.291	0.508
$\frac{3}{2}$[512]	0.329	0.400	0.470	0.448	0.542	0.730	0.646	0.648	0.328	0.372	0.409	0.432	0.390	0.762	0.695	0.533
$\frac{1}{2}$[510]	0.543	0.396	0.227	0.283	0.739	0.555	0.411	0.588	0.474	0.332	0.209	0.178	0.256	0.639	0.457	0.569
$\frac{7}{2}$[503]	0.537	0.617	0.911	0.648	0.325	0.422	0.463	0.468	0.570	0.645	0.770	0.978	0.544	0.447	0.475	0.189
$\frac{9}{2}$[505]	0.461	0.507	0.565	0.948	0.284	0.208	0.208	0.430	0.458	0.497	0.542	0.659	0.998	0.309	0.455	0.091
$\frac{13}{2}$[606]	0.385	0.422	0.426	0.815	0.274	0.177	0.459	0.402	0.409	0.440	0.476	0.538	0.957	0.287	0.443	0.079
$\frac{3}{2}$[501]	0.349	0.443	0.449	0.231	0.476	0.650	0.576	0.613	0.370	0.421	0.421	0.341	0.160	0.614	0.618	0.618
$\frac{5}{2}$[503]	0.276	0.321	0.398	0.535	0.518	0.509	0.851	0.419	0.275	0.306	0.345	0.410	0.478	0.634	0.842	0.207
$\frac{1}{2}$[501]	0.321	0.342	0.315	0.229	0.432	0.476	0.504	0.695	0.315	0.317	0.296	0.256	0.191	0.529	0.526	0.639

Table 5.3: (continued) c) For deformation $\epsilon_2 = 0.30$.

	$\frac{1}{2}[431]$	$\frac{3}{2}[422]$	$\frac{5}{2}[413]$	$\frac{7}{2}[404]$	$\frac{1}{2}[420]$	$\frac{3}{2}[411]$	$\frac{5}{2}[402]$	$\frac{1}{2}[550]$	$\frac{3}{2}[541]$	$\frac{5}{2}[532]$	$\frac{7}{2}[523]$	$\frac{9}{2}[514]$	$\frac{11}{2}[505]$	$\frac{1}{2}[411]$	$\frac{3}{2}[402]$	$\frac{1}{2}[400]$
$\frac{1}{2}[541]$	0.752	0.514	0.520	0.333	0.621	0.487	0.351	0.631	0.640	0.453	0.481	0.493	0.315	0.528	0.362	0.451
$\frac{3}{2}[532]$	0.828	0.807	0.549	0.505	0.452	0.605	0.452	0.701	0.752	0.900	0.600	0.512	0.530	0.601	0.465	0.605
$\frac{5}{2}[523]$	0.556	0.914	0.766	0.521	0.388	0.556	0.471	0.637	0.700	0.727	0.972	0.647	0.527	0.555	0.477	0.251
$\frac{7}{2}[514]$	0.605	0.582	0.941	0.650	0.414	0.302	0.494	0.581	0.584	0.641	0.682	0.994	0.606	0.322	0.486	0.116
$\frac{1}{2}[530]$	0.649	0.563	0.428	0.400	0.742	0.540	0.373	0.776	0.625	0.502	0.519	0.376	0.383	0.575	0.386	0.492
$\frac{3}{2}[521]$	0.606	0.596	0.437	0.423	0.662	0.683	0.453	0.560	0.640	0.631	0.401	0.408	0.359	0.695	0.471	0.532
$\frac{5}{2}[512]$	0.414	0.557	0.569	0.330	0.376	0.845	0.543	0.392	0.436	0.502	0.581	0.425	0.241	0.840	0.566	0.352
$\frac{1}{2}[660]$	0.710	0.594	0.473	0.334	0.673	0.433	0.343	0.957	0.781	0.648	0.568	0.483	0.401	0.454	0.350	0.429
$\frac{3}{2}[651]$	0.736	0.645	0.503	0.351	0.580	0.498	0.357	0.831	0.900	0.725	0.595	0.518	0.415	0.508	0.367	0.410
$\frac{5}{2}[642]$	0.693	0.722	0.534	0.376	0.394	0.555	0.373	0.667	0.862	0.834	0.661	0.532	0.437	0.550	0.385	0.342
$\frac{7}{2}[633]$	0.559	0.767	0.615	0.412	0.301	0.532	0.403	0.657	0.584	0.897	0.767	0.594	0.460	0.529	0.412	0.248
$\frac{9}{2}[624]$	0.441	0.697	0.719	0.477	0.360	0.387	0.440	0.547	0.664	0.533	0.929	0.697	0.509	0.405	0.439	0.152
$\frac{11}{2}[615]$	0.566	0.446	0.778	0.594	0.381	0.197	0.451	0.556	0.519	0.611	0.520	0.949	0.607	0.221	0.441	0.078
$\frac{1}{2}[521]$	0.590	0.495	0.291	0.321	0.690	0.676	0.367	0.533	0.562	0.500	0.327	0.243	0.252	0.713	0.388	0.590
$\frac{3}{2}[512]$	0.404	0.516	0.540	0.320	0.428	0.852	0.557	0.370	0.408	0.464	0.509	0.426	0.215	0.860	0.581	0.405
$\frac{1}{2}[510]$	0.437	0.277	0.141	0.100	0.567	0.423	0.241	0.484	0.410	0.257	0.132	0.087	0.071	0.446	0.255	0.603
$\frac{7}{2}[503]$	0.436	0.342	0.424	0.543	0.570	0.399	0.855	0.321	0.323	0.328	0.362	0.446	0.462	0.429	0.851	0.124
$\frac{9}{2}[505]$	0.608	0.561	0.542	0.948	0.261	0.131	0.406	0.486	0.509	0.511	0.547	0.612	0.999	0.113	0.399	0.042
$\frac{13}{2}[606]$	0.579	0.506	0.422	0.821	0.205	0.100	0.384	0.488	0.508	0.483	0.518	0.512	0.957	0.074	0.378	0.036
$\frac{3}{2}[501]$	0.351	0.395	0.355	0.190	0.341	0.475	0.530	0.294	0.325	0.354	0.345	0.266	0.148	0.498	0.537	0.614
$\frac{5}{2}[503]$	0.431	0.337	0.403	0.528	0.560	0.422	0.855	0.312	0.315	0.318	0.350	0.413	0.451	0.447	0.852	0.135
$\frac{1}{2}[501]$	0.362	0.386	0.336	0.184	0.359	0.459	0.519	0.309	0.331	0.346	0.326	0.252	0.145	0.484	0.527	0.633

5.4 0[110] pairs and development of collectivity and deformation

Proton - neutron orbital pairs of the type $\Delta K[\Delta N \Delta n_z \Delta \Lambda] = 0[110]$ can be related to the development of collectivity and deformation in nuclei. In order to make this clear we will be using Fig. 5.6 and Table 5.4, which show a schematic illustration of the proton and neutron orbitals of the $Z = 50 - 82$ and $N = 82 - 126$ shells and a list of proton and neutron Nilsson orbitals appearing in different major shells of the nuclear shell model, respectively. Fig. 5.6 was used in Section 3.1 to show that the peaking of δV_{pn} in specific isotopes of Er, Yb, Hf and W, took place when the last proton and last neutron of these nuclei occupied orbitals which differed by $\Delta K[\Delta N \Delta n_z \Delta \Lambda] = 0[110]$. The peaking of δV_{pn} was also related through Fig. 5.5 to the onset of deformation. Here, we shall take these findings a little further.

From Fig. 5.6 we first note that every one of the 16 Nilsson proton orbitals, including the unique parity orbitals (here, the orbitals that stem from the $h_{11/2}$ orbit), has a 0[110] neutron partner. Proton and neutron 0[110] partners are colored the same way and appear to have the same behavior. In Table 5.4, to exhibit the correspondence between 0[110] partner orbitals, the proton orbitals are numerically labelled by their order and the number which precedes the neutron orbitals indicates the neutron partner. A more critical look at Fig. 5.6, reveals a general pattern, not heretofore recognized, namely that these 0[110] pairs fill almost synchronously as the protons and neutrons shells fill. Also, since the behavior of partners is similar in the two shells, ie, similar up- and down- sloping orbits and orbit crossings, the synchronous filling persists both for small and large deformations. For example, for small deformations, one has the successive p-n combinations: 1/2[431]-1/2[541], 3/2[422]-3/2[532], 5/2[413]-5/2[523], 1/2[420]-1/2[530] and so on. For larger deformations, eg for $\epsilon \sim 0.3$, near midshell, for example for the $^{168}_{68}\text{Er}_{100}$, which was used again before, the 18 valence protons and neutrons, except some interchanges of adjacent orbits, fill highly overlapping 0[110] combinations. The same happens for $^{172}_{70}\text{Yb}_{102}$. From Table 5.4 and Fig. 5.6 it is clear that the 20 valence protons and neutrons occupy the lowest 10 proton and neutron orbitals, all of them forming 0[110] pairs. It should be emphasized that proton and neutron orbitals might not be filled in exactly the same order, but once they are filled for a given nucleus, the order is not important any more.

Table 5.4: Nilsson orbitals appearing in different major shells of the nuclear shell model.

	p:28-50		n:50-82		p:50-82		n:82-126		p:82-126		n:126-184
1	1/2[321]	1	1/2[431]	1	1/2[431]	1	1/2[541]	1	1/2[541]	1	1/2[651]
2	3/2[312]	3	1/2[420]	2	3/2[422]	3	1/2[530]	2	3/2[532]	2	3/2[642]
3	1/2[310]	2	3/2[422]	3	1/2[420]	2	3/2[532]	3	1/2[660]	4	1/2[640]
4	3/2[301]	7	1/2[550]	4	1/2[550]	4	1/2[660]	4	1/2[530]	6	5/2[633]
5	5/2[303]	8	3/2[541]	5	3/2[541]	5	3/2[651]	5	3/2[651]	8	3/2[631]
6	1/2[301]	4	3/2[411]	6	5/2[532]	6	5/2[642]	6	5/2[523]	3	1/2[770]
7	1/2[440]	9	5/2[532]	7	5/2[413]	8	3/2[521]	7	5/2[642]	5	3/2[761]
8	3/2[431]	5	5/2[413]	8	3/2[411]	7	5/2[523]	8	3/2[521]	7	5/2[752]
9	5/2[422]	6	1/2[411]	9	7/2[523]	9	7/2[633]	9	7/2[633]	12	5/2[622]
10	7/2[413]		5/2[402]	10	1/2[411]	10	1/2[521]	10	7/2[514]	17	1/2[631]
11	9/2[404]		7/2[404]	11	7/2[404]	12	5/2[512]	11	9/2[624]	9	7/2[743]
		10	7/2[523]	12	5/2[402]	11	7/2[514]	12	5/2[512]	10	7/2[624]
			1/2[400]	13	9/2[514]		7/2[503]	13	9/2[505]	15	7/2[613]
		11	9/2[514]	14	11/2[505]		9/2[505]	14	11/2[615]	11	9/2[734]
			3/2[402]	15	3/2[402]	13	9/2[624]	15	7/2[503]	13	9/2[615]
			11/2[505]	16	1/2[400]	16	1/2[510]	16	13/2[606]	19	1/2[620]
						15	3/2[512]	17	1/2[521]	18	3/2[622]
						14	11/2[615]	18	3/2[512]	14	11/2[725]
							13/2[606]	19	1/2[510]		9/2[604]
							3/2[501]	20	5/2[503]	16	13/2[716]
							5/2[503]	21	3/2[501]		11/2[606]
							1/2[501]	22	1/2[501]	21	3/2[611]
										20	5/2[613]
											15/2[707]
											5/2[602]
										22	1/2[611]
											7/2[604]
											1/2[600]
											3/2[602]

Past midshell, neutron orbitals start to occur, that do not have a 0[110] partner. These are the orbitals that are shown as black dashed lines in the neutron Nilsson diagram of Fig. 5.6. The characteristic of these orbitals is that they all have an up-sloping behavior and they are characterized by $n_z = 0$, that is, they are oblate orbitals that do not contribute to prolate deformation. These $n_z = 0$ neutron orbitals explain the white dots that lie away from the $Z_{val} = N_{val}$ line, in Fig. 5.5 or better they explain the shifts in peaks in δV_{pn} to $N_{val} = Z_{val} + 2$. For example, $^{176}_{72}\text{Hf}_{104}$, has 22 valence protons and neutrons. From Table 5.4 and Fig. 5.6 it is seen that the lowest 10 proton and neutron orbitals are occupied by forming 0[110] pairs. However, the last protons occupy the 7/2[404] orbital and the last neutrons the 5/2[512] orbital, which do not make a 0[110] pair. Thus, no maximum δV_{pn} appears for this nucleus. The maximum appears for the $^{178}_{72}\text{Hf}_{106}$ nucleus (22 valence protons, 24 valence neutrons), where the neutron orbital 7/2[514] is filled, which makes a 0[110] partner with the 7/2[404] proton orbital.

5.5 Possible new pseudoshell approach to heavy nuclei

The synchronous filling of 0[110] pairs in proton and neutron shells is not a characteristic just of the $Z = 50 - 82$ and $N = 82 - 126$ shells, but, as it can be seen from Table 5.4, this characterizes Nilsson orbitals appearing in different major shells of the nuclear shell model. This characteristic may suggest a new coupling scheme, similar in spirit to the idea of pseudo-SU(3) [3, 4], but different in content.

5.5.1 Pseudo-SU(3) model

As has already been mentioned, nuclear shell structure, at least for light nuclei belonging to the sd shell, is not much different from that of the harmonic oscillator which is characterized by SU(3) symmetry. So, the SU(3) model was proposed by Elliott [2] for the description of light nuclei, belonging maximum to the sd shell. However, as the nucleus becomes larger, the spin orbit interaction completely destroys the harmonic oscillator shell structure and new major shells are constructed. The new major shells have the same subshells as the corresponding harmonic oscillator major shells, but the subshell with the largest j is moved to the lower major shell and is "replaced" by the subshell with the largest j of the next harmonic oscillator shell. The subshells in the new major shell which are the same as the corresponding subshells in the harmonic oscillator major shells, are called normal parity orbitals of the new shell. The subshell that comes from the next major shell is called intruder level or abnormal parity level, because it has parity opposite to the other levels in the major shell. For example, the N=3 major shell of the harmonic oscillator (or 28-50 major shell) has the degenerate subshells $2p_{1/2}, 2p_{3/2}, 1f_{5/2}, 1f_{7/2}$, the N=4 major shell (or 50-82 major shell) has the degen-

erate subshells $3s_{1/2}, 2d_{3/2}, 2d_{5/2}, 1g_{7/2}, 1g_{9/2}$, the N=5 major shell (or 82-126 major shell) has the degenerate subshells $3p_{1/2}, 3p_{3/2}, 3f_{5/2}, 3f_{7/2}, 1h_{9/2}, 1h_{11/2}$, the N=6 major shell (or 126-184 major shell) has the degenerate subshells $4s_{1/2}, 3d_{3/2}, 3d_{5/2},$ $2g_{7/2}, 2g_{9/2}, 1i_{11/2}, 1i_{13/2}$ and so on. After the spin orbit coupling is applied, the subshells are split in energy. The N=3 major shell loses the $1f_{7/2}$ subshell which makes its own 20-28 major shell and takes the intruder level $1g_{9/2}$ from the N=4 shell. The N=4 shell having lost the $1g_{9/2}$ subshell, has it replaced by the $1h_{11/2}$ subshell from the N=5 shell. The N=5 shell loses the $1h_{11/2}$ subshell and replaces it by the intruder level $1i_{13/2}$ of the next major shell and so on. The new major shells that are contructed are the 20-28 major shell, comprised by the $1f_{7/2}$ subshell, the 28-50 major shell, comprised by the $2p_{1/2}, 2p_{3/2}, 1f_{5/2}, 1g_{9/2}$ subshells, the 50-82 major shell, comprised by the $3s_{1/2}, 2d_{3/2}, 2d_{5/2}, 1g_{7/2}, 11h_{11/2}$ subshells, the 82-126 major shell, comprised by the $3p_{1/2}, 3p_{3/2}, 3f_{5/2}, 3f_{7/2}, 1h_{9/2}, 1i_{13/2}$ subshells, the 126-184 major shell, comprised by the $4s_{1/2}, 3d_{3/2}, 3d_{5/2}, 2g_{7/2}, 2g_{9/2}, 1i_{11/2}, 1j_{15/2}$ and so on. In an effort to describe this movement of subshells beyond the sd shell, the pseudo SU(3) scheme was developed.

It was observed that the normal parity subshells in the new major shells, those that would belong to the N major shell of the harmonic oscillator, have the same j values as the subshells belonging to the N-1 major shell of the harmonic oscillator. For example, the normal parity orbits of the 50-82 major shell, $3s_{1/2}, 2d_{3/2},$ $2d_{5/2}, 1g_{7/2}$, which would belong to the N=5 harmonic oscillator major shell, have the same j values as the subshells belonging to the N=4 major shell of the harmonic oscillator, $2p_{1/2}, 2p_{3/2}, 1f_{5/2}, 1f_{7/2}$. This suggests a mapping of the values of the l and s of the normal parity orbits $3s_{1/2}, 2d_{3/2}, 2d_{5/2}, 1g_{7/2}$ onto pseudo $\tilde{l}$ and $\tilde{s}$, by keeping j constant, i.e. $j = l + s \rightarrow \tilde{l} + \tilde{s} = j$, so as to get the subshells of the major oscillator shell. For example $s_{1/2}, d_{3/2}, d_{5/2}, g_{7/2} \rightarrow \tilde{p}_{1/2}, \tilde{p}_{3/2}, \tilde{f}_{5/2}, \tilde{f}_{7/2}$. The opposite parity orbital, coming from the next major shell is not taken into account in this mapping. So, in total, for the 28-50 shell, one has the mapping $2p_{1/2},$ $2p_{3/2}, 1f_{5/2} \rightarrow \tilde{s}_{1/2}, \tilde{d}_{3/2}, \tilde{d}_{5/2}$. For the 50-82 shell, one has the mapping $3s_{1/2}, 2d_{3/2},$ $2d_{5/2}, 1g_{7/2} \rightarrow \tilde{p}_{1/2}, \tilde{p}_{3/2}, \tilde{f}_{5/2}, \tilde{f}_{7/2}$. For the 82-126 shell, the mapping is $3p_{1/2}, 3p_{3/2},$ $3f_{5/2}, 3f_{7/2}, 1h_{9/2} \rightarrow \tilde{s}_{1/2}, \tilde{d}_{3/2}, \tilde{d}_{5/2}, \tilde{g}_{7/2}, \tilde{g}_{9/2}$. For the 126-184 shell, the mapping is $4s_{1/2}, 3d_{3/2}, 3d_{5/2}, 2g_{7/2}, 2g_{9/2}, 1i_{11/2} \rightarrow \tilde{p}_{1/2}, \tilde{p}_{3/2}, \tilde{f}_{5/2}, \tilde{f}_{7/2}, \tilde{h}_{9/2}, \tilde{h}_{11/2}$. From the mapping, the angular momentum changes by one and the spin is inverted. In terms of Nilsson quantum numbers, the new Nilsson orbitals would have Λ changed by one unit, either positive or negative, the Σ quantum number would be inverted, but the projection of the total angular momentum, K would be the same. In the Nilsson diagram, the Nilsson levels with their new pseudo symbols, $\tilde{\Omega}[\tilde{N}\tilde{n}_z\tilde{\Lambda}]$, are grouped into pseudo spin orbit doublets having $\tilde{\Omega} = \tilde{\Lambda} \pm 1/2$. This implies that the pseudo spin-orbit splitting is small, so the SU(3) symmetry of the harmonic oscillator is back. It should be noticed that this is applied separately to the proton and neutron major shells.

Without wanting to get into details, in order to apply the pseudo-SU(3) to real

nuclei, one needs to know the symmetry of each shell. For example, if one wanted to apply the pseudo-SU(3) scheme to rare earth nuclei, one should consider the following. The positive parity protons occupy the pseudo-pf shell, which has a U(10) symmetry, possessing an SU(3) subalgebra. The negative parity protons occupy the $1h_{11/2}$ orbital, which has a U(12) symmetry, possessing an Sp(12) subalgebra. The negative parity neutrons occupy the pseudo-sdg shell, which has a U(15) symmetry, possessing an SU(3) subalgebra, while the positive parity neutrons occupy the $1i_{13/2}$ orbital, which has a U(14) symmetry, possessing an Sp(14) subalgebra. Finding the basis states and by selecting an appropriate Hamiltonian, the energies and other observables can be derived for comparison with the experiment.

5.5.2 Approximate SU(3) symmetry

In the new coupling scheme, the idea of 0[110] partners is exploited. In order to understand this idea, one can follow Tables 5.5, 5.6, where the Nilsson orbitals of the major shells created after the spin-orbit interaction and the Nilsson orbitals of the harmonic oscillator major shells, N, are listed. For example, comparing the Nilsson orbitals of the 28-50 major shell with those of the N=3 harmonic oscillator shell, one sees that all orbitals are the same, except for those of the $1g_{9/2}$ and $1f_{7/2}$ subshells, whose orbitals differ by 0[110]. So, one can replace the Nilsson orbitals of the $1g_{9/2}$ subshell with their 0[110] counterparts of the $1f_{7/2}$ subshell of the harmonic oscillator, leaving out the single orbital, 9/2[404], which lies highest in energy and has no 0[110] partner. Then, the 28-50 major shell can be approximated as a pf shell. A similar approximation can also be made in the other major shells as well. So, the 50-82 major shell can be approximated as an sdg shell, plus the single orbital 11/2[505] which stays out. The 82-126 major shell can be considered as an approximate pfh shell, ruling out the single orbital 13/2[606]. The 126-184 major shell can be considered as an approximate sdgi shell, ruling out the single orbital 15/2[707].

In the new coupling scheme, it is clear that the Nilsson orbitals of the normal parity orbits are mapped onto themselves, in other words, they remain intact and those that change are the Nilsson orbitals of the abnormal parity subshell. By this mapping parity is changed, but the projections of angular momentum Λ, spin, Σ and total angular momentum K remain intact. Also, n_z is changed by one unit. As before, one needs to know the symmetries of each approximate shell in the new coupling scheme. The approximate pf shell has a U(10) symmetry, the approximate sdg shell has a U(15) symmetry, the pfh shell has a U(21) symmetry and the sdgi shell has a U(28) symmetry. All algebras have an SU(3) subalgebra. For example, for the rare earth nuclei, in the new coupling scheme, protons occupy the approximate sdg shell, having a U(15) symmetry, and neutrons the approximate pfh shell, having U(21) symmetry. Both symmetries possess SU(3) subalgebras, which can be combined into an SU(3) algebra for the system. Thus, one can work in the scheme

$$U_p(15) \times U_n(21) \supset SU_p(3) \times SU_n(3) \supset SU_((3). \tag{5.16}$$

Table 5.5: Nilsson orbitals appearing in different major shells of the nuclear shell model and in different shells of the 3D harmonic oscillator.

28-50		N=4		50-82		N=5	
2p1/2	1/2[301]	2p1/2	1/2[301]	3s1/2	1/2[411]	3s1/2	1/2[411]
2p3/2	1/2[321]	2p3/2	1/2[321]	2d3/2	1/2[400]	2d3/2	1/2[400]
	3/2[312]		3/2[312]		3/2[402]		3/2[402]
1f5/2	1/2[310]	1f5/2	1/2[310]	2d5/2	1/2[431]	2d5/2	1/2[431]
	3/2[301]		3/2[301]		3/2[422]		3/2[422]
	5/2[303]		5/2[303]		5/2[413]		5/2[413]
1g9/2	1/2[440]	1f7/2	1/2[330]	1g7/2	1/2[420]	1g7/2	1/2[420]
	3/2[431]		3/2[321]		3/2[411]		3/2[411]
	5/2[422]		5/2[312]		5/2[402]		5/2[402]
	7/2[413]		7/2[303]		7/2[404]		7/2[404]
	9/2[404]			1h11/2	1/2[550]	1g9/2	1/2[440]
					3/2[541]		3/2[431]
					5/2[532]		5/2[422]
					7/2[523]		7/2[413]
					9/2[514]		9/2[404]
					11/2[505]		

So, in the new coupling scheme one has two different algebras involved. The existence of an SU(3) subalgebra for the total system allows for an analytical solution relevant to deformed nuclei.

As an example, ^{154}Sm is considered, for which the Nilsson deformation parameter is $\epsilon \approx 0.95, \beta_2 \approx 0.32$ [1, 148]. From Fig. 5.6 it is clear that 6 out of 12 valence protons occupy normal parity orbitals in the 50-82 shell, while the other six occupy $1h_{11/2}$ orbitals. In addition, six out of ten valence neutrons occupy normal parity orbitals in the 82-126 shell, while the other four occupy $1i_{13/2}$ orbitals. In the new coupling scheme all valence protons are accomodated within the [222222] irrep of U(15), while all valence neutrons are accomodated within the [22222] irrep of U(21). The most leading SU(3) irrep of U(15) is the (24,0) irrep, while the most leading SU(3) irrep of U(21) is the (30,4) irrep. Then, the total SU(3) irrep for the system will be (54,4). This symmetry involves all valence protons and all valence neutrons, not only the normal parity ones.

To proceed further, one has to choose a Hamiltonian containing, in addition to the usual quadrupole-quadrupole and the angular momentum terms, SU(3) symmetry preserving third-order and/or fourth-order terms [4, 149].

Table 5.6: Nilsson orbitals appearing in different major shells of the nuclear shell model and in different shells of the 3D harmonic oscillator.

82-126		N=6		126-184		N=7	
3p1/2	1/2[501]	3p1/2	1/2[501]	4s1/2	1/2[611]	4s1/2	1/2[611]
3p3/2	1/2[521]	3p3/2	1/2[521]	3d3/2	1/2[600]	3d3/2	1/2[600]
	3/2[512]		3/2[512]		3/2[602]		3/2[602]
2f5/2	1/2[510]	3f5/2	1/2[510]	3d5/2	1/2[631]	3d5/2	1/2[631]
	3/2[501]		3/2[501]		3/2[622]		3/2[622]
	5/2[503]		5/2[503]		5/2[613]		5/2[613]
2f7/2	1/2[541]	3f7/2	1/2[541]	2g7/2	1/2[620]	2g7/2	1/2[620]
	3/2[532]		3/2[532]		3/2[611]		3/2[611]
	5/2[523]		5/2[523]		5/2[602]		5/2[602]
	7/2[514]		7/2[514]		7/2[604]		7/2[604]
1h9/2	1/2[530]	1h9/2	1/2[530]	2g9/2	1/2[651]	2g9/2	1/2[651]
	3/2[521]		3/2[521]		3/2[642]		3/2[642]
	5/2[512]		5/2[512]		5/2[633]		5/2[633]
	7/2[503]		7/2[503]		7/2[624]		7/2[624]
	9/2[505]		9/2[505]		9/2[615]		9/2[615]
1i13/2	1/2[660]	1h11/2	1/2[550]	1i11/2	1/2[640]	1i11/2	1/2[640]
	3/2[651]		3/2[541]		3/2[631]		3/2[631]
	5/2[642]		5/2[532]		5/2[622]		5/2[622]
	7/2[633]		7/2[523]		7/2[613]		7/2[613]
	9/2[624]		9/2[514]		9/2[604]		9/2[604]
	11/2[615]		11/2[505]		11/2[606]		11/2[606]
	13/2[606]			1j15/2	1/2[770]	1i13/2	1/2[660]
					3/2[761]		3/2[651]
					5/2[752]		5/2[642]
					7/2[743]		7/2[633]
					9/2[734]		9/2[624]
					11/2[725]		11/1[615]
					13/2[716]		13/2[606]
					15/2[707]		

Conclusions

The search for approximate symmetries in collective models of nuclear structure has lead to many different methods by which an approximate symmetry can emerge, their common characteristic being the breaking of a symmetry. We have presented the application of statistical measures of chaos on the energy spectrum and the transition strengths of exhited 0^+ states, for N=175 bosons, in the context of the IBM, around the arc of regularity. The statistical measures of chaos reveal regularity on the U(5)-O(6) leg, due to the common O(5) subalgebra of the two limits and also minimum chaoticity on the arc of regularity, which is in agreement with previous studies performed with much smaller number of bosons and levels with angular momentum $L > 2$. Chaotic behavior dominates in all the other caluated points. As the number of bosons gets larger, the quantum statistical parameters seem to reach steady values, however they always show qualitatively the same results; that the point on the arc of regularity is always more regular than the points away from the arc. The study of chaos as a function of energy showed that the degree of chaos reduces significantly as one moves to the high part of the spectrum, or in other words, as the energy increases. The arc of regularity obviously exists due to some underlying approximate symmetry, which lowers the degree of chaos.

A possible explanation for the existence of the arc of regularity is given by the analytical derivation of a line based on an approximate SU(3) symmetry. This line is extracted by the study of Hamiltonians that in the large boson limit of the IBM, approximately commute with the SU(3) generators. The approximate SU(3) symmetry found, extends from the SU(3) vertex until close to the critical line, following the Alhassid-Whelan arc of regular behavior amidst chaotic regions. That was also the first analytical evidence for the existence of an approximate symmetry inside the symmetry triangle of the IBM. The method can be in general used for algebraic Hamiltonians known to possess symmetries due to existing subalgebras.

The last approximate symmetry, an SU(3) approximate symmetry, was derived in the context of the Nilsson model, with the help of which a new coupling scheme for shell model calculations can be developed, which bears many similarities to the pseudo-SU(3) scheme, though it is much more inclusive. The thought of an approximate SU(3) symmetry came up, after the study of enhanced proton-neutron interactions and their possible explanation as having wavefunctions that greatly overlap. These highly interacting pairs of protons and neutrons, which are responsible for the saturation of deformation in nuclei, have a special relation characterizing

their Nilsson quantum number. They are pairs differing by 0[110]. A closer look at the Nilsson orbitals of the 3D harmonic oscillator shells and those of the nuclear shell model, reveals that Nilsson orbitals are either the same, or differ by 0[110]. A whole new coupling scheme can be developed when the Nilsson orbitals of the nuclear shell model are replaced by their 0[110] counterparts of the 3D harmonic oscillator.

Appendices

Appendix A

Application of statistical measures on energy eigenvalues

The program used for the production of eigenvalues and transition strenghts between the states of the IBM Hamiltonian is the IBAR of R. J. Casperson, which can handle up to 1000 bosons [150]. Once the energies are calculated using IBAR, they need to be unfolded in order to apply the statistical measures, $P(S)$, $\Delta_3(L)$ and $P(y)$. As already mentioned, the statistical measures $P(S)$ and $\Delta_3(L)$ are used for the statistical analysis of the eigenvalues produced by IBAR, while $P(y)$ is used for the statistical analysis of the transition strengths. The way the statistical analysis is performed, is described in this appendix. The puprose, is to find, by fitting, the quantum statistical parameters ω, q, ν of each statistic, which will reveale the amount of chaos of each point studied on the symmetry triangle.

First, one constructs a staircase function of the data, which is the number of energies versus the energies. Then, one fits a sixth order polynomial $N(E)$ to the staircase function. The normalised energies are found as

$$\epsilon_i = N(E_i). \tag{17}$$

Now, one applies the statistical measures $P(S)$ and $\Delta_3(L)$ to the normalised energies.

For the statistical measure $P(S)$, one first finds the normalised spacings $S_i = \epsilon_{i+1} - \epsilon_i$ and then puts them to bins, so an histogram of normalised spacings is produced. Then, one fits the Brody distribution, which is multiplied by a factor A, for scaling reasons $(P_\omega(S) = A\,\alpha(1+\omega)S^\omega exp(-\alpha S^{1+\omega}))$, to the histogram, by minimising the function

$$\chi^2(\omega) = \sum_{i \in bins} \left(\frac{P_{bin}(S_i) - P_\omega(S_i)}{\sigma_i} \right)^2, \tag{18}$$

in order to find the best value of ω. $P_{bin}(S_i)$ is the total number of normalised spacings in the i'th bin and σ_i is the statistical error of the number of elements in each bin, given by $\sigma_i = \sqrt{n_i}$, where n_i is the number of spacings at the i'th bin.

In order to calculate the Δ_3 statistics, in terms of the normalised energies $E_1, E_2, \ldots, E_n$, one uses the function of $\Delta_3(L)$ given in eq. (22) in [89],

$$\Delta_3(\alpha, L) = \frac{n^2}{16} - \frac{1}{L^2}\left(\sum_{i=1}^{n} \epsilon_i\right)^2 + \frac{3n}{2L^2}\left(\sum_{i=1}^{n} \epsilon_i^2\right)$$
$$- \frac{3}{L^4}\left(\sum_{i=1}^{n} \epsilon_i^2\right)^2 + \frac{1}{L}\left(\sum_{i=1}^{n}(n - 2i + 1)\epsilon_i\right), \qquad (19)$$

where $\epsilon_i = E_i - (\alpha + L/2)$ is the measure of the normalised energies with respect to the center of energy interval $(\alpha, \alpha + L)$. One calculates the $\Delta_3(L)$ in the energy intervals of length $L = 0.5, 1, 1.5, \ldots, 10$, which span the whole normalised spectrum, once for energy intervals that start from $\alpha = 0$ and once for energy intervals that start from $\alpha = L/2$. Then, the $\Delta_3(L)$ is found as the average over all the $\Delta_3(\alpha, L)$. In order to find the best value of q, one minimizes the function

$$\Delta(q) = \sum_{Lvalues} [\Delta_3(L) - \Delta_3^q(L)]^2, \qquad (20)$$

where $\Delta_3(L)$ is the value for each energy interval of length L, calculated with the procedure described before, while $\Delta_3^q(L)$ is the expression given by eq. (2.17).

For the last statistical measure, $P(y)$, one needs first to normalize the transition strengths to the local average strengths. The local average strengths are found by using Gaussians of width γ, centered around each level E_i [89, 90, 91, 29],

$$\bar{y}(E, E') = \frac{\sum_{k,l} |\langle k|T|l\rangle|^2 \, exp[-(E - E_k)^2/2\gamma^2] \, exp[-(E' - E_l)^2/2\gamma^2]}{\sum_{k,l} exp[-(E - E_k)^2/2\gamma^2] \, exp[-(E' - E_l)^2/2\gamma^2]}. \qquad (21)$$

The width γ was chosen to be 2. Then, the normalised transition strengths are defined as

$$y_{fi} = \frac{|\langle f|T|i\rangle|^2}{\bar{y}(E = E_i, E' = E_f)}. \qquad (22)$$

In order to calculate the local average strengths and the normalized transition strenghts, one should use the unfolded energies, computed for the statistical measures, $P(S)$ and $\Delta_3(L)$. Then, one should approximate the logarithms of the normalized transition strengths to bins and produce an histogram of normalized transition strengths. Then, the interpolating function

$$P_\nu(y) = A \left(\frac{\nu}{2 < y >}\right)^{\nu/2} \frac{y^{\frac{\nu}{2} - 1} exp(-\nu y/2 < y >)}{\Gamma\left(\frac{\nu}{2}\right)}, \qquad (23)$$

where A is a factor added for scaling reasons, is fitted to the histogram, by minimizing the function

$$\chi^2(\nu) = \sum_{i \in bins} \left(\frac{P_{bin}(y_i) - P_\nu(y_i)}{\sigma_i}\right)^2 \qquad (24)$$

in order to find the best value of ν. However, since the y_{fi}s are the logarithms of the normalized transition strengths, one should change the variable y of the intepolating function (7) to $z = \log_{10}(y)$ and use for the fitting the form of the interpolating function after the change of variable. $P_{bin}(y_i)$ is the total number of the logarithms of the normalized transition strengths in the i'th bin and σ_i is, as already explained for the statistical measure $P(S)$, the statistical error of the number of elements in each bin.

Appendix B

Commutation Relations

We list here the commutation relations needed for obtaining the results of Sections 3–6. They are obtained through standard angular momentum coupling techniques [151].

$$[\hat{n}_d, (d^\dagger s + s^\dagger \tilde{d})_\xi^{(2)}] = (d^\dagger s - s^\dagger \tilde{d})_\xi^{(2)}, \tag{25}$$

$$[(d^\dagger \tilde{d})_\xi^{(2)}, (d^\dagger s + s^\dagger \tilde{d})_\nu^{(2)}] = (2\xi 2\nu|2\xi+\nu)(d^\dagger s - s^\dagger \tilde{d})_{\xi+\nu}^{(2)}, \tag{26}$$

$$[\hat{n}_d, (d^\dagger \tilde{d})_\xi^{(k)}] = 0, \quad k = 0,1,2,3,4, \tag{27}$$

$$[(d^\dagger \tilde{d})_\xi^{(2)}, (d^\dagger \tilde{d})_\nu^{(2)}] = -10 \sum_{k=1,3} (2\xi 2\nu|k\xi+\nu) \begin{Bmatrix} 2 & 2 & k \\ 2 & 2 & 2 \end{Bmatrix} (d^\dagger \tilde{d})_{\xi+\nu}^{(k)}, \tag{28}$$

$$[(d^\dagger s + s^\dagger \tilde{d})_\xi^{(2)}, (d^\dagger s + s^\dagger \tilde{d})_\nu^{(2)}] = 2 \sum_{k=1,3} (2\xi 2\nu|k\xi+\nu)(d^\dagger \tilde{d})_{\xi+\nu}^{(k)}, \tag{29}$$

$$[(d^\dagger s + s^\dagger \tilde{d})_\xi^{(2)}, (d^\dagger \tilde{d})_\nu^{(1)}] = -\sqrt{\frac{3}{5}}(2\xi 1\nu|2\xi+\nu)(d^\dagger s + s^\dagger \tilde{d})_{\xi+\nu}^{(2)}, \tag{30}$$

$$[(d^\dagger s + s^\dagger \tilde{d})_\xi^{(2)}, (d^\dagger \tilde{d})_\nu^{(3)}] = -\sqrt{\frac{7}{5}}(2\xi 3\nu|2\xi+\nu)(d^\dagger s + s^\dagger \tilde{d})_{\xi+\nu}^{(2)}, \tag{31}$$

$$[(d^\dagger \tilde{d})_\xi^{(1)}, (d^\dagger \tilde{d})_\nu^{(1)}] = -\frac{1}{\sqrt{5}}(1\xi 1\nu|1\xi+\nu)(d^\dagger \tilde{d})_{\xi+\nu}^{(1)}, \tag{32}$$

$$[(d^\dagger \tilde{d})_\xi^{(2)}, (d^\dagger \tilde{d})_\nu^{(1)}] = 2\sqrt{15}(2\xi 1\nu|2\xi+\nu) \begin{Bmatrix} 2 & 2 & 1 \\ 2 & 2 & 2 \end{Bmatrix} (d^\dagger \tilde{d})_{\xi+\nu}^{(2)}, \tag{33}$$

$$[(d^\dagger \tilde{d})_\xi^{(2)}, (d^\dagger \tilde{d})_\nu^{(3)}] = 2\sqrt{35} \sum_{k=2,4} (2\xi 3\nu|k\xi+\nu) \begin{Bmatrix} 2 & 3 & k \\ 2 & 2 & 2 \end{Bmatrix} (d^\dagger \tilde{d})_{\xi+\nu}^{(k)}. \tag{34}$$

Appendix C

Calculation of commutators of IBA generators

As already mentioned in Section 4.1.1, in order to calculate the commutation relations, the expression found in [6], Eq. (2.6) or in [15], Eq. (7.51) is used

$$[G_\kappa^{(k)}(l,l'), G_{\kappa'}^{(k')}(l'',l''')] = \sum_{k'',\kappa''} \sqrt{(2k+1)(2k'+1)}(k\kappa k'\kappa'|k''\kappa'')(-1)^{k-k'}$$

$$\left[(-1)^{k+k'+k''} \begin{Bmatrix} k & k' & k'' \\ l''' & l & l' \end{Bmatrix} \delta_{l'l''} G_{\kappa''}^{(k'')}(l,l''') - \begin{Bmatrix} k & k' & k'' \\ l'' & l' & l \end{Bmatrix} \delta_{ll'''} G_{\kappa''}^{(k'')}(l'',l') \right], \quad (35)$$

where,
$$G_\kappa^{(k)}(l,l') = (b_l^\dagger \tilde{b}_{l'})_\kappa^{(k)}, \qquad (l,l'=0,2). \quad (36)$$

In this expression, one needs to calculate Glebsch-Gordan coefficients, $(l_1 m_1 l_2 m_2 | l_3 m_3)$, which are related to 3-j symbols through the relation

$$\begin{pmatrix} l_1 & l_2 & l_3 \\ m_1 & m_2 & m_3 \end{pmatrix} = \frac{(-1)^{l_1-l_2-m_3}}{\sqrt{2l_3+1}} (l_1 m_1 l_2 m_2 | l_3 m_3) \quad (37)$$

and 6-j symbols
$$\begin{Bmatrix} l_1 & l_2 & l_3 \\ m_1 & m_2 & m_3 \end{Bmatrix}. \quad (38)$$

If one wants, for some reason, to do the calculations "the hard way", then the symmetry relations of the Glebsch-Gordan coefficients, 3-j and 6-j symbols are needed, as well as the expressions given on pages 125-127 and 130-132 of Ref. [151] for the calculation of 3-j and 6-j symbols. For the sake of completeness we give the symmetry relations mentioned before.

The symmetry relations for the Glebsch-Gordan coefficients are:

$$< l_1 m_1 l_2 m_2 | lm >= (-1)^{l_1+l_2-l} < l_2 m_2 l_1 m_1 | lm >, \quad (39)$$

$$< l_1 m_1 l_2 m_2 | l_3 m_3 >= (-1)^{l_2+m_2} \sqrt{\frac{2l_3+1}{2l_1+1}} < l_2 -m_2 l_3 m_3 | l_1 m_1 >, \quad (40)$$

$$< l_1 m_1 l_2 m_2 | l_3 m_3 > = (-1)^{l_1 - m_1} \sqrt{\frac{2l_3 + 1}{2l_2 + 1}} < l_3 m_3 l_1 - m_1 | l_2 m_2 > . \tag{41}$$

The symmetry relations for the 3-j symbols are:

$$\begin{pmatrix} l_1 & l_2 & l_3 \\ m_1 & m_2 & m_3 \end{pmatrix} = \begin{pmatrix} l_2 & l_3 & l_1 \\ m_2 & m_3 & m_1 \end{pmatrix} = \begin{pmatrix} l_3 & l_1 & l_2 \\ m_3 & m_1 & m_2 \end{pmatrix} \tag{42}$$

which means that the 3-j symbol remains invariant by an even permutation of its columns and

$$(-1)^{l_1 + l_2 + l_3} \begin{pmatrix} l_1 & l_2 & l_3 \\ m_1 & m_2 & m_3 \end{pmatrix} = \begin{pmatrix} l_2 & l_1 & l_3 \\ m_2 & m_1 & m_3 \end{pmatrix}$$

$$= \begin{pmatrix} l_1 & l_3 & l_2 \\ m_1 & m_3 & m_2 \end{pmatrix} = \begin{pmatrix} l_3 & l_2 & l_1 \\ m_3 & m_2 & m_1 \end{pmatrix} \tag{43}$$

so that every odd permutation of its columns introduces a factor $(-1)^{l_1 + l_2 + l_3}$.

Last, the symmetry relations of the 6-j symbols have the following characteristics,

$$\begin{Bmatrix} l_1 & l_2 & l_3 \\ l_4 & l_5 & l_6 \end{Bmatrix} = \begin{Bmatrix} l_2 & l_3 & l_1 \\ l_5 & l_6 & l_4 \end{Bmatrix} = \begin{Bmatrix} l_3 & l_1 & l_2 \\ l_6 & l_4 & l_5 \end{Bmatrix}$$

$$= \begin{Bmatrix} l_2 & l_1 & l_3 \\ l_5 & l_4 & l_6 \end{Bmatrix} = \begin{Bmatrix} l_1 & l_3 & l_2 \\ l_4 & l_6 & l_6 \end{Bmatrix} = \begin{Bmatrix} l_3 & l_2 & l_1 \\ l_6 & l_5 & l_4 \end{Bmatrix}. \tag{44}$$

The 6-j symbol remains invariant by an even or odd permutation of its columns and

$$\begin{Bmatrix} l_1 & l_2 & l_3 \\ l_4 & l_5 & l_6 \end{Bmatrix} = \begin{Bmatrix} l_1 & l_5 & l_6 \\ l_4 & l_2 & l_3 \end{Bmatrix} \tag{45}$$

also remains invariant if two columns get upside down simultaneously.

As an example, we are going to explicitly derive Eq. (4.8). The commutator of the first part of the Hamiltonian with the quadrupole operators is

$$\begin{aligned} [\hat{H}_1, \hat{Q}^{(2)}_{SU(3),\nu}] &= c\eta[\hat{n}_d, \hat{Q}^{(2)}_{SU(3),\nu}] = c\eta[\sqrt{5}(d^\dagger \tilde{d})^{(0)}_0, \hat{Q}^{(2)}_{SU(3),\nu}] \\ &= c\eta[\sqrt{5}(d^\dagger \tilde{d})^{(0)}_0, (s^\dagger \tilde{d})^{(2)}_\nu + (d^\dagger \tilde{s})^{(2)}_\nu - \frac{\sqrt{7}}{2}(d^\dagger \tilde{d})^{(2)}_\nu] \\ &= c\eta\sqrt{5}[(d^\dagger \tilde{d})^{(0)}_0, (s^\dagger \tilde{d})^{(2)}_\nu] + c\eta\sqrt{5}[(d^\dagger \tilde{d})^{(0)}_0, (d^\dagger \tilde{s})^{(2)}_\nu] \\ &\quad - c\eta\frac{\sqrt{35}}{2}[(d^\dagger \tilde{d})^{(0)}_0, (d^\dagger \tilde{d})^{(2)}_\nu]. \end{aligned} \tag{46}$$

In this form, we can directly apply Eq. (35) to the three terms of (46). For the first term, $[(d^\dagger \tilde{d})^{(0)}_0, (s^\dagger \tilde{d})^{(2)}_\nu]$, one has $k = 0$, $k' = 2$, $k'' = 2$, $\kappa = 0$, $\kappa' = \nu$, $\kappa'' = \nu$, $l = l' = l''' = 2$, $l'' = 0$ and $\delta_{l'l''} = 0$, $\delta_{ll'''} = 1$, so that

$$[(d^\dagger \tilde{d})^{(0)}_0, (s^\dagger \tilde{d})^{(2)}_\nu] = \sum_\nu \sqrt{5}(002\nu|2\nu)\left[-(-1)^{2+0+0+2}\begin{Bmatrix} 0 & 2 & 2 \\ 0 & 2 & 2 \end{Bmatrix} G^{(2)}_\nu(0,2)\right], \tag{47}$$

where we have applied the fact that $\kappa + \kappa' = \kappa''$ and that when one couples angular momentum 2 with angular momentum 0, $G(0,2)$, the only possible result is that they couple to angular momentum 2, $k'' = 2$, so that finaly one has,

$$[(d^\dagger \tilde{d})_0^{(0)}, (s^\dagger \tilde{d})_\nu^{(2)}] = -\frac{1}{\sqrt{5}}(s^\dagger \tilde{d})_\nu^{(2)}. \tag{48}$$

The second term, $[(d^\dagger \tilde{d})_0^{(0)}, (d^\dagger \tilde{s})_\nu^{(2)}]$, has $k = 0$, $k' = 2$, $k'' = 2$, $\kappa = 0$, $\kappa' = \nu$, $\kappa'' = \nu$, $l = l' = l'' = 2$, $l''' = 0$ and $\delta_{l'l''} = 1$, $\delta_{ll'''} = 0$, so that

$$\begin{aligned}
[(d^\dagger \tilde{d})_0^{(0)}, (d^\dagger \tilde{s})_\nu^{(2)}] &= \sum_\nu \sqrt{5}(002\nu|2\nu)(-1)^{2+0+2} \begin{Bmatrix} 2 & 0 & 2 \\ 2 & 0 & 2 \end{Bmatrix} G_\nu^{(2)}(2,0) \\
&= \frac{1}{\sqrt{5}}(d^\dagger \tilde{s})_\nu^{(2)}. \tag{49}
\end{aligned}$$

Then for the third and last term, $[(d^\dagger \tilde{d})_0^{(0)}, (d^\dagger \tilde{d})_\nu^{(2)}]$, one has $k = 0$, $k' = 2$, $k'' = 2$, $\kappa = 0$, $\kappa' = \nu$, $\kappa'' = \nu$, $l = l' = l'' = l''' = 2$ and $\delta_{l'l''} = 1$, $\delta_{ll'''} = 1$, so that

$$[(d^\dagger \tilde{d})_0^{(0)}, (d^\dagger \tilde{s})_\nu^{(2)}] = \sum_\nu \sqrt{5}(002\nu|2\nu) \left[(-1)^{2+2+2} \begin{Bmatrix} 2 & 2 & 2 \\ 2 & 0 & 2 \end{Bmatrix} G_\nu^{(2)}(2,2) \right.$$

$$\left. -(-1)^{2+2+0+2} \begin{Bmatrix} 2 & 2 & 2 \\ 0 & 2 & 2 \end{Bmatrix} G_\nu^{(2)}(2,2) \right] = 0. \tag{50}$$

In total, all three terms of Eq. (46) give

$$\begin{aligned}
c\eta[\hat{n}_d, \hat{Q}_{SU(3),\nu}^{(2)}] &= -c\eta\sqrt{5}\frac{1}{\sqrt{5}}(s^\dagger \tilde{d})_\nu^{(2)} + c\eta\sqrt{5}\frac{1}{\sqrt{5}}(d^\dagger \tilde{s})_\nu^{(2)} \\
&= c\eta(d^\dagger \tilde{s} - s^\dagger \tilde{d})_\nu^{(2)}, \tag{51}
\end{aligned}$$

which is indeed Eq. (4.8).

Appendix D

Analytic derivation of Eq. (4.15)

We will show the analytic derivation of Eq. (4.15) from Eq. (4.13), which we rewrite here for convenience,

$$[\hat{Q}_\chi^{(2)} \cdot \hat{Q}_\chi^{(2)}, \hat{Q}_{SU(3),\nu}^{(2)}] = \sum_\xi (-1)^\xi \left\{ [\hat{Q}_{SU(3),\xi}^{(2)}, \hat{Q}_{SU(3),\nu}^{(2)}]\hat{Q}_{\chi,-\xi}^{(2)} + \hat{Q}_{\chi,\xi}^{(2)}[\hat{Q}_{SU(3),-\xi}^{(2)}, \hat{Q}_{SU(3),\nu}^{(2)}] \right.$$

$$\left. + \left(\chi + \frac{\sqrt{7}}{2}\right) \left\{ [(d^\dagger \tilde{d})_\xi^{(2)}, \hat{Q}_{SU(3),\nu}^{(2)}]\hat{Q}_{\chi,-\xi}^{(2)} + \hat{Q}_{\chi,\xi}^{(2)}[(d^\dagger \tilde{d})_{-\xi}^{(2)}, \hat{Q}_{SU(3),\nu}^{(2)}] \right\} \right\}. \qquad (52)$$

Eq. (4.13) has four terms which need to be "expanded" in order to get Eq. (4.15). For the first term, $[\hat{Q}_{SU(3),\xi}^{(2)}, \hat{Q}_{SU(3),\nu}^{(2)}]\hat{Q}_{\chi,-\xi}^{(2)}$, we first need to calculate the commutator $[\hat{Q}_{SU(3),\xi}^{(2)}, \hat{Q}_{SU(3),\nu}^{(2)}]$, which is

$$[\hat{Q}_{SU(3),\xi}^{(2)}, \hat{Q}_{SU(3),\nu}^{(2)}] =$$
$$[(s^\dagger \tilde{d} + d^\dagger \tilde{s})_\xi^{(2)} - \tfrac{\sqrt{7}}{2}(d^\dagger \tilde{d})_\xi^{(2)}, (s^\dagger \tilde{d} + d^\dagger \tilde{s})_\nu^{(2)} - \tfrac{\sqrt{7}}{2}(d^\dagger \tilde{d})_\nu^{(2)}] =$$
$$[(s^\dagger \tilde{d})_\xi^{(2)}, (s^\dagger \tilde{d})_\nu^{(2)}] + [(s^\dagger \tilde{d})_\xi^{(2)}, (d^\dagger \tilde{s})_\nu^{(2)}] - \tfrac{\sqrt{7}}{2}[(s^\dagger \tilde{d})_\xi^{(2)}, (d^\dagger \tilde{d})_\nu^{(2)}]$$
$$+[(d^\dagger \tilde{s})_\xi^{(2)}, (s^\dagger \tilde{d})_\nu^{(2)}] + [(d^\dagger \tilde{s})_\xi^{(2)}, (d^\dagger \tilde{s})_\nu^{(2)}] - \tfrac{\sqrt{7}}{2}[(d^\dagger \tilde{s})_\xi^{(2)}, (d^\dagger \tilde{d})_\nu^{(2)}]$$
$$-\tfrac{\sqrt{7}}{2}[(d^\dagger \tilde{d})_\xi^{(2)}, (s^\dagger \tilde{d})_\nu^{(2)}] - \tfrac{\sqrt{7}}{2}[(d^\dagger \tilde{d})_\xi^{(2)}, (d^\dagger \tilde{s})_\nu^{(2)}] + \tfrac{7}{4}[(d^\dagger \tilde{d})_\xi^{(2)}, (d^\dagger \tilde{d})_\nu^{(2)}]. \qquad (53)$$

With the help of (35) we have

$$[\hat{Q}_{SU(3),\xi}^{(2)}, \hat{Q}_{SU(3),\nu}^{(2)}] =$$
$$\sqrt{5}(2\xi 2\nu|0\xi + \nu)(s^\dagger \tilde{s})_{\xi+\nu}^{(0)} - \sum_{k''}(-1)^{k''}(2\xi 2\nu|k''\xi + \nu)(d^\dagger \tilde{d})_{\xi+\nu}^{(k'')}$$
$$-\tfrac{\sqrt{7}}{2}(2\xi 2\nu|2\xi + \nu)(s^\dagger \tilde{d})_{\xi+\nu}^{(2)} + \sum_{k''}(2\xi 2\nu|k''\xi + \nu)(d^\dagger \tilde{d})_{\xi+\nu}^{(k'')}$$
$$+\tfrac{\sqrt{7}}{2}(2\xi 2\nu|2\xi + \nu)(d^\dagger \tilde{s})_{\xi+\nu}^{(2)} - \sqrt{5}(2\xi 2\nu|0\xi + \nu)(s^\dagger \tilde{s})_{\xi+\nu}^{(0)}$$

89

$$+\tfrac{\sqrt{7}}{2}(2\xi 2\nu|2\xi+\nu)(s^\dagger\tilde{d})^{(2)}_{\xi+\nu}-\tfrac{\sqrt{7}}{2}(2\xi 2\nu|2\xi+\nu)(d^\dagger\tilde{s})^{(2)}_{\xi+\nu}$$

$$-\tfrac{7}{4}10\sum_{k''=1,3}(2\xi 2\nu|k''\xi+\nu)\begin{Bmatrix}2&2&2\\k''&2&2\end{Bmatrix}(d^\dagger\tilde{d})^{(k'')}_{\xi+\nu}=$$

$$\sum_{k''}(2\xi 2\nu|k''\xi+\nu)(d^\dagger\tilde{d})^{(k'')}_{\xi+\nu}(1-(-1)^{k''})$$

$$-\tfrac{35}{2}\sum_{k''=1,3}(2\xi 2\nu|k''\xi+\nu)\begin{Bmatrix}2&2&2\\k''&2&2\end{Bmatrix}(d^\dagger\tilde{d})^{(k'')}_{\xi+\nu}. \tag{54}$$

From the first sum one has $k''=1,3$, due to the $(1-(-1)^{k''})$ term. After calculating the 6-j symbol one is left with

$$[\hat{Q}^{(2)}_{SU(3),\xi},\hat{Q}^{(2)}_{SU(3),\nu}]=\frac{15}{4}(2\xi 2\nu|1\xi+\nu)(d^\dagger\tilde{d})^{(1)}_{\xi+\nu}. \tag{55}$$

However, we need the product $[\hat{Q}^{(2)}_{SU(3),\xi},\hat{Q}^{(2)}_{SU(3),\nu}]\hat{Q}^{(2)}_{\chi,-\xi}$, which is

$$[\hat{Q}^{(2)}_{SU(3),\xi},\hat{Q}^{(2)}_{SU(3),\nu}]\hat{Q}^{(2)}_{\chi,-\xi}=\frac{15}{4}(2\xi 2\nu|1\xi+\nu)(d^\dagger\tilde{d})^{(1)}_{\xi+\nu}\hat{Q}^{(2)}_{\chi,-\xi}. \tag{56}$$

For this, we need to recouple the angular momentums by using the tensor product (4.14)

$$[T^{(k_1)}\times T^{(k_2)}]^{(k)}_q=\sum_{q_1=-k_1}^{k_1}\sum_{q_2=-k_2}^{k_2}<k_1q_1k_2q_2|kq>T^{(k_1)}_{q_1}T^{(k_2)}_{q_2}. \tag{57}$$

In our case, it is obvious that, $k_1=1$, $q_1=\xi+\nu$, $k_2=2$, $q_2=-\xi$, so one needs to use Eq. (41) in order to rearrange in a desired way the Glebsch-Gordan coefficients, so as to get

$$\begin{aligned}[\hat{Q}^{(2)}_{SU(3),\xi},\hat{Q}^{(2)}_{SU(3),\nu}]\hat{Q}^{(2)}_{\chi,-\xi}&=\frac{15}{4}(-1)^{-\xi}\sqrt{\frac{3}{5}}(1\ \xi+\nu\ 2\ -\xi|2\ \nu)(d^\dagger\tilde{d})^{(1)}_{\xi+\nu}\hat{Q}^{(2)}_{\chi,-\xi}\\&=(-1)^{-\xi}\frac{3}{4}\sqrt{15}\left((d^\dagger\tilde{d})^{(1)}\hat{Q}^{(2)}_{\chi}\right)^{(2)}_{\nu}.\end{aligned} \tag{58}$$

The case of $\hat{Q}^{(2)}_{\chi,\xi}[\hat{Q}^{(2)}_{SU(3),-\xi},\hat{Q}^{(2)}_{SU(3),\nu}]$ is exactly the same as the one just examined, if we replace ξ by $-\xi$, so it is

$$\begin{aligned}\hat{Q}^{(2)}_{\chi,\xi}[\hat{Q}^{(2)}_{SU(3),-\xi},\hat{Q}^{(2)}_{SU(3),\nu}]&=\frac{15}{4}(2\ -\xi\ 2\ -\nu|1\ -\xi+\nu)\hat{Q}^{(2)}_{\chi,\xi}(d^\dagger\tilde{d})^{(1)}_{-\xi+\nu}\\&=-(-1)^\xi\sqrt{\frac{3}{5}}\frac{15}{4}(2\ \xi\ 1\ -\xi+\nu|2\ \nu)\hat{Q}^{(2)}_{\chi,\xi}(d^\dagger\tilde{d})^{(1)}_{-\xi+\nu}\\&=-(-1)^\xi\frac{3}{4}\sqrt{15}\left(\hat{Q}^{(2)}_{\chi}(d^\dagger\tilde{d})^{(1)}\right)^{(2)}_{\nu}.\end{aligned} \tag{59}$$

We see that if we add Eqs. (58) and (59) and replace them to (4.13), we take one part of Eq. (4.15). By applying the same method, as above, to the other two terms of Eq. (4.13), $[(d^\dagger\tilde{d})^{(2)}_{\xi},\hat{Q}^{(2)}_{SU(3),\nu}]\hat{Q}^{(2)}_{\chi,-\xi}$ and $\hat{Q}^{(2)}_{\chi,\xi}[(d^\dagger\tilde{d})^{(2)}_{-\xi},\hat{Q}^{(2)}_{SU(3),\nu}]$, one gets the full Eq. (4.15).

Appendix E

İnőnű - Wigner contraction

İnőnű and Wigner [110] had described the contraction as the operation of obtaining a new group (or a new algebra associated with the group), by a singular transformation of the generators (or basis vectors of the algebra) of the old group. The X_i's, $i = 1, 2, \ldots, n$ can either be refered to as the generators of a group G, where n is the number of generators, or as the basis vectors of the associatied with the group G, algebra g [152]. From now on we will be sticking with the first meaning.

Let X_i be the generators of the group G, which obey the commutation relations

$$[X_i, X_j] = c_{i,j}^k X_k. \tag{60}$$

If one subjects the X_i to a nonsingular transformation U, one obtains new generators Y_i,

$$Y_i = U_i^j X_j. \tag{61}$$

U has the form

$$U = \begin{pmatrix} I & 0 \\ 0 & \epsilon I \end{pmatrix}, \tag{62}$$

with

$$U^{-1} = \begin{pmatrix} I & 0 \\ 0 & I/\epsilon \end{pmatrix}, \tag{63}$$

where I, ϵI and I/ϵ are $r \times r$ and $(n-r) \times (n-r)$ matrices respectively. As long as $0 < \epsilon < \epsilon_0$, the determinant of U will be different from zero and thus, the transformation will be non-singular.

The generatos Y_i will have the same commutation relations as the X_i's, but with different structure constants, C_{ij}^k, up to a constant. The structure constants with respect to the new basis will be

$$
\begin{aligned}
{[Y_i, Y_j]} &= C_{i,j}^k Y_k \Rightarrow \\
\left[U_i^m X_m, U_j^n X_n \right] &= C_{i,j}^k U_k^l X_l \Rightarrow \\
U_i^m U_j^n c_{mn}^l (U^{-1})_l^k &= C_{i,j}^k.
\end{aligned}
\tag{64}
$$

But, what happens of U is singular, that is, if $\epsilon \to 0$? In this limit we have contraction and the transformation U leads to a new group, the contacted group G'. For convenience, it is useful to symbolise the operators that transform using the upper left part, I, of the the tranformation matrix U, as X_α, X_β, X_γ, ... and those that transform from the lower right part, ϵI, as X_i, X_j, X_k,.... Then, one has

$$\begin{aligned} UX_\alpha &= X_\alpha = Y_\alpha \\ UX_i &= \epsilon X_i = Y_i. \end{aligned} \tag{65}$$

From (62), (63) and (64), one can find the relationship between the old and the new structure constants. Since, only the diagonal elements of U are diffenent from zero, the relationship between the old and the new structure constants becomes

$$C'^\lambda_{\mu,\nu} = U^\mu_\mu U^\nu_\nu c^\lambda_{\mu,\nu} (U^{-1})^\lambda_\lambda. \tag{66}$$

It turns out that the result depends only on where μ, ν and λ belong, that is to the upper left or lower right part of U. Then, one has the following cases at the contraction limit.

$$\begin{aligned} C^k_{ij} &= \epsilon\epsilon c^k_{ij}\epsilon^{-1} = \epsilon c^k_{ij} \to 0 \tag{67} \\ C^\alpha_{ij} &= \epsilon\epsilon c^\alpha_{ij} 1 = \epsilon^2 c^\alpha_{ij} \to 0 \tag{68} \\ C^j_{\alpha i} &= 1\epsilon c^j_{\alpha i}\epsilon^{-1} = c^j_{\alpha i} \tag{69} \\ C^\beta_{\alpha i} &= 1\epsilon c^\beta_{\alpha i} 1 = \epsilon c^\beta_{\alpha i} \to 0 \tag{70} \\ C^\gamma_{\alpha\beta} &= 11 c^\gamma_{\alpha\beta} 1 = c^\gamma_{\alpha\beta} \tag{71} \\ C^i_{\alpha\beta} &= 11 c^i_{\alpha\beta}\epsilon^{-1} = \frac{1}{\epsilon} c^i_{\alpha\beta}. \tag{72} \end{aligned}$$

The last one converges only if $c^i_{\alpha\beta} = 0$, so, $C^i_{\alpha\beta} = 0$. From the above series of equations, the last two say that the X_α and Y_α which are closed under commutation span sugroups of G and G' respectively. The third from the end sais that the Y_i span an invariant subgroup of G', which is also abelian, (derived by the first equation).

The contractions of SU(3) to R^5[SO(3)] and O(6) to R^5[SO(5)] are based on the idea of contraction of groups of İnőnű and Wigner and are discussed in more detail in appendices F and G, respectively.

Appendix F

The SU(3)→ [R^5]SO(3) contraction

The SU(3)→ [R^5]SO(3) contraction has been studied in Refs. [111, 112]. It is a procedure in which the full SU(3) algebra, consisting of eight noncommuting generators, is reduced into an SO(3) algebra (consisting of three noncommuting generators), accompanied by five mutually commuting operators (the quadrupole operators). This simplification occurs in the limit of large boson number, in which, in SU(3), all intrinsic excitations rise in energy, isolating the ground state band so that SU(3) goes over, approximately, into a simple rigid rotator. The resulting algebraic structure is, indeed, known [153] to be the algebra of the rigid rotator. The scaling of Ref. [6] is used here. (The quadrupole operator in Refs. [111, 112] is $2\sqrt{2}$ times the quadrupole operator of Ref. [6].)

The SU(3) commutation relations read

$$[\hat{L}_\xi, \hat{L}_\nu] = -\sqrt{2}(1\xi 1\nu|1\xi+\nu)\hat{L}_{\xi+\nu}, \tag{73}$$

$$[\hat{L}_\xi, \hat{Q}^{(2)}_{SU(3),\nu}] = -\sqrt{6}(1\xi 2\nu|2\xi+\nu)\hat{Q}^{(2)}_{SU(3),\xi+\nu}, \tag{74}$$

$$[\hat{Q}^{(2)}_{SU(3),\xi}, \hat{Q}^{(2)}_{SU(3),\nu}] = \frac{3}{4}\sqrt{\frac{5}{2}}(2\xi 2\nu|1\xi+\nu)\hat{L}_{\xi+\nu}. \tag{75}$$

The second order Casimir operator is

$$\hat{C}_2[SU(3)] = \frac{2}{3}\left[2\hat{Q}_{SU(3)}\cdot\hat{Q}_{SU(3)} + \frac{3}{4}\hat{L}\cdot\hat{L}\right], \tag{76}$$

while its eigenvalues in the Elliott basis, (λ,μ), are

$$C_2(\lambda,\mu) = \frac{2}{3}(\lambda^2 + \mu^2 + \lambda\mu + 3\lambda + 3\mu). \tag{77}$$

If we consider, for example, SU(3) irreducible representations (irreps) with large values of $C_2(\lambda,\mu)$ - that is, for large boson numbers- we can rescale the quadrupole operator as

$$\hat{q}^{(2)}_{SU(3),\xi} = \frac{\hat{Q}^{(2)}_{SU(3),\xi}}{\sqrt{C_2(\lambda,\mu)}}. \tag{78}$$

The first two commutation relations remain unchanged by the rescaling, while the last one becomes

$$[\hat{q}^{(2)}_{SU(3),\xi}, \hat{q}^{(2)}_{SU(3),\nu}] = \frac{3}{4}\sqrt{\frac{5}{2}}(2\xi 2\nu|1\xi+\nu)\frac{\hat{L}_{\xi+\nu}}{C_2(\lambda,\mu)}. \tag{79}$$

Then, in the limit of large values of $C_2(\lambda,\mu)$, one gets

$$[\hat{q}^{(2)}_{SU(3),\xi}, \hat{q}^{(2)}_{SU(3),\nu}] = 0. \tag{80}$$

This result, which is obtained for large boson numbers, is called the contraction of SU(3) to [R^5]SO(3), where [R^5]SO(3) is the algebra of the rigid rotator[153], generated by the angular momentum operators of SO(3) and the five commuting operators $\hat{q}^{(2)}_{SU(3),\xi}$, $\xi = -2,-1,0,1,2$.

An immediate consequence of Eqs. (76) and (77) is that, in the contraction limit, terms propotional to the angular momentum $\hat{L}$ can be ignored. In the IBA framework, in which $\hat{L}$ is proportional to $(d^\dagger \tilde{d})^{(1)}$, as seen in Eq. (4.4), this implies that $(d^\dagger \tilde{d})^{(1)}$ terms can be ignored.

In the limit of large values of $C_2(\lambda,\mu)$ and $\lambda \geq \mu$, the intrinsic quadrupole moments become [112, 154]

$$q_0 = \frac{1}{2\sqrt{2}}(2\lambda + \mu + 3), \quad q_2 = \frac{1}{4}\sqrt{3(\mu - K)(\mu + K + 2)}, \tag{81}$$

where K is the eigenvalue of the angular momentum projection on the body-fixed z-axis, for which $K \leq L$ is valid, as one can see from the algorithm of the SU(3)⊃SO(3) reduction [6]. (Remember at this point, that the quadrupole operator used in Refs. [111, 112, 154] is $2\sqrt{2}$ times the quadrupole operator used in the present work.) For states with $\lambda \gg L$ (and therefore also $\lambda \gg K$) and $\lambda \gg \mu$, one then obtains [111]

$$q_0 = \frac{\lambda}{\sqrt{2}}, \tag{82}$$

while q_2 becomes negligible. Since the ground-state band belongs to the $(2N,0)$ irrep of SU(3), while other low-lying bands belong to irreps $(2N - 4i - 6j, 2i)$, $i = 0,1,2,\ldots$, $j = 0,1,2,\ldots$, with relatively low i, j, the contraction occurs in the large-N limit. Thus, in the case of interest, the intrinsic quadrupole moment becomes

$$q_0 = N\sqrt{2}. \tag{83}$$

An equivalent statement is that one can approximately replace the operator $\hat{Q}^{(2)}_{SU(3)}$ by the scalar $\lambda/\sqrt{2}$, as one can see from Eq. (76) and (77), since the terms containing $\hat{L}$ and μ are negligible in this limit, having as a consequence that only the first term in the rhs of these equations survives.

It should be noticed that the above results have been obtained in irreps with $\lambda \gg L$ and thus, they regard the low-lying part of the spectrum.

In the SU(3), the irreps are built out of the (2,0) irrep, while in the case of $\overline{SU(3)}$ the irreps are built out of the (0,2) irrep [6]. As a result, in the $\overline{SU(3)}$ framework one is interested in states with large values of $C_2(\lambda, \mu)$ and $\lambda < \mu$, in which the intrinsic quadrupole moments become [111, 112]

$$q_0 = -\frac{1}{2\sqrt{2}}(2\lambda + \mu + 3), \quad q_2 = -\frac{1}{4}\sqrt{3(\mu - K)(\mu + K + 2)}, \tag{84}$$

For states with $\mu \gg L$ and $\mu \gg \lambda$, one then obtains

$$q_0 = -\frac{\mu}{\sqrt{2}}, \tag{85}$$

while q_2 becomes negligible. Since the ground-state band belongs to the $(0, 2N)$ irrep of $\overline{SU(3)}$, while other low-lying bands belong to irreps $(2i, 2N - 4i - 6j)$, $i = 0, 1, 2, \ldots$, $j = 0, 1, 2, \ldots$ with relatively low i, j, the contraction does occur in the large-N limit, the intrinsic quadrupole moment becoming

$$q_0 = -N\sqrt{2}. \tag{86}$$

Since SU(3) is associated with prolate shapes, while $\overline{SU(3)}$ is related to oblate shapes, the signs in Eqs. (83) and (86) are consistent with the fact that intrinsic quadrupole moments are known to be positive for prolate nuclei and negative for oblate nuclei [14].

Appendix G

The O(6)→ [R^5]SO(5) contraction

A similar procedure to that of appendix F is followed in the contraction of O(6) to [R^5]SO(5) [113, 114]. This is a procedure in which the full O(6) algebra, consisting of 15 noncommuting generators, is reduced into an SO(5) algebra (consisting of 10 noncommuting generators), accompanied by 5 mutually commuting operators (the quadrupole operators). The resulting algebraic structure is known [114] to be the algebra of the γ-unstable rotator.

The commutation relation for the quadrupole operators reads

$$[\hat{Q}^{(2)}_{O(6),\xi}, \hat{Q}^{(2)}_{O(6),\nu}] = 2 \sum_{k=1,3} (2\xi 2\nu | k\xi + \nu)(d^\dagger \tilde{d})^{(k)}_{\xi+\nu}. \tag{87}$$

The second order Casimir operator is [6]

$$\hat{C}_2[O(6)] = 2\hat{Q}^{(2)}_{O(6)} \cdot \hat{Q}^{(2)}_{O(6)} + 4 \sum_{k=1,3} (d^\dagger \tilde{d})^{(k)} \cdot (d^\dagger \tilde{d})^{(k)}. \tag{88}$$

Its eigenvalues are

$$C_2(\sigma) = 2\sigma(\sigma + 4), \tag{89}$$

where σ is the quantum number characterizing the irreps of O(6).

If we consider O(6) irreps with large σ, we can rescale the quadrupole operator as

$$\hat{q}^{(2)}_{O(6),\xi} = \frac{\hat{Q}^{(2)}_{O(6)),\xi}}{\sqrt{C_2(\sigma)}}. \tag{90}$$

Then the commutation relation for the quadrupole operators becomes

$$[\hat{q}^{(2)}_{O(6),\xi}, \hat{q}^{(2)}_{O(6),\nu}] = 2 \sum_{k=1,3} (2\xi 2\nu | k\xi + \nu)\frac{(d^\dagger \tilde{d})^{(k)}_{\xi+\nu}}{C_2[\sigma]}. \tag{91}$$

Then, in the limit of large σ (and small τ, where τ is the quantum number characterizing the irreps of O(5)) [114] one gets

$$[\hat{q}^{(2)}_{O(6),\xi}, \hat{q}^{(2)}_{O(6),\nu}] = 0. \tag{92}$$

This procedure is called the contraction of O(6) to $[R^5]SO(5)$, where $[R^5]SO(5)$ is the algebra of the γ-unstable rotator, generated by the operators of SO(5) and the five commuting operators $q^{(2)}_{O(6),\xi}$, $\xi = -2, -1, 0, 1, 2$, which are the coordinates [114].

An immediate consequence of Eqs. (88) and (89) is that, in the contraction limit, terms proportional to $(d^\dagger \tilde{d})^{(k)}$ can be ignored.

The most leading O(6) irrep, to which the ground state band belongs, is (N). Thus, in the large-boson number limit, it is appropriate to use this contraction. The intrinsic quadrupole moment will then be

$$q'_0 = \sigma, \tag{93}$$

as can be seen from Eqs. (88) and (89). Thus, in the case of interest, the intrinsic quadrupole moment becomes

$$q'_0 = N. \tag{94}$$

It should be noticed that the above results have been obtained in irreps with $\sigma >> \tau$, and thus they regard the low lying part of the spectrum (since $L \leq 2\tau$, as seen from the algorithm of the SO(5)$\supset$SO(3) reduction [6]).

Appendix H

An alternative basis

The Nilsson vectors used in Eq. (5.7) can easily be expressed in terms of the total angular momentum j

$$|Nl\Lambda\Sigma\rangle = \sum_j (l\Lambda\frac{1}{2}\Sigma|j\Omega)|Nlj\Omega\rangle, \tag{95}$$

where a Clebsch–Gordan coefficient appears in the rhs.

Then the expansion of Eq. (5.7) can be written as

$$\chi_{N\Omega} = \sum_{lj} \left[\Sigma_\Lambda a_{l\Lambda}^\Omega (l\Lambda\frac{1}{2}\Sigma|j\Omega) \right] |Nlj\Omega\rangle. \tag{96}$$

Actually the sum over l can be omitted. This can be seen as follows. The wave function $\chi_{N\Omega}$ is assumed to have a definite parity. As seen from Eq. (5.9), the parity of the vectors in the rhs of Eq. (5.7) is dictated by the spherical harmonic. As a consequence, only even or only odd values of l can occur in the expansion. Since $j = l \pm \frac{1}{2}$, we see that j and the parity of $\chi_{N\Omega}$ fix which of the two possible values of l will contribute.

The expansion of Eq. (95) can be easily inverted

$$|Nlj\Omega\rangle = \sum_\Sigma (l\Lambda\frac{1}{2}\Sigma|j\Omega)|Nl\Lambda\Sigma\rangle, \tag{97}$$

where there is no summation over Λ since $\Omega = \Lambda + \Sigma$.

An example is provided of how one goes from one basis to the other. In the Nilsson code used, results are found in the $|Nlj\Omega\rangle$ basis, for deformation $\epsilon_2 = 0.22$.

The expansion obtained for the $\frac{1}{2}[550]$ level is

$$\left|\frac{1}{2}[550]\right\rangle = -0.0132\left|51\frac{1}{2}\frac{1}{2}\right\rangle + 0.0692\left|51\frac{3}{2}\frac{1}{2}\right\rangle - 0.0179\left|53\frac{5}{2}\frac{1}{2}\right\rangle$$

$$+0.2966\left|53\frac{7}{2}\frac{1}{2}\right\rangle - 0.0258\left|55\frac{9}{2}\frac{1}{2}\right\rangle + 0.9519\left|55\frac{11}{2}\frac{1}{2}\right\rangle. \tag{98}$$

The orbital $\left|\frac{1}{2}[550]\right\rangle$ has odd parity. Therefore, only odd values of l will appear in the rhs. For example, in the term with $j = 5/2$, the possible l values are $l = 2$, 3, since $s = 1/2$. Out of these, only $l = 3$ is eligible. Thus the relevant vector reads $\left|53\frac{5}{2}\frac{1}{2}\right\rangle$.

On the other hand, in the original Nilsson paper [1] the same orbital $\frac{1}{2}[550]$ is expanded in terms of $|Nl\Lambda\Sigma\rangle$ vector as

$$\left|\frac{1}{2}[550]\right\rangle_{\eta=4} = 1.000\left|550\frac{1}{2}\right\rangle + 0.479\left|530\frac{1}{2}\right\rangle + 0.183\left|510\frac{1}{2}\right\rangle$$
$$+0.843\left|551-\frac{1}{2}\right\rangle + 0.343\left|531-\frac{1}{2}\right\rangle + 0.071\left|511-\frac{1}{2}\right\rangle. \qquad (99)$$

The numerical coefficients correspond to $\eta = 4$. For $\eta = 2$ the expansion reads

$$\left|\frac{1}{2}[550]\right\rangle_{\eta=2} = 1.000\left|550\frac{1}{2}\right\rangle + 0.237\left|530\frac{1}{2}\right\rangle + 0.046\left|510\frac{1}{2}\right\rangle$$
$$+0.888\left|551-\frac{1}{2}\right\rangle + 0.192\left|531-\frac{1}{2}\right\rangle + 0.024\left|511-\frac{1}{2}\right\rangle. \qquad (100)$$

In order to compare the two results, and in order to be able to use the configuration space wave functions described in Section 2, we have to expand the vectors appearing in Eq. (98) in terms of the vectors appearing in Eqs. (99) and (100). For example, one has

$$\left|55\frac{11}{2}\frac{1}{2}\right\rangle = (50\frac{1}{2}\frac{1}{2}|\frac{11}{2}\frac{1}{2})\left|550\frac{1}{2}\right\rangle + (51\frac{1}{2}-\frac{1}{2}|\frac{11}{2}\frac{1}{2})\left|551-\frac{1}{2}\right\rangle. \qquad (101)$$

The reasoning behind writing this equation is the following. From the lhs we know that $N = 5$, $j = 11/2$, $\Omega = 1/2$. Since the parity has to be odd, from the possible values of $l = 5, 6$, only $l = 5$ is allowed. Then in the rhs the summation is limited only over Σ. Since $\Omega = \Lambda + \Sigma$ and $\Omega = 1/2$, we have only two terms: $(\Lambda = 0, \Sigma = 1/2)$ and $(\Lambda = 1, \Sigma = -1/2)$.

In the same way one finds

$$\left|55\frac{9}{2}\frac{1}{2}\right\rangle = (50\frac{1}{2}\frac{1}{2}|\frac{9}{2}\frac{1}{2})\left|550\frac{1}{2}\right\rangle + (51\frac{1}{2}-\frac{1}{2}|\frac{9}{2}\frac{1}{2})\left|551-\frac{1}{2}\right\rangle, \qquad (102)$$

$$\left|53\frac{7}{2}\frac{1}{2}\right\rangle = (30\frac{1}{2}\frac{1}{2}|\frac{7}{2}\frac{1}{2})\left|530\frac{1}{2}\right\rangle + (31\frac{1}{2}-\frac{1}{2}|\frac{7}{2}\frac{1}{2})\left|531-\frac{1}{2}\right\rangle, \qquad (103)$$

$$\left|53\frac{5}{2}\frac{1}{2}\right\rangle = (30\frac{1}{2}\frac{1}{2}|\frac{5}{2}\frac{1}{2})\left|530\frac{1}{2}\right\rangle + (31\frac{1}{2}-\frac{1}{2}|\frac{5}{2}\frac{1}{2})\left|531-\frac{1}{2}\right\rangle, \qquad (104)$$

$$\left|51\frac{3}{2}\frac{1}{2}\right\rangle = (10\frac{1}{2}\frac{1}{2}|\frac{3}{2}\frac{1}{2})\left|510\frac{1}{2}\right\rangle + (11\frac{1}{2}-\frac{1}{2}|\frac{3}{2}\frac{1}{2})\left|511-\frac{1}{2}\right\rangle, \qquad (105)$$

$$\left|51\frac{1}{2}\frac{1}{2}\right\rangle = \left(10\frac{1}{2}\frac{1}{2}\Big|\frac{1}{2}\frac{1}{2}\right)\left|510\frac{1}{2}\right\rangle + \left(11\frac{1}{2}-\frac{1}{2}\Big|\frac{1}{2}\frac{1}{2}\right)\left|511-\frac{1}{2}\right\rangle. \tag{106}$$

Then one finds

$$\left|55\frac{11}{2}\frac{1}{2}\right\rangle = 0.7385\left|550\frac{1}{2}\right\rangle + 0.6742\left|551-\frac{1}{2}\right\rangle, \tag{107}$$

$$\left|55\frac{9}{2}\frac{1}{2}\right\rangle = -0.6742\left|550\frac{1}{2}\right\rangle + 0.7385\left|551-\frac{1}{2}\right\rangle, \tag{108}$$

$$\left|53\frac{7}{2}\frac{1}{2}\right\rangle = 0.7559\left|530\frac{1}{2}\right\rangle + 0.6547\left|531-\frac{1}{2}\right\rangle, \tag{109}$$

$$\left|53\frac{5}{2}\frac{1}{2}\right\rangle = -0.6547\left|530\frac{1}{2}\right\rangle + 0.7559\left|531-\frac{1}{2}\right\rangle, \tag{110}$$

$$\left|51\frac{3}{2}\frac{1}{2}\right\rangle = 0.8165\left|510\frac{1}{2}\right\rangle + 0.5774\left|511-\frac{1}{2}\right\rangle, \tag{111}$$

$$\left|51\frac{1}{2}\frac{1}{2}\right\rangle = -0.5774\left|510\frac{1}{2}\right\rangle + 0.8165\left|511-\frac{1}{2}\right\rangle. \tag{112}$$

Substituting these results in Eq. (98) we get

$$\left|\frac{1}{2}[550]\right\rangle = 0.7204\left|550\frac{1}{2}\right\rangle + 0.2359\left|530\frac{1}{2}\right\rangle + 0.0641\left|510\frac{1}{2}\right\rangle$$
$$+0.6227\left|551-\frac{1}{2}\right\rangle + 0.1806\left|531-\frac{1}{2}\right\rangle + 0.0292\left|511-\frac{1}{2}\right\rangle. \tag{113}$$

The vector of Eq. (113) is normalized to 1, while the vectors of Eq. (99), (100) are not (they are normalized to the coefficient of the first vector in the expansion instead). In order to facilitate comparisons, we normalize (113) in the same way (by dividing all coefficients by 0.7204), obtaining

$$\left|\frac{1}{2}[550]\right\rangle = 1.000\left|550\frac{1}{2}\right\rangle + 0.327\left|530\frac{1}{2}\right\rangle + 0.089\left|510\frac{1}{2}\right\rangle$$
$$+0.864\left|551-\frac{1}{2}\right\rangle + 0.251\left|531-\frac{1}{2}\right\rangle + 0.040\left|511-\frac{1}{2}\right\rangle. \tag{114}$$

Bibliography

[1] S. G. Nilsson, Mat. Fys. Medd. K. Dan. Vidensk. Selsk. **29**, 16 (1955)

[2] J. P. Elliott, Proc. Roy. Soc. Lon. **245**, 128 (1958).

[3] R. D. Ratna Raju, J. P. Draayer, K. T. Hecht, Nucl. Phys. A **202**, 433 (1973).

[4] J. P. Draayer, K. J. Weeks, Ann. Phys. (NY) **156**, 41 (1984).

[5] A. Bohr, Mat. Fys. Medd. K. Dan. Vidensk. Selsk. **26**, no.14 (1952).

[6] F. Iachello and A. Arima, The interacting boson model, Cambridge University Press, (1987).

[7] D. Bonatsos, Interacting Boson Models of Nuclear Structure, Clarendon Press, (1987).

[8] A. Arima and F. Iachello, Phys. Rev. Lett. **35**, 1069 (1975).

[9] A. Arima and F. Iachello, Ann. Phys. **99**, 253 (1976).

[10] A. Arima and F. Iachello, Ann. Phys. **111**, 201 (1978).

[11] A. Arima and F. Iachello, Ann. Phys. **123**, 468 (1979).

[12] P. Van Isacker, Rep. Prog. Phys. **62**, 1661 (1999).

[13] M. Hamermesh, Group theory and its application to physical problems, Dover Publications, NY, (1962).

[14] R. F. Casten, Nuclear Structure from a simple perspective, Oxford University Press, Oxford (1990).

[15] F. Iachello, Lie Algebras and Applications (Springer Berlin Heidelberg, 2006).

[16] N. V. Zamfir, P. von Brentano, R. F. Casten, J. Jolie, Phys. Rev. C **66**, 021304(R) (2002).

[17] V. Werner, P. von Brentano, R.F. Casten, J. Jolie, Phys. Lett. B **527**, 55 (2002).

[18] E. A. McCutchan, N. V. Zamfir, R. F. Casten, Phys. Rev. C **69**, 064306 (2004).

[19] R.F. Casten, Prog. Part. Nucl. Phys. **62**, 183 (2009).

[20] D. H. Feng, R. Gilmore, S. R. Deans, Phys. Rev. C **23**, 1254 (1981).

[21] J. N. Ginocchio, M. W. Kirson, Phys. Rev. Lett. **44**, 1744 (1980).

[22] A. E. L. Dieperink, O. Scholten, F. Iachello, Phys. Rev. Lett. **44**, 1747 (1980).

[23] F. Iachello, N. V. Zamfir, R. F. Casten, Phys. Rev. Lett. **81**, 1191 (1998).

[24] F. Iachello, Phys. Rev. Lett. **85**, 3580 (2000).

[25] F. Iachello, Phys. Rev. Lett. **87**, 052502 (2001).

[26] Y. Alhassid, N. Whelan, Phys. Rev. C **43**, 2637 (1991)

[27] Y. Alhassid, N. Whelan, Phys. Rev. Lett. **67**, 816 (1991)

[28] Y. Alhassid, N. Whelan, B. Lauritzen, Phys. Rev. Lett. **70**, 572 (1993)

[29] N. Whelan, Y. Alhassid, Nucl. Phys. A **556**, 42 (1993)

[30] N. Whelan, PhD thesis, Yale University (1993)

[31] Y. Alhassid, A. Leviatan, J. Phys. A: Math. Gen. **25**, L1265 (1992).

[32] A. Leviatan, Phys. Rev. Lett. **77**, 818 (1996).

[33] A. Leviatan, P. Van Isacker, Phys. Rev. Lett. **89**, 222501 (2002).

[34] A. Leviatan, Phys. Rev. Lett. **98**, 242502 (2007).

[35] A. Leviatan, Prog. Part. Nucl. Phys. **66**, 93 (2011).

[36] D. J. Rowe, Phys. Rev. Lett. **93**, 122502 (2004).

[37] D. J. Rowe, P. S. Turner, and G. Rosensteel, Phys. Rev. Lett. **93**, 232502 (2004).

[38] D. J. Rowe, Nucl. Phys. A **745**, 47 (2004).

[39] P. S. Turner and D. J. Rowe, Nucl. Phys. A **756**, 333 (2005).

[40] G. Rosensteel and D. J. Rowe, Nucl. Phys. A **759**, 92 (2005).

[41] C. Kremer, J. Beller, A. Leviatan, N. Pietralla, G. Rainovski, R. Trippel, P. Van Isacker, Phys. Rev. C **89**, 041302(R) (2014).

[42] H. Goldstein, C. Poole, J. Safko, Classical Mechanics, (Addison Wesley, 2002), chap. 11

[43] Martin C. Gutzwiller, Chaos in Classical and Quantum Mechanics, (Springer-Verlag, New York, 1990)

[44] Fritz Haake, Quantum Signatures of Chaos, (Springer-Verlag, 2010)

[45] T. A. Brody, J. Flores, P. A. Mello, A. Pandey, S. S. M. Wong, Rev. Mod. Phys. **53**, No. 3, 385 (1981)

[46] O. Bohigas, H. A. Weidenmüller, Annu. Rev. Nucl. Part. Sci. **38**, 421 (1988)

[47] H. A. Weidenmüller, G. E. Mitchell, Rev. Mod. Phys. **81**, 539 (2009)

[48] J. L. Rosen, J. S. Desjardins, J. Rainwater, W. W. Havens, Phys. Rev. **118**, 687 (1960)

[49] J. L. Rosen, J. S. Desjardins, J. Rainwater, W. W. Havens, Phys. Rev. **120**, 2214 (1960)

[50] C. E. Porter and N. Rosenzweig, Phys. Rev. **120**, 1698 (1960)

[51] M. L. Mehta, Nucl. Phys. **18**, 395 (1960)

[52] M. L. Mehta, M. Gaudin, Nucl. Phys. **18**, 420 (1960)

[53] M. Gaudin, Nucl. Phys. **25**, 447 (1961)

[54] R. G. Thomas, C. E. Porter, Phys. Rev. **104**, 483 (1956)

[55] I. I. Gurevich , M. I. Pevsner, Nuclear Phys. **2**, 575 (1957)

[56] E. P. Wigner, Ann. Math. **53**, 36 (1951)

[57] E. P. Wigner, Ann. Math. **62**, 548 (1955)

[58] E. P. Wigner, Ann. Math. **65**, 203 (1957)

[59] E. P. Wigner, Ann. Math. **67**, 325 (1958)

[60] F. J. Dyson, J. Math. Phys. **3**, 140 (1962)

[61] F. J. Dyson, J. Math. Phys. **3**, 157 (1962)

[62] F. J. Dyson, J. Math. Phys. **3**, 166 (1962)

[63] F. J. Dyson and M. L. Mehta, J. Math. Phys. **4**, 701 (1963)

[64] M. L. Mehta and F. J. Dyson, J. Math. Phys. **4**, 713 (1963)

[65] J. Von Neumann, E. P. Wigner, Phys. Z. **30**, 467 (1929)

[66] H. S. Camarda, P. D. Georgopoulos, Phys. Rev. Lett. **50**, 7 (1983)

[67] O. Bohigas, M. J. Giannoni, C. Schmit, Phys. Rev. Lett. **52**, 1 (1984)

[68] M.R. Schroeder, J. Audio Eng. Soc. **35**, 307 (1987)

[69] H. J. Stöckmann, J. Stein, Phys. Rev. Lett. **64**, 2215 (1990)

[70] H. Alt, H. D. Gräf, H. L. Harney, R. Hofferbert, H. Lengeler, A. Richter, P. Schart, H. A. Weidenmüller, Phys. Rev. Lett. **74**, 62 (1995)

[71] H. Alt, H. D. Gräf, R. Hofferbert, C. Rangacharyulu, H. Rehfeld, A. Richter, P. Schart, A. Wirzba, Phys. Rev. E **54**, 2303 (1996)

[72] Th. Zimmermann, H. Köppel, L. S. Cederbaum, C. Persch, W. Demtröder, Phys. Rev. Lett. **61**, 3 (1988)

[73] G. Persch, E. Mehdizadeh, W. Demtröder, T. Zimmermann, L. S. Cederbaum, Ber. Bunsenges. Phys. Chem. **92**, 312 (1988)

[74] H. Held, J. Schlichter, G. Raithel, H. Walther, Europhys. Lett. **43**, 392 (1998)

[75] C. Ellegaard, T. Guhr, K. Lindemann, H.Q. Lorensen, J. Nygård, M. Oxborrow, Phys. Rev. Lett. **75**, 1546 (1995)

[76] C. Ellegaard, T. Guhr, K. Lindemann, J. Nygård, M. Oxborrow, Phys. Rev. Lett. **77**, 4918 (1996)

[77] P. So, S. M. Anlage, E. Ott, R. N. Oerter, Phys. Rev. Lett. **74**, 2662 (1995)

[78] U. Stoffregen, J. Stein, H. J. Stockmann, M. Kus, F. Haake, Phys. Rev. Lett. **74**, 2666 (1995)

[79] K. Sacha, J. Zakrzewski, D. Delande, Phys. Rev. Lett. **83**, 2922, (1999)

[80] K. Sacha, Jour. Phys. B: At. Mol. Opt. Phys. **33**, 2617, (2000)

[81] A. Hoenig, D. Wintgen, Phys. Rev. A **39**, 5642 (1989)

[82] M. Oxborrow, C. Ellegaard, In Proceedings of the 3rd Experimental Chaos Conference (Edinburgh, 1995)

[83] S. Deus, P.M. Koch, L. Sirko, Phys. Rev. E **52**, 1146 (1995)

[84] O. Legrand, C. Schmit, D. Sornette, Europhys. Lett. **18**, 101 (1992)

[85] A. Pandey, Ann. Phys. **119**, 170 (1979)

[86] R. U. Haq, A. Pandey, O. Bohigas, Phys. Rev. Lett. **48**, 1086 (1982)

[87] M. V. Berry, Ann. Phys. **131**, 163 (1981)

[88] M. V. Berry, M. Tabor, Proc. R. Soc. Lond. A **356**, 375 (1977)

[89] Y. Alhassid, A. Novoselsky, Phys. Rev. C **45**, 4 (1992)

[90] Y. Alhassid, R. D. Levine, Phys. Rev. Lett. **57**, 2879 (1986)

[91] Y. Alhassid, M. Feingold, Phys. Rev. A **39**, 374 (1989)

[92] J. Jolie, R. F. Casten, P. Cejnar, S. Heinze, E. A. McCutchan, N. V. Zamfir, Phys. Rev. Lett. **93**, 132501 (2004)

[93] P. Cejnar, J. Jolie, Phys. Rev. E **58**, 387 (1998)

[94] M. Macek, Jan Dobeš, P. Cejnar, Phys. Rev. C **80**, 014319 (2009)

[95] D. Bonatsos, E. A. McCutchan, R. F. Casten, Phys. Rev. Lett. **104**, 022502 (2010)

[96] D. Bonatsos, S. Karampagia, R. F. Casten, Phys. Rev. C **83**, 054313 (2011)

[97] M. Macek, P. Stránský, P. Cejnar, Phys. Rev. C **75**, 064318 (2007)

[98] Y. Alhassid and N. Whelan, Phys. Rev. Lett. **67**, 816 (1991).

[99] N. Whelan and Y. Alhassid, Nucl. Phys. A **556**, 42 (1993).

[100] P. Cejnar and J. Jolie, Phys. Rev. E **58**, 387 (1998).

[101] M. Macek, P. Stránský, P. Cejnar, S. Heinze, J. Jolie, and J. Dobeš, Phys. Rev. C **75**, 064318 (2007).

[102] F. Iachello, N. V. Zamfir, and R. F. Casten, Phys. Rev. Lett. **81**, 1191 (1998).

[103] D. J. Rowe, Phys. Rev. Lett. **93**, 122502 (2004).

[104] D. J. Rowe, Phys. Rev. Lett. **93**, 232502 (2004).

[105] D. J. Rowe, Nucl. Phys. A **745**, 47 (2004).

[106] P. S. Turner and D. J. Rowe, Nucl. Phys. A **756**, 333 (2005).

[107] G. Rosensteel and D. J. Rowe, Nucl. Phys. A **759**, 92 (2005).

[108] M. Macek, J. Dobeš, and P. Cejnar, Phys. Rev. C **80**, 014319 (2009).

[109] M. Macek, J. Dobeš, and P. Cejnar, Phys. Rev. C **82**, 014308 (2010).

[110] E. İnőnű and E. P. Wigner, Proc. Natl. Acad. Sci. (N.Y.) **39**, 510 (1953).

[111] R. Le Blanc, J. Carvalho, and D. J. Rowe, Phys. Lett. B **140**, 155 (1984).

[112] D. J. Rowe, Prog. Part. Nucl. Phys. **37**, 265 (1996).

[113] J. Meyer-ter-Vehn, Phys. Lett. B **84**, 10 (1979).

[114] J. P. Elliott, P. Park, and J. A. Evans, Phys. Lett. B **171**, 145 (1986).

[115] E. A. McCutchan, Dennis Bonatsos, N. V. Zamfir, Phys. Rev. C , 034306 (2006).

[116] A. Leviatan, A. Novoselsky, I. Talmi, Phys. Lett. B **172**, 144 (1986)

[117] A. de-Shalit, M. Goldhaber, Phys. Rev. **92**, 1211 (1953)

[118] I. Talmi, Rev. Mod. Phys. **34**, 704 (1962)

[119] P. Federman, S. Pittel, Phys. Lett. B **69**, 385 (1977)

[120] P. Federman, S. Pittel, Phys. Lett. B **77**, 29 (1978)

[121] P. Federman, S. Pittel, Phys. Rev. C **20**, 820 (1979)

[122] J. Dobaczewski, W. Nazarewicz, J. Skalski, T. Werner, Phys. Rev. Lett. **60**, 2254 (1988)

[123] W. Nazarewicz, Prog. Part. Nucl. Phys. **28**, 307 (1992)

[124] T. R. Werner, J. Dobaczewski, M. V. Guidry, W. Nazarewicz, J. A. Sheikh, Nucl. Phys. A **578**, 1 (1994)

[125] P. Cejnar, J. Jolie, R. F. Casten, Rev. Mod. Phys. **82**, 2155 (2010)

[126] R. F. Casten, D. S. Brenner, P. E. Haustein, Phys. Rev. Lett. **58**, 658 (1987)

[127] R. Casten, Nuclear Structure from a Simple Perspective, (Oxford University Press, 2nd Edition, 2000)

[128] M.G. Mayer, Phys. Rev. **78**, 16 (1950).

[129] A. de Shalit and H. Feshbach, Theoretical Nuclear Physics Vol. I: Nuclear Structure (Wiley, New York, 1974).

[130] M. Moshinsky, T. H. Seligman, and K. B. Wolf, J. Math. Phys. **13**, 901 (1972).

[131] W. Greiner, *Quantum Mechanics* (Springer, Berlin, 1989).

[132] R. F. Casten, Phys. Rev. Lett. **54**, 1991 (1985)

[133] R. F. Casten, K. Heyde, A. Wolf, Phys. Lett. B **208**, 33 (1988)

[134] J.-Y. Zhang, R. F. Casten, D. S. Brenner, Phys. Lett. B **227**, 1 (1989)

[135] P. Van Isacker, D. D. Warner, D. S. Brenner, Phys. Rev. Lett. **74**, 4607 (1995)

[136] D. S. Brenner, R. B. Cakirli, R. F. Casten, Phys. Rev. C **73**, 034315 (2006)

[137] D. S. Brenner, C. Wesselborg, R. F. Casten, E. A. Millman, Phys. Lett. B **243**, 1 (1990)

[138] R. B. Cakirli, D. S. Brenner, R. F. Casten, E. A. Millman, Phys. Rev. Lett. **94**, 092501 (2005)

[139] D. D. Warner, M. A. Bentley, P. Van Isacker, Nature Phys. **2**, 315 (2006)

[140] R. B. Cakirli, R. F. Casten, Phys. Rev. Lett. **96**, 132501 (2006)

[141] M. Stoitsov, R. B. Cakirli, R. F. Casten, W. Nazarewicz, W. Satula, Phys. Rev. Lett. **98**, 132502 (2007)

[142] D. Neidherr *et al.* , Phys. Rev. C **80**, 044323 (2009)

[143] L. Chen *et al.* , Phys. Rev. Lett. **102**, 122503 (2009)

[144] D. Neidherr *et al.* , Phys. Rev. Lett. **102**, 112501 (2009)

[145] M. Breitenfeldt *et al.* , Phys. Rev. C **81**, 034313 (2010)

[146] R. B. Cakirli, K. Blaum, R. F. Casten, Phys. Rev. C **82**, 061304(R) (2010)

[147] D. Bonatsos, S. Karampagia, R. B. Cakirli, R. F. Casten, K. Blaum, L. Amon Susam, Phys. Rev. C **88**, 054309 (2013)

[148] S. Raman, C. W. Nestor, Jr., P. Tikkanen, At. Data Nucl. Data Tables **78**, 1 (2001).

[149] G. Vanden Berghe, H. E. De Meyer, P. Van Isacker, Phys. Rev. C **32**, 1049 (1985).

[150] R. J. Casperson, Comp. Phys. Commun. **183**, 1029 (2012)

[151] A. R. Edmonds, Angular Momentum in Quantum Mechanics, (Princeton University Press, Princeton, 1957).

[152] Gilmore, Lie groups, lie algebras, and some of their applications (John Wiley and Sons, Inc, 1974).

[153] H. Ui, Prog. Theor. Phys. **44**, 153 (1970).

[154] D. J. Rowe, M. G. Vassanji, J. Carvalho, Nucl. Phys. A **504**, 76 (1989).